United States
Consumer Product Safety Commission

October 20, 2023

CPSC[1] Staff Statement on: Exposure Assessment of Carbon Nanotubes in Sports Equipment (Phase I and II)

The reports titled, “Exposure Assessment of Carbon Nanotubes in Sports Equipment” (the Phase I study) and “Exposure Assessment of Carbon Nanotubes in Sports Equipment, Phase II” describe studies performed by the National Institute of Standards and Technology (NIST). The studies were supported by interagency agreements CPSC-I-08-0008 and CPSC-I-12-0009 between the Consumer Product Safety Commission (CPSC) and NIST.

NIST’s Material Measurement Laboratory (MML) conducts measurement science research, provides technical expertise to the development of standards, and performs fundamental and applied research to assure the quality of measurement results. MML staff developed analytical methods in the Phase I study and optimized those methods in the Phase II study to assess if and where carbon nanotubes (CNTs) were located in two commercially available baseball bats. In addition, NIST also determined whether CNTs were released from the bats during normal use conditions and in the worst-case scenarios (e.g., bat breakage).

Nanoparticles are of concern because their small nanoscale size enables these particles to penetrate to the deep lung when inhaled and potentially move across lung cell walls and become systemically distributed. Published literature from in vivo studies has shown that CNTs and carbon nanofibers (CNF)[2] can cause persistent pulmonary inflammation, granulomatosis, and fibrosis. In addition, immunosuppression, neuroinflammation, and cardiovascular effects, such as endothelial dysfunction, may occur from systemic inflammation in laboratory animals following inhalation exposure to CNTs. While these health effects have been observed in animal studies, epidemiological studies in CNT/CNF workplaces have not shown consistent patterns in the health effects assessed (e.g., respiratory symptoms and illnesses; blood pressure; heart rate; hematology; as well as serum markers of oxidative stress, inflammation, fibrosis, and immunosuppression).

CNTs are used as additives in sports equipment to achieve performance advantages (e.g., lighter weight, greater strength). NIST notes that composite bats have better bending resistance and elasticity than aluminum and wood bats. Adding CNTs, especially multiwall carbon nanotubes (MWCNTs), to the composite polymer resin can improve the durability of composite bats which have tended to break more easily, especially in cold temperatures.

In the Phase I study, NIST noted that based on a literature and patent search, they expected that the bat barrels were hollow and CNTs were most likely present in the inner composite layers. In order to confirm the location of the CNTs, NIST cut bat sections with a wet bandsaw and analyzed the cut sections with various microscopic techniques, including light microscopy (LM), scanning

[1] This statement was prepared by the CPSC staff, and the attached report was prepared by NIST for CPSC staff. The statement and reports have not been reviewed or approved by, and do not necessarily represent the views of, the Commission.
[2] Please note that NIST includes carbon nanofibers under the term CNTs in both study reports.

electron microscopy (SEM), energy dispersive x-ray spectrometry (EDS), focused ion beam (FIB) SEM, transmission electron microscopy (TEM), and Raman spectroscopy.

LM, SEM, and EDS analyses confirmed the laminated structure of the bat barrels and the presence of carbon fiber composite layers which were located more than 1 mm below the bat surface layers. Because of the depth of the carbon composite layer, NIST stated that incidental release of CNTs from minor abrasion or scratches to the bat surface is not likely to occur. FIB SEM and TEM analyses did not detect any CNTs in the resin around the carbon fiber composite layers, although other nanometer-sized silicon particles were observed. However, Raman spectroscopy did detect CNTs in the cross-sectional samples of the bats

To investigate wear (including bat breakage) and the potential release of CNTs during consumer use, NIST cut, sawed and shredded the bats. Sawdust and released particles were analyzed by NIST with different microscopic techniques. SEM images of the sawdust showed many large particles (hundreds of micrometers in size) containing CNT-like fibrous protrusions covered in composite resin; bare CNT-like particles were not common. SEM analysis could not clearly confirm the presence of CNTs. Analysis of the released fine particles showed two types of CNT-like particles, rod-like particles and resin-covered particles, occurring singly and as aggregates, in large nanometer and small submicron sizes. High-resolution TEM analysis confirmed the presence of CNTs.

From the Phase I analysis studies of bat sawdust and fine particles, NIST stated that CNTs can be released as bare CNTs or CNT aggregates of nanocomposite material. Although SEM and TEM analyses were microscopically effective in detecting the presence of CNTs, NIST noted that the technologies were time-consuming and laborious methods and do not appear to be viable approaches for quantitative analysis of CNTs.

NIST noted that the Phase I study had extremely low collection efficiency for the TEM analyses, such that many of the released fine particles were lost to surrounding surfaces. Therefore, the Phase II study focused on a more systematic and controlled evaluation of CNT particle release. The objectives of the Phase II study were to (1) develop and optimize the Raman spectroscopy for MWCNT detection procedure, (2) determine MWCNT release in different use-case scenarios (e.g., abrasion) by SEM analysis, and (3) evaluate the feasibility of performing quantitative SEM analysis of MWCNTs.

Similar to the Phase I studies, the bats were cut into smaller pieces. In addition, a specially designed sample abrader and a sample collection system were used in Phase II. Furthermore, a step of selectively dissolving the polymer matrix was added to facilitate MWCNT detection.

NIST evaluated the test system with positive controls consisting of custom fabricated epoxy nanocomposite samples with known concentrations of MWCNTs. In addition, a prototype Raman microscope system was used for analyzing MWCNTs in the positive control samples and in the baseball bat released particles.

The initial Phase II aerosol sampling system consisted of a Taber linear abrader, a customized sampling chamber, a scanning mobility particle sizer (SMPS) for particle sizing and counting, and a Nanometer Aerosol Sampler (NAS) electrostatic precipitator and a personal sampler for sample collection. NIST determined that sampling close to the abrading surface was necessary to collect sufficient particles. The particle size distribution peaked at 100 nm. However, the particle number

concentration was extremely low, such that NIST stated conclusions could not be made based on the SMPS results.

The positive control studies found that abrasion nanoparticles were not effectively aerosolized for collection, and there was a significant loss of nanoparticles during the sampling process (i.e., transport loss from generating sites to sampling site). To address the low sampling efficiency problem, NIST modified the aerosol sampling system to include additional real-time particle analyzers and a micro-orifice uniform deposit impactor (MOUDI) with customized impaction plates.

Unlike the Phase I study, Raman spectrometry in Phase II study did not identify the presence of MWCNTs from the bat samples although it detected the presence of MWCNTs from the positive controls. NIST believes the lack of MWCNT signals in the bat samples is due to the MWCNT loading in the bats falling below the Raman detection limit. NIST noted that the resin fragments appeared translucent rather than black; MWCNT nanocomposites with MWCNT concentrations greater than 0.1% mass should appear black. NIST also cited that another potential cause for the lower MWCNT detection in samples may be due to particle dispersion. Raman signals are stronger on MWCNT agglomerated samples than well-dispersed samples. NIST indicated that there is a need to better understand MWCNT dispersion in polymer matrices in order to determine whether Raman imaging can be used routinely to detect CNTs in nanocomposites and their release products.

NIST stated that SEM and TEM at this time are the most effective and reliable methods to identify MWCNTs due to the extreme small size of MWCNTs and their lack of unique elemental and chemical signatures. However, the methods are time-consuming processes and may not be appropriate for a high throughput analysis of a large number of samples.

While the Phase II study was not able to determine a MWCNT release rate, the MOUDI analysis provided information on the characteristics of released MWCNT and non-MWCNT particles and potential artifacts generated during sampling. MWCNTs detected at the inlet stage appear to be generally longer than those detected on the subsequent stages of the MOUDI system. This observation indicates that the released MWCNT particles may have been broken into smaller particles upon impact while traveling from the inlet stage to the subsequent stages in the MOUDI system. Therefore, nanoparticles obtained by the MOUDI system may not be representative of released samples in a real-world scenario.

In conclusion, the Phase II study demonstrated that free MWCNTs and MWCNTs embedded in polymer resin can be released from commercially available nanocomposite bats. Because of the small number of detected MWCNTs compared to the number of total released particles, NIST stated that the environmental release of MWCNTs from these commercially available bats is limited. NIST indicated that a more sophisticated system to obtain information on real-time analysis of released particles and realistic estimates of particles loss during sample collection would be required for a quantitative assessment of MWCNTs released from the baseball bats.

Exposure Assessment of Carbon Nanotubes in Sports Equipment

Report of Analysis for the CPSC-NIST Interagency Agreement # CPSC-I-08-0008; Mod#3

May 15, 2012

Performed by:

Keana Scott, NIST
Christopher Marvel, SURF Student, Lehigh University
Stephan Stranick, NIST
John Henry Scott, NIST
Andrew Herzing, NIST

Submitted by:

Keana Scott
Microanalysis Research Group
National Institute of Standards and Technology
100 Bureau Drive, MS-8372
Gaithersburg, MD 20877
(301) 975-4579
keana.scott@nist.gov

Table of Contents

1. Executive Summary

Two commercially available carbon nanotube (CNT) containing baseball/softball bats were analyzed. The main focus of this study was to evaluate several different imaging and spectroscopy based techniques for the detection and characterization of CNTs in the bat and in the release products of different use scenarios. Both bats had barrels made up of multiple layers of composite materials. The CNTs were found in the polymer resin in the carbon nanocomposite layers, initially by Raman spectroscopy of the polished cross-sectional samples of the bat barrels and subsequently by SEM analysis of the carbon nanocomposite chunks. Based on the structure of the bat barrel where CNT containing nanocomposite layers were located relatively far (> 1 mm) below the surface, incidental release of CNTs from minor abrasion or scratching of the bat surface was considered not likely. The release of CNTs from broken bats and during the disposal scenarios was also considered. These release scenarios were simulated in the lab by sawing and cutting the bats. Released particles were collected using several different sampling methods and analyzed using SEM and TEM. SEM analysis detected nano-sized release particles that looked like CNTs or resin covered CNTs. Subsequent TEM analysis of the same particles confirmed the multi-wall structures of these particles. Although we were able to detect and analyze the CNTs in the bats and in the release products, quantitative analysis of the released CNTs was not performed at this time. Several improvements in the sampling methods and analysis techniques are needed to perform robust quantitative analysis of CNT release from the bats.

2. Introduction

The National Institute of Standards and Technology (NIST) performed microscopy-based analysis on two different commercially available carbon nanotube (CNT) containing baseball/softball bats for the Consumer Product Safety Commission (CPSC) in accordance with Interagency Agreement # CPSC-I-08-0008; Mod#3. As outlined in the agreement, NIST was tasked to evaluate and develop methods to confirm the presence of CNTs in commercially available bats and analyze the detected CNTs for their distribution, identification and morphological characterization.

3. Approach Summary

Several CNT containing consumer products (based on the manufacturer's labeling) were considered and two types of baseball bats were identified by CPSC and NIST as the initial sample products and purchased by NIST. Several sampling/sectioning methods and the risks associated with each method were considered. Glove bags were used for the initial sample preparation tasks such as dry sawing and cutting to meet NIST's nanoparticle handling guidelines.

The proposed areas of analysis were:

1. Detection and confirmation of the presence of CNTs via SEM and LM
2. Analysis of detected CNTs and surrounding matrix via FIB/SEM and TEM
3. Test for the incidental release of CNTs SEM and LM of wipe test samples
4. Test for air release of CNTs

5. Quantitation of CNT in consumer products and released CNTs

Cross-sectional samples of the bats were analyzed for the presence of CNTs (items 1 and 2) using various microscopy and spectroscopy techniques including light microscopy (LM), environmental scanning electron microscopy (ESEM), focused ion beam (FIB) SEM, Raman spectroscopy, and transmission electron microscopy (TEM). Several CNT release scenarios (bat breakage and disposal) were simulated by cutting and shredding sectioned bat pieces. Debris from the simulated release scenarios were analyzed using SEM and TEM (items 3, 4 and 5).

4. Results

4.1 Sample Preparation

Two CNT containing bats were purchased. They were[1]:

Sample 1: Manufacturer 1 Youth Baseball Bat 32 inch/21 oz.
Sample 2: Manufacturer 2 Senior League Baseball Bat, 30 inch/22 oz.

Based on the literature and patent search, it was determined that the CNT bat barrels are hollow and the CNTs are most likely to be present in one or more of the inner composite layers. Figure 1 is a diagram from bat patents (U.S. Patent No. 5593158, 6764419, and 6866598) showing the multilayer structure of the hollow barrel.

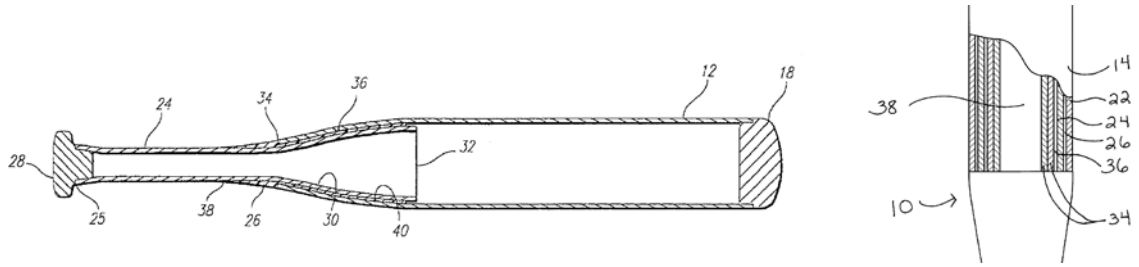

Figure 1: Structure of CNT composite bats, U.S. Patent No. 5593158, 6764419, and 6866598

A temporary glove box (Figure 2) was set up on a lab bench using a large transparent plastic bag. Two large armholes were made in the plastic bag and two rubber gloves were attached through the holes, sealing the bag-glove seams with plastic tape. A CNT containing bat, a clean hacksaw with a replaceable blade, a clean file, two vices, several pieces of sticky tape, several sample stubs, small plastic re-sealable bags and several sheets of wet wipes were put inside the plastic bag and then the bag was sealed with additional plastic tape. The bat was held in place with the vices and sectioned into several pieces using the hacksaw. Sectioned pieces were deburred using the file and loose particles on the sectioned pieces were removed using the sticky tape. A small slit was made in the glovebag (away from the center area to minimize the incidental release of the saw dust) and the sectioned pieces were wiped with clean wet wipes as they were transferred out of the glove bag. Once out of the glove bag,

[1] Certain commercial equipment, instruments, or materials are identified in this talk to foster understanding. Such identification does not imply recommendation or endorsement by NIST, nor does it imply that the materials or equipment identified are necessarily the best available for the purpose.

the pieces were carefully wiped with wet wipes again. The slit in the glove bag was sealed with another piece of tape. When all samples were cut, the inside of the plastic bag was sampled using a piece of double-sided carbon tape on an SEM stub. Also a small amount of saw dust accumulated in the plastic bag was transferred to a re-sealable plastic bag for further analysis. All samples, reusable tools and the remainder of the bat were removed from the glove box in a similar manner as before (wiped clean with wet wipes and extracted through a small incision in the plastic bag followed by another wet wipe). To minimize cross contamination from one bat to the other, all reusable tools were cleaned with Stripcoat TLC Free™ (latex coating commonly used to remove particulate contamination). Once all samples and tools were removed from the plastic bag, the bag was re-sealed and disposed of as nanoparticle waste.

Figure 2: Temporary glove box constructed with a large plastic bag, plastic gloves and 80-20 framing. This photo illustrates how the bat was held in place during the cutting process.

Sectioned pieces of the bats were further processed into roughly 5 mm by 5 mm pieces using a wet band saw. Figure 3 shows several sections cut using a wet band saw.

Figure 3: Larger open ring shaped piece is from the original hack saw cut in the glove bag. Smaller pieces were obtained from the ring shaped piece using a wet band saw.

Several small pieces of the bat samples were embedded in epoxy and polished for subsequent cross-sectional LM and SEM analysis. Possible release of CNTs during the wet sawing and wet

polishing step was considered negligible since the sample pieces were relatively small and the wet polishing minimized the nanoparticle (if any) dispersal. Liquid from the wet sawing and polishing steps was retained and disposed as nanoparticle waste.

4.2 Detection of CNTs in the Product

Several imaging and spectroscopic techniques were applied to confirm the presence of CNTs in the bat samples. Light microscopy provided information about the overall structure of the bat barrel (composite laminates). Scanning electron microscopy (SEM) and energy dispersive x-ray spectrometry (EDS) were used for the compositional analysis of the various layers in the barrels and for locating specific regions of interest for the subsequent focused ion beam (FIB) SEM and transmission electron microscopy (TEM) analyses. Raman spectroscopy was used to see if CNT signature was detectable in the samples.

4.2.1 Light Microscopy (LM)

Based on the product patent documents and published literature on related products, it was assumed that the CNTs in sports equipment are in the form of CNT-reinforced polymer composites. In most nanocomposites, carbon nanomaterial used is in the form of long fibers. However, for this report the term carbon nanotubes are used for both the long carbon nano fibers (CNFs) and carbon nanotubes. Figure 4 is a simplified diagram of an example CNT-reinforced polymer composite material. Basic components of a CNT-reinforced polymer composite (or carbon nanocomposite) are carbon fibers, polymer resin and CNTs. Depending on the application and manufacturing process used, several different types of polymer resin can be used (e.g. epoxy, polyester, vinyl ester and urethane) and CNTs can either be mixed in the resin or be bonded to the carbon fibers.

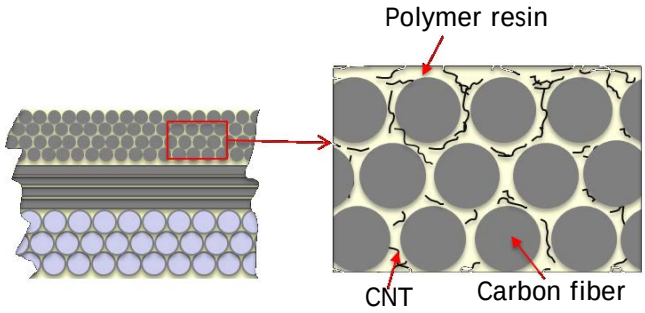

Figure 4: Schematic of CNT-reinforced polymer composite laminate.

Bright field LM images of the polished cross-section and thin section samples were collected for the macro level understanding of the bat structure and as navigational aids in the subsequent higher resolution microscopy and spectroscopy analyses. Figures 5 and 6 show the bright field images of Sample 1 and Sample 2 respectively. Here, the outer wall of the barrel is shown on the left and the inner edge is shown on the right. As expected, both bats had multi-layered structures similar to what is shown in Figure 4. However, the arrangement of the layers was very different in the two bats. In the Sample 1, there were four distinct layers (light/dark/light/dark) in addition to a thin outer paint layer and a thin adhesion layer and these layers were clearly separated. Further analysis showed that these four layers

correspond to fiberglass/carbon fiber/fiberglass/carbon fiber layers. Additionally, each carbon fiber or fiberglass layer consisted of several differently oriented and thinner carbon fiber or fiberglass layers (see Figure A1). Sample 2 also had layers of carbon fibers and fiberglass. However, the layers are not as clearly defined as in the Sample 1 and instead of having a stacked layer structure, fibers show braided or twisted structure (See Figure A2). The nominal bat barrel wall thicknesses were about 4.4 mm for the Sample 1 and about 4 mm for the Sample 2. Precise wall thickness was difficult to measure because the composite layers tended to separate and expand during the cutting and polishing steps.

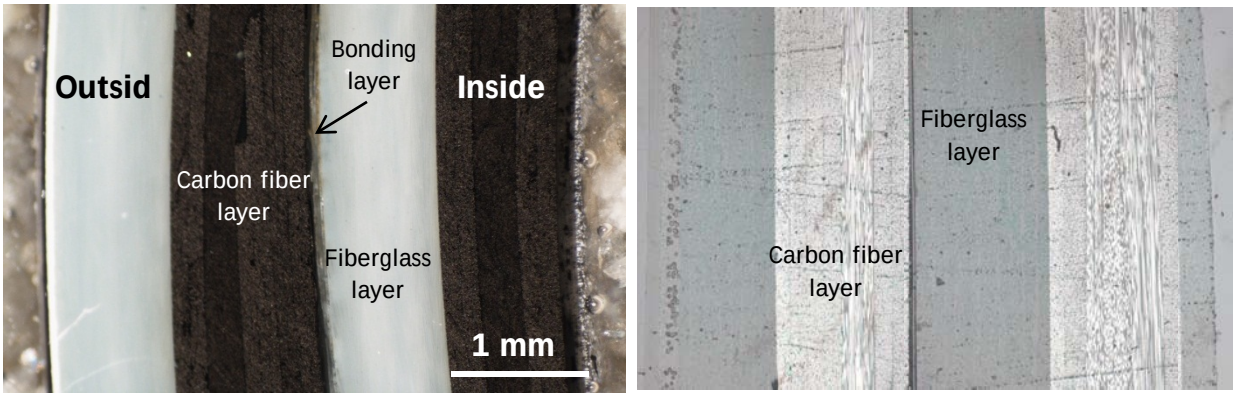

Figure 5: Bright field image of the Sample 1 barrel cross-section (left). Image on the right is from a thin section of the same sample. Thin section highlights the different orientations of the carbon fibers in the composite layers.

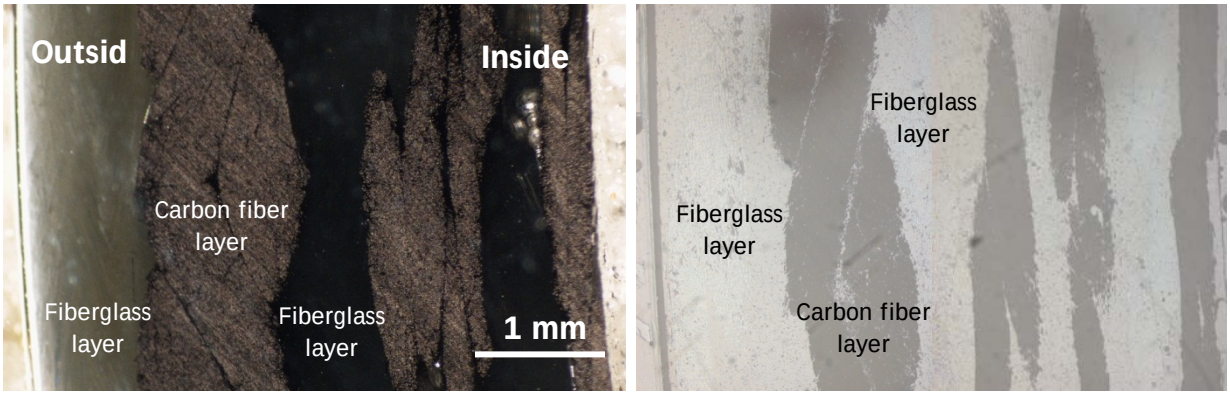

Figure 6: Bright field image of the Sample 2 barrel cross-section (left). Image on the right is from a thin section of the same sample. In this sample, fibers seem to be in braided sheets rather than in stacked layers.

4.2.2 Scanning Electron Microscopy (SEM)

Once the overall structures of the samples were obtained from the bright field LM images, the polished crossed-section samples were sputter coated with carbon and analyzed using SEM and energy dispersive x-ray spectrometry (EDS). SEM-EDS analysis confirmed the locations of different composite layers (carbon fiber layer and fiberglass layer) in each sample.

Sample 1 consisted of several types of layers:

- Carbon fiber layer (Figure 7a) – arranged in longitudinal (right) or circumferential (left) orientations
- Fiberglass layer (Figure 7b) – arranged in circumferential orientation
- Bonding layer (Figure 4) – bonding layer between two sets of composite layers
- Metallic layer (Figure 7c, arrow) – outer layer with micrometer sized metallic chips

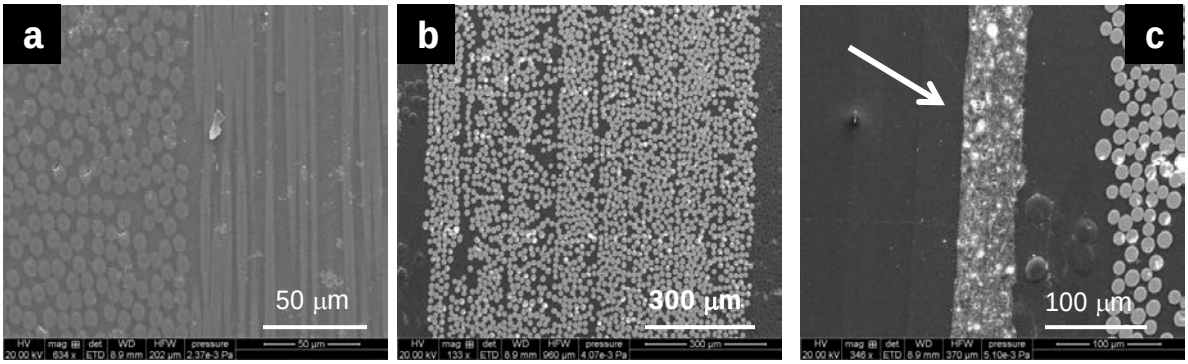

Figure 7: ESEM images of the Sample 1. (a) two different orientations of carbon fibers, (b) fiberglass layer and (c) metallic layer on the outside surface of the bat.

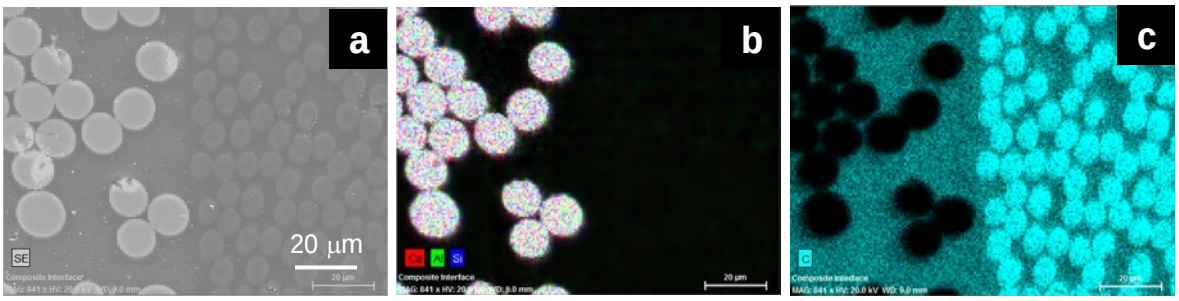

Figure 8: ESEM image (a) and corresponding X-ray maps of the fiberglass (b) and carbon fibers (c) in the Sample 1. Panel (b) is the Ca, Al, Si composite map of fiberglass (bright circles) and (c) is the carbon map showing the circumferential carbon fibers (cyan regions).

Sample 2 also consists of multiple layers but the layers are less clearly defined compared to the Sample 1:

- Carbon fiber layer (Figure 9a, central region with dark gray ovals) – arrangement of carbon fibers are less regular than those in the Sample 1.
- Fiberglass layer (Figure 9a, light gray ovals) - fiberglass bundles also show twisted/braided structure
- Metallic layer (Figure 9c, arrow) – outer layer with micrometer sized metallic chips

Carbon fiber layer consists of twisted layers of carbon fiber bundles. Fiberglass layer is also present but not as separate layers but as irregular bundles. This is shown in Figure 9.

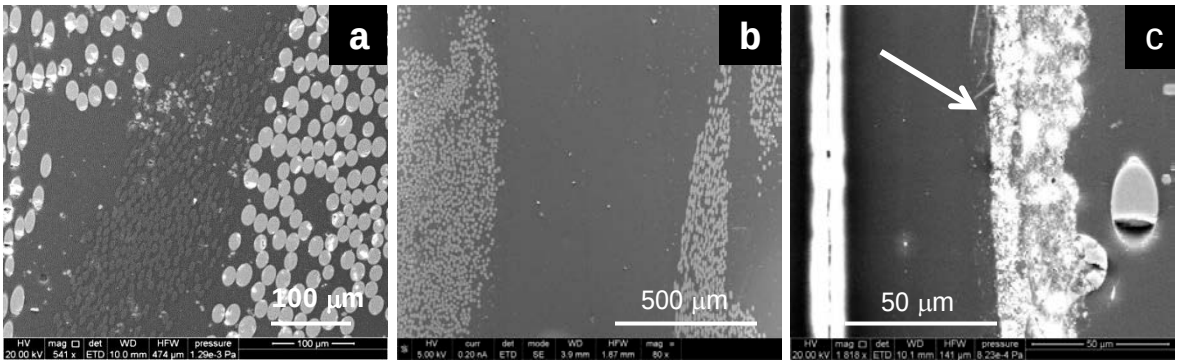

Figure 9: ESEM images of the Sample 2. (a & b) show that the carbon fiber (dark gray ovals) layer and the fiberglass (light gray ovals) layers are not cleanly separated and (c) shows the metallic layer on the outside surface of the bat.

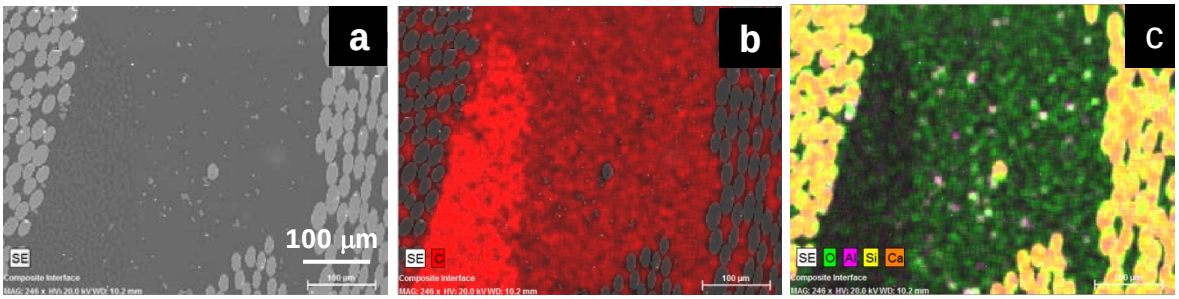

Figure 10: ESEM image (a) and corresponding X-ray maps of the carbon fibers (b) and fiberglass (c) in the Sample 2. (b) is the carbon map showing the location of the carbon fiber bundles (red) and (c) is the Al, Ca, Si, O composite map showing the fiberglass (bright yellow regions).

4.2.3 Focused Ion Beam Scanning Electron Microscopy (FIB SEM)

To confirm the presence of CNTs in the resin, high resolution SEM analysis of the resin filled regions between carbon fibers was performed on the polished cross-section samples. In a flat polished sample, the main contrast mechanism for an SEM image is the compositional variations within the sample. Since most polymer resins are highly carbonaceous, it was assumed that detecting CNTs in resin would be very challenging. However, we did expect to detect some of the surface exposed CNTs. SEM analysis of the samples did not show any CNTs in the resin around carbon fibers. One possible explanation is that the surface exposed CNTs are pulled out during the polishing step, making it difficult to detect CNTs in the polished surfaces.

FIB SEM is a technique where a focused ion beam is used to remove portions of a sample in a site specific manner. Nascent exposed sample surface can then be imaged and analyzed using the electron beam as in a traditional SEM. Figure 11 shows the schematic of a FIB SEM chamber and a commonly adopted sample orientation.

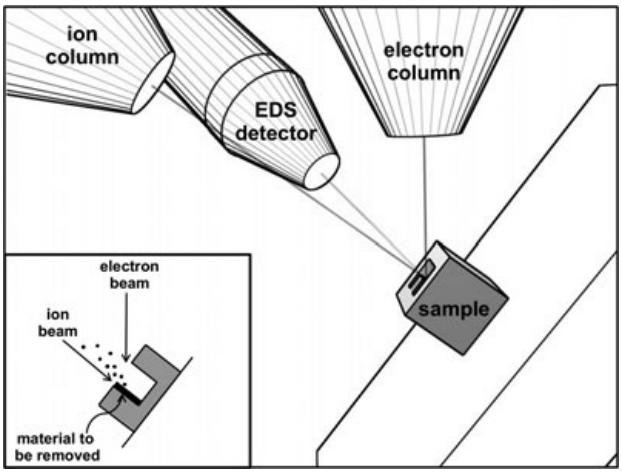

Figure 11: Schematic of a FIB SEM chamber. Inset is the schematic of material removal by ion beam. (*from J.Microsc. (2011) 242, 86-93*)

As shown in Figure 11, FIB SEM allows the examination of the internal structure of a sample that has not been affected by mechanical polishing. Pristine sections of carbon fiber layer were exposed using FIB milling and examined for the presence of CNTs. Again, CNTs were not detectable in any of the SEM images although other nanometer sized features such as silicon containing particles shown in Figure 12 were detected in both bat samples.

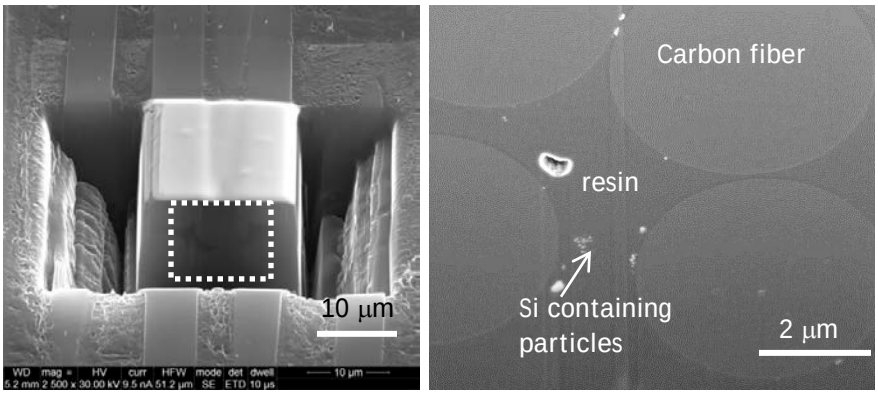

Figure 12: Left panel shows the FIB milled sample geometry. White dashed rectangle marks the newly exposed analysis face that is imaged. Right panel shows a typical high resolution image of the FIB milled carbon fiber region. Large circular features are the carbon fibers (cross-sectional view) and the darker region between the fibers is the resin. EDS analysis showed that the bright particulate features were silicon containing particles and were present in both bat samples.

TEM thin sections were also created from these carbon fiber regions of both samples. Figure 13 shows the SEM images of the TEM thin sections from the Sample 1 and the Sample 2, respectively.

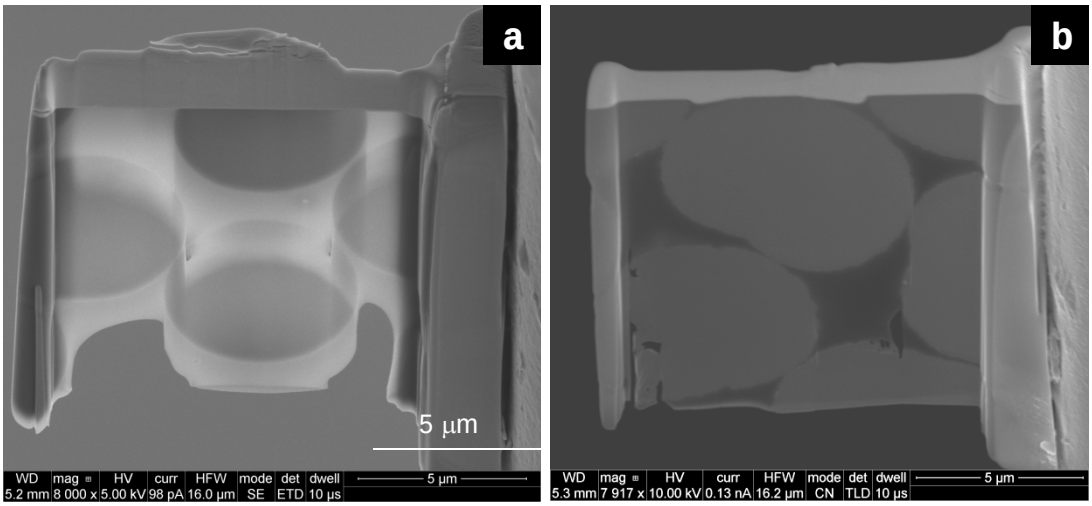

Figure 13: TEM samples from the Sample 1 (a) and the Sample 2 (b).

4.2.4 Transmission Electron Microscopy (TEM) FIB Prepared Thin Sections

Bright field TEM images and the EELS analysis of the FIB prepared thin sections from the carbon fiber regions did not show any CNTs.

4.2.5 Raman Analysis

Raman spectroscopy was also performed on the Sample 1 and the Sample 2. Preliminary analysis was done using a 633 nm excitation beam. Figure 14 shows a spectrum from one of the carbon fibers in the Sample 1. Two main peaks on the right are most likely from the amorphous carbon in the fiber. Figure 15 was collected from the resin area between carbon fibers in the Sample 1. Because the probe used for this analysis was relatively large (several micrometers in diameter), the Raman spectrum shows contributions from the carbon fiber as well as several sharp peaks that represent CNTs.

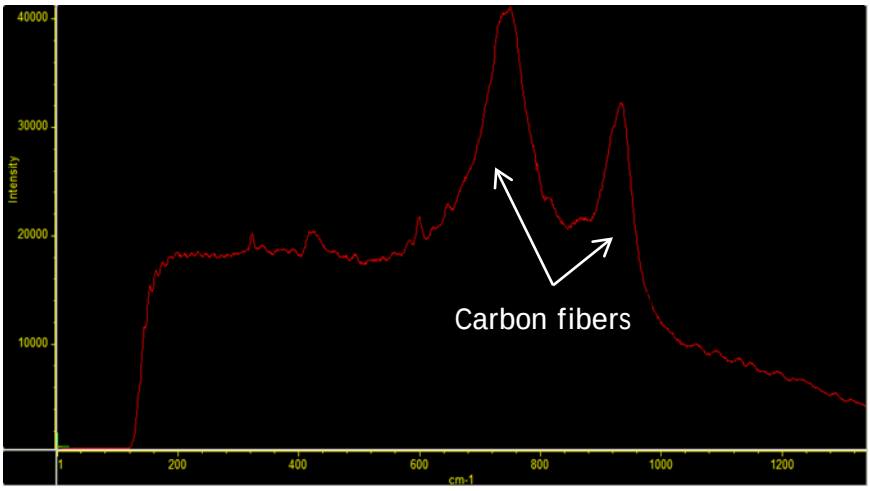

Figure 14: Raman spectrum from the carbon fiber of the Sample 1.

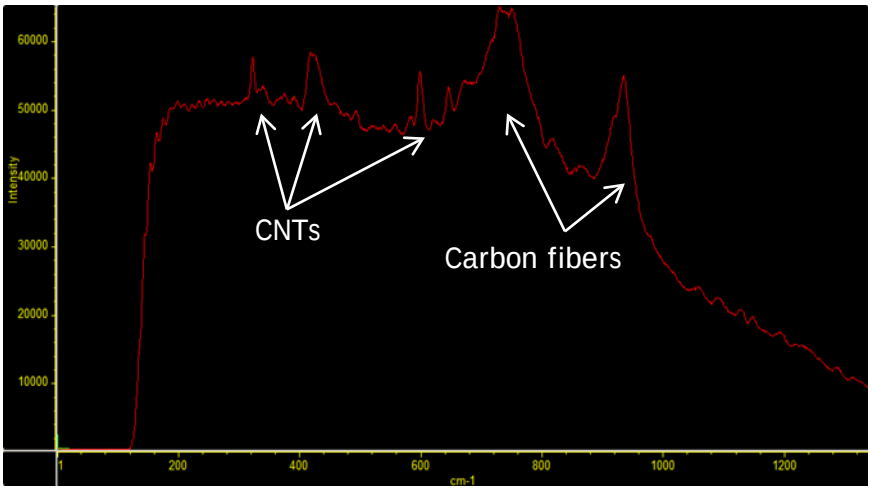

Figure 15: Raman spectrum from the resin area of the carbon fiber region of the Sample 1.

Raman spectra from the Sample 2 show similar results. Carbon fibers show broad but clear peaks around wavenumbers 750 cm^{-1} and 900 cm^{-1} while the resin around the carbon fibers show several narrower peaks between 200 cm^{-1} and 700 cm^{-1}.

4.3 Detection of CNTs in Released Material

Two different types of release particles were collected.

1. Sawdust from cutting up the bats
2. Particles released from cutting and shredding of bat pieces

4.3.1 Scanning Electron Microscopy (SEM)

For the SEM analysis, commonly used 10 mm SEM stub with double-sided carbon tape was used to collect the particle samples from the sawdust accumulated in the glove bags (See Sample Preparation section) or the inside surface of the glove bags. Particles and the dust from the cutting and shredding operation were collected by placing the sample stub on a clean surface and cutting or shredding bat pieces directly over the sample stub. Each sample stub was lightly sputter coated with carbon to avoid charging during the SEM analysis.

4.3.1.1. Control Stub

Two blank stubs were prepared with double-sided carbon tape and left in the open laboratory condition for 24 hours. One stub was carbon coated using the same sputter coating settings used by all other SEM samples. One stub was left uncoated.

Figure 15 shows a typical surface of the carbon coated stub and Figure 16 shows some of the particles collected on the control stub with carbon coating. Although most of the stub surface is clean, there were occasional micrometer and even nanometer sized particles and features. None of the nanometer sized particles resembled fine particles released from the bats.

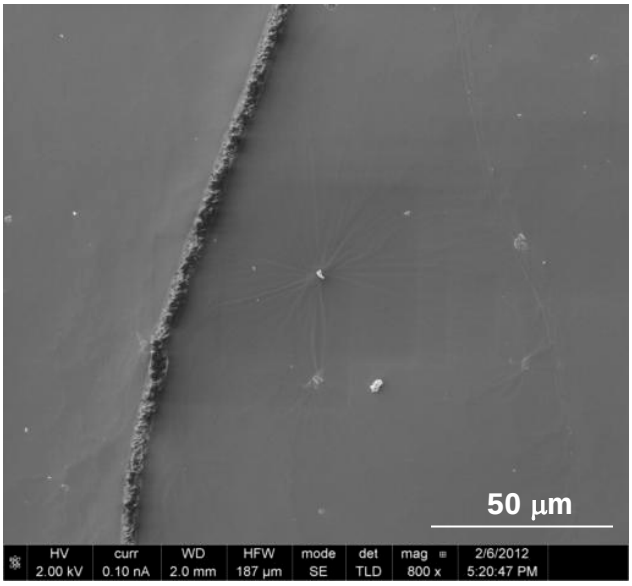

Figure 15: Typical carbon coated blank stub surface. Large vertical feature in the image is the crack that was formed on the adhesive layer. The stub showed a network of these cracks all over the surface.

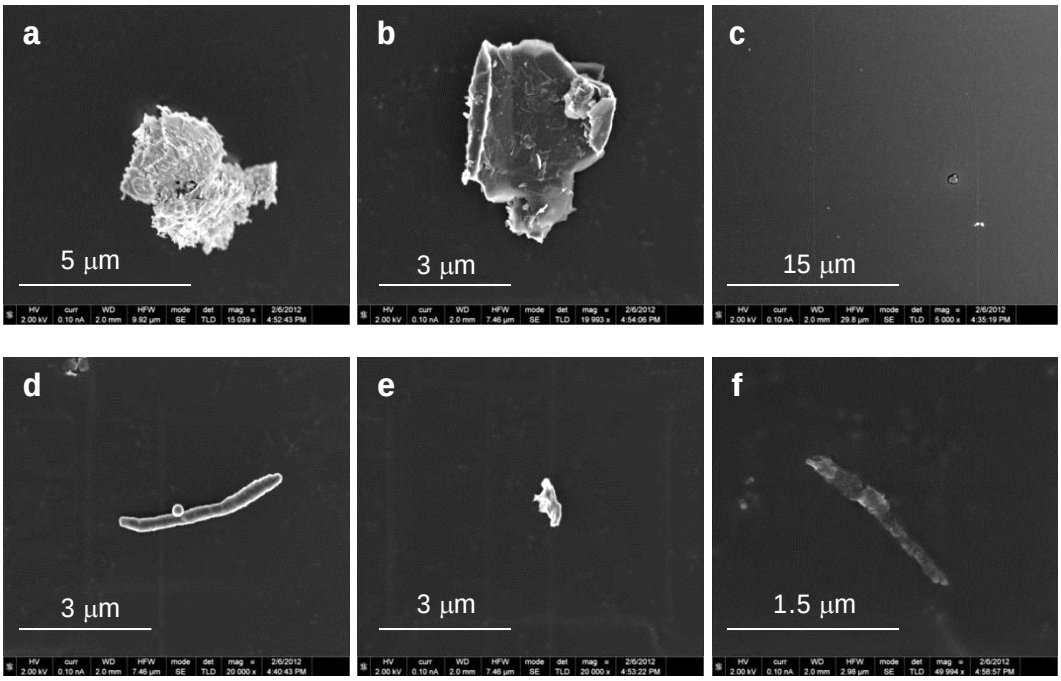

Figure 16: Typical particles detected on the carbon coated blank stub. (f) is a surface feature that can easily be mistaken for a particle.

Uncoated blank stub had almost no particles on it.

4.3.1.2. Sample 1

Samples of the sawdust, fine particles from inside the glove bag, cutting debris and fine particles from cutting/shredding were analyzed.

Sawdust

Figure 17 shows typical sawdust particles. Most of the particles are hundreds of micrometers in size and consist of various components of the composite material.

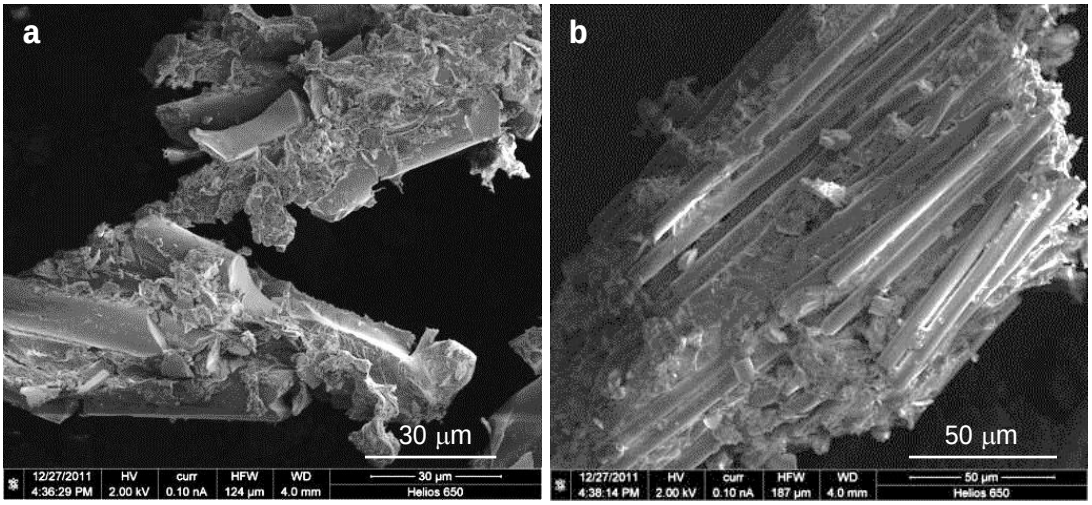

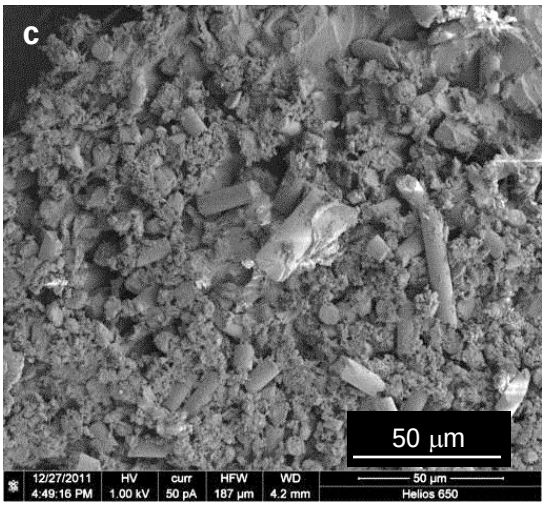

Figure 17: Typical sawdust particles. (a)resin and fiberglass, (b) resin and carbon fibers and (c) matted chunks of resin material.

Cutting Debris

Although the morphology of the cut particles was very similar to that of the saw dust particles, sample loading was much lighter with cutting debris. This made it easier to control the charging problem and we were able to perform high resolution analysis of the cut particles. Figure 18 shows the details of the large particles typically seen in the sawdust and the cutting debris. Figure 18a shows a carbon fiber bundle that came loose. In a typical bundle, fibers are held together with polymer resin and this can be seen in Figures 18b and 18e. When the material is cut or torn apart, resin between the fibers can come off as shown in Figure 18 c. In some cases, fibrous features were seen between resin pieces (Figure 18d) but whether these are CNTs covered in resin is not clear based on SEM imaging alone. Figures 18d and 18f show features similar to those seen in Zyvex™ product literature (see Figures A3, A4 and A5). Based on these similarities, the small fibrous protrusions could be CNT bundles covered in resin, but we cannot confirm this based on the SEM images.

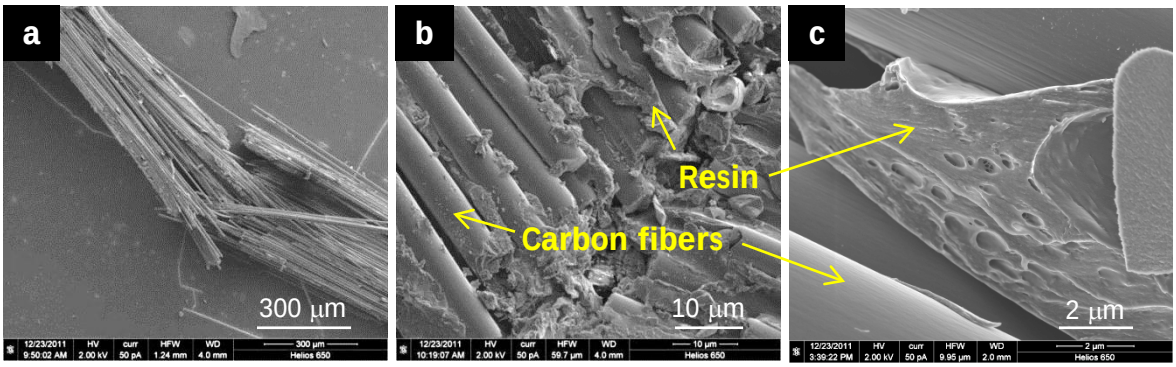

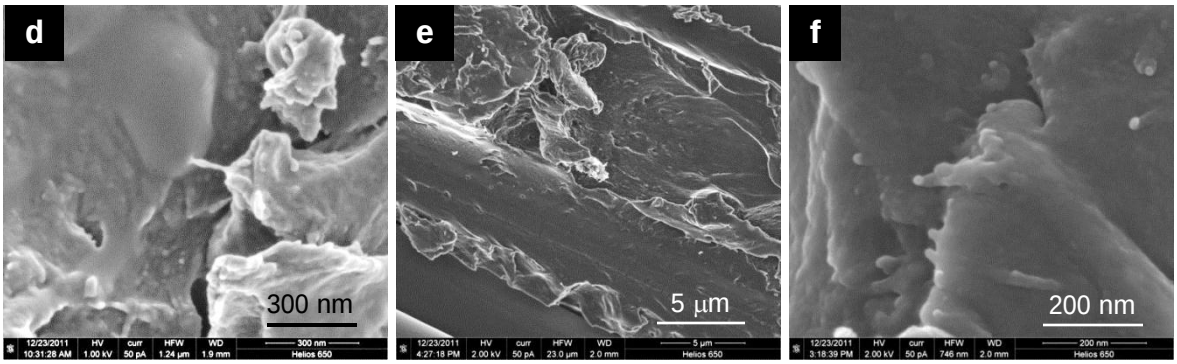

Figure 18: Typical cut particles from the Sample 1.

Several of these large particles were decorated with nano-sized features. Figure 19 shows several of these nano-sized decorations. Figure 19a and 19c show aggregates of roughly cylindrical particles with ~20 nm diameter. There were larger aggregates of similar particles as well. These short cylinders could be shortened CNTs covered in resin. Although most CNT nanocomposites use long carbon nano fibers (CNFs) as nanofillers, depending on the manufacturing process used, CNFs can be broken into shorter pieces. In Figures 19b and 19e, thin tube like features can be seen. These features are reminiscent of fibers seen in the Zyvex™ literature. The diameters of these features are mostly in the range of 10 nm to 20 nm. Figure 19e shows another common type of particles that looks like a crumpled up graphene sheet.

Figures 19f – 19k show more traditional bare nanotube shaped decorations – long thin straight tubes. Figure 19l is a close up of Figure 19k. Some of these decorations seemed to be loosely attached to the larger particle surface and others seemed to be protruding out of the surface. Most had diameters of about 10 nm and some were as long as 1 μm or more.

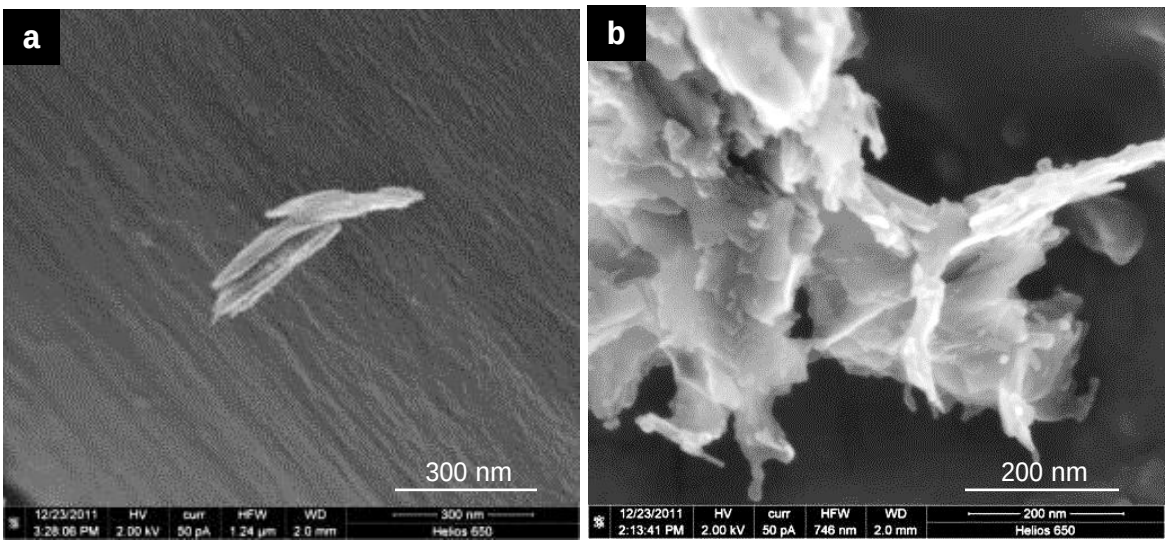

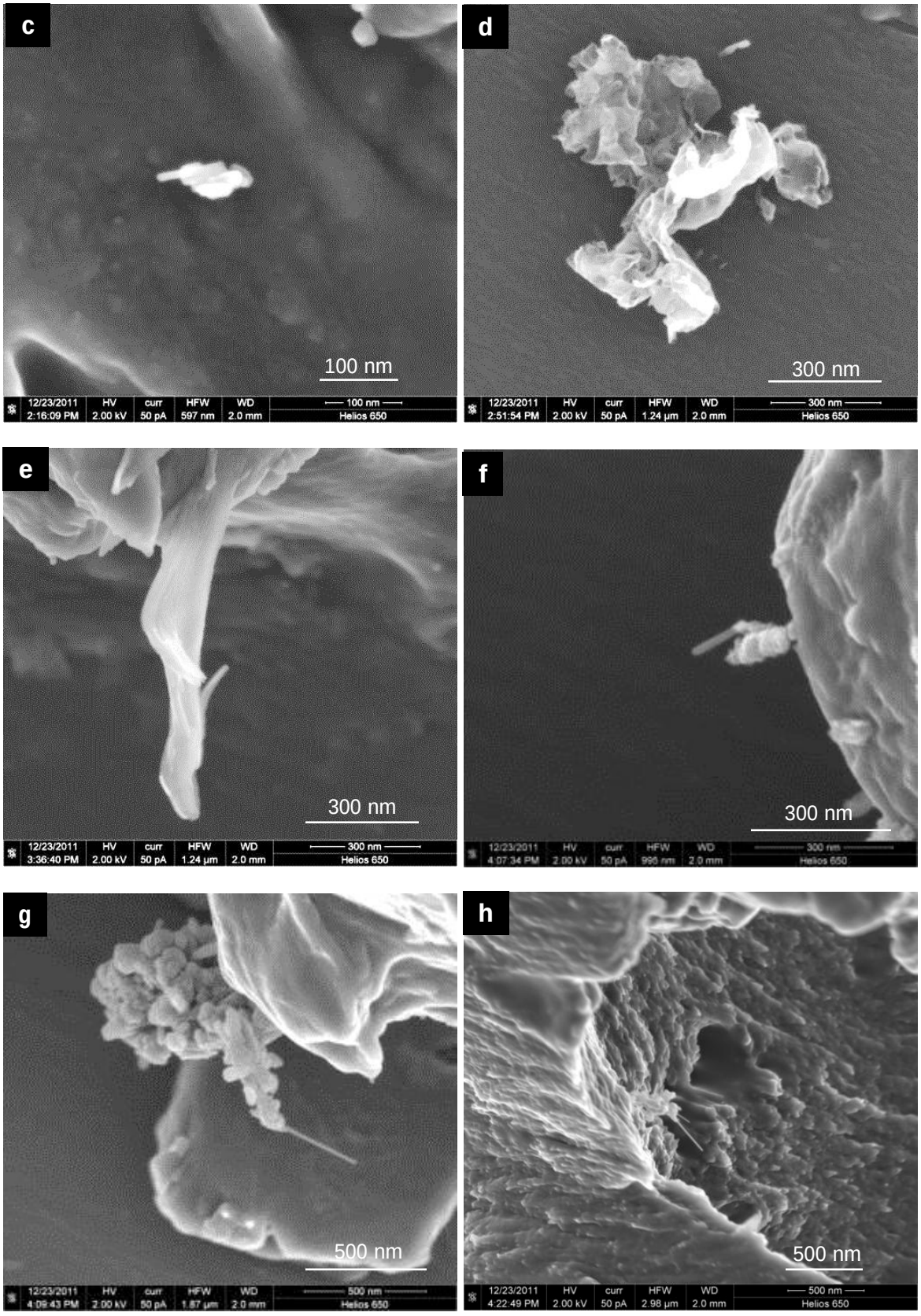
c
100 nm
12/23/2011 2:16:09 PM HV 2.00 kV curr 50 pA HFW 597 nm WD 2.0 mm 100 nm Helios 650
d
300 nm
12/23/2011 2:51:54 PM HV 2.00 kV curr 50 pA HFW 1.24 µm WD 2.0 mm 300 nm Helios 650
e
300 nm
12/23/2011 3:36:40 PM HV 2.00 kV curr 50 pA HFW 1.24 µm WD 2.0 mm 300 nm Helios 650
f
300 nm
12/23/2011 4:07:34 PM HV 2.00 kV curr 50 pA HFW 996 nm WD 2.0 mm 300 nm Helios 650
g
500 nm
12/23/2011 4:09:43 PM HV 2.00 kV curr 50 pA HFW 1.87 µm WD 2.0 mm 500 nm Helios 650
h
500 nm
12/23/2011 4:22:49 PM HV 2.00 kV curr 50 pA HFW 2.98 µm WD 2.0 mm 500 nm Helios 650

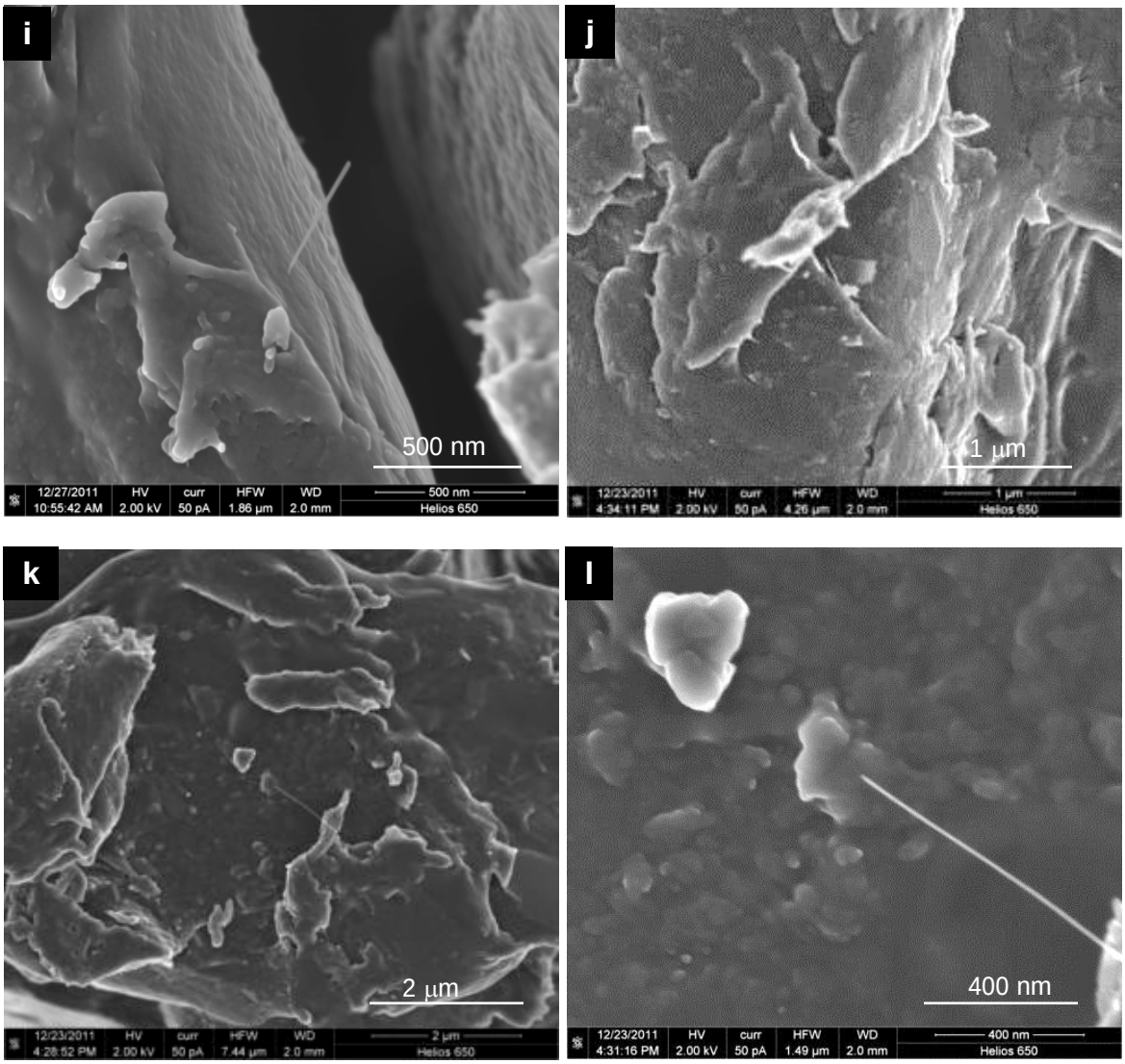

Figure 19: Nano-sized decorations attached to larger particles/chunks (Sample 1).

Although we were able to detect bare CNT-like particles (Figures 19f-19k), they were not very common. Over the entire sample stub, we were able to identify about a dozen of these particles. There were many more particles that looked like particles shown in Figures 19a – 19e.

Fine Particles

Fine particles collected from the inside of the glove bag and the cutting operation both showed similar morphology. Figure 20 shows several types of nanoparticles found in the fine particle sample stubs. There were mainly two types of particles that looked like CNTs. One type was a straight, high aspect ratio rod-like particle with occasional bends or changes in the diameter (Figures 20d – 20k). The other type looked more like a resin covered CNT where the resin formed a flexible casing around the CNT (Figures 20a - 20c). For the lack of a better term, we will call these nano-casings in this report. Both the nano-rods and nano-casings

occurred singly and as aggregates. Sometimes they showed up complexed with other materials (Figures 20c, 20g and 20k).

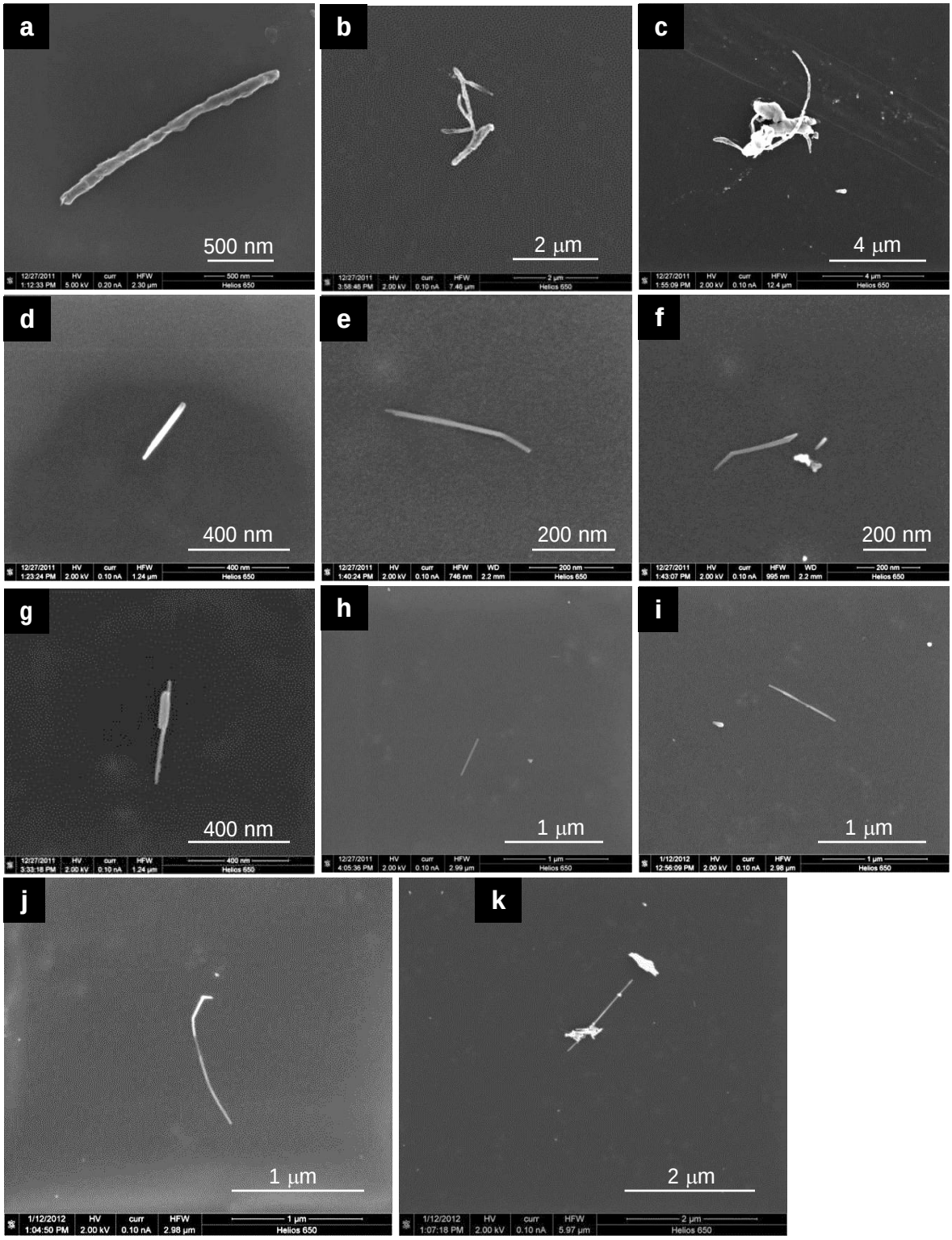

Figure 20: Nanoparticles found from fine particle sample stubs (Sample 1).

Fine Particles on TEM Grids

Although many particles found on the SEM stubs do look like CNTs, we could not confirm that the particles were indeed CNTs since the hollow center/multi-wall structure was not visible in the SEM images. TEM or STEM (scanning transmission electron microscopy) analysis was needed to confirm that these particles are CNTs. TEM samples were collected by placing several Cu TEM grids with holey carbon film on a clean surface and cutting the bat pieces immediately above the grids (dusting method). A control TEM grid was also prepared by leaving a clean grid out in the open lab environment for 24 hours. All TEM grids were lightly sputter coated with carbon to minimize charging.

Because the field of view in TEM is extremely limited, the most efficient way to perform TEM analysis is to identify the exact locations of the nanoparticles of interest on the grid using SEM and then perform the TEM analysis of these specific nanoparticles.

Figure 20 shows images from the control grid. There were some tears and holes in the holey carbon film (c) but no particles were detected on the control grid.

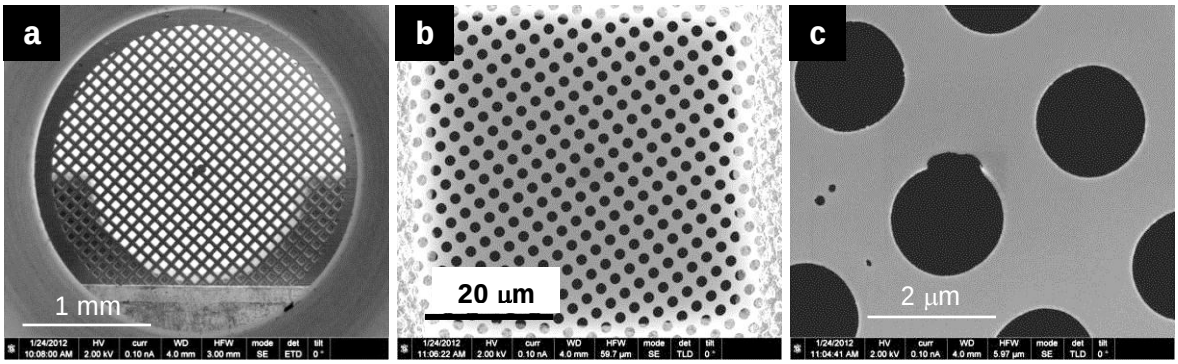

Figure 20: Control grid. (a) grid overview, (b) one of the grid square covered with holey carbon film and (c) occassional tears and holes in the carbon film.

The collection efficiency of our particle depositing method was found to be extremely poor. Although we were able to detect many bare CNT-like particles as well as other nanometer and micrometer size particles on the SEM stubs with carbon tape, very few particles of any size were deposited onto the TEM grid from the dusting method described earlier.

Figure 21 shows one of the TEM grid squares with deposited nanoparticles. Average particle loading per grid square was somewhat lower than what is shown here. To quickly locate the nanoparticles during TEM analysis, each grid square coordinate was noted and specific particle location within the grid square was noted using navigational aids shown in this figure.

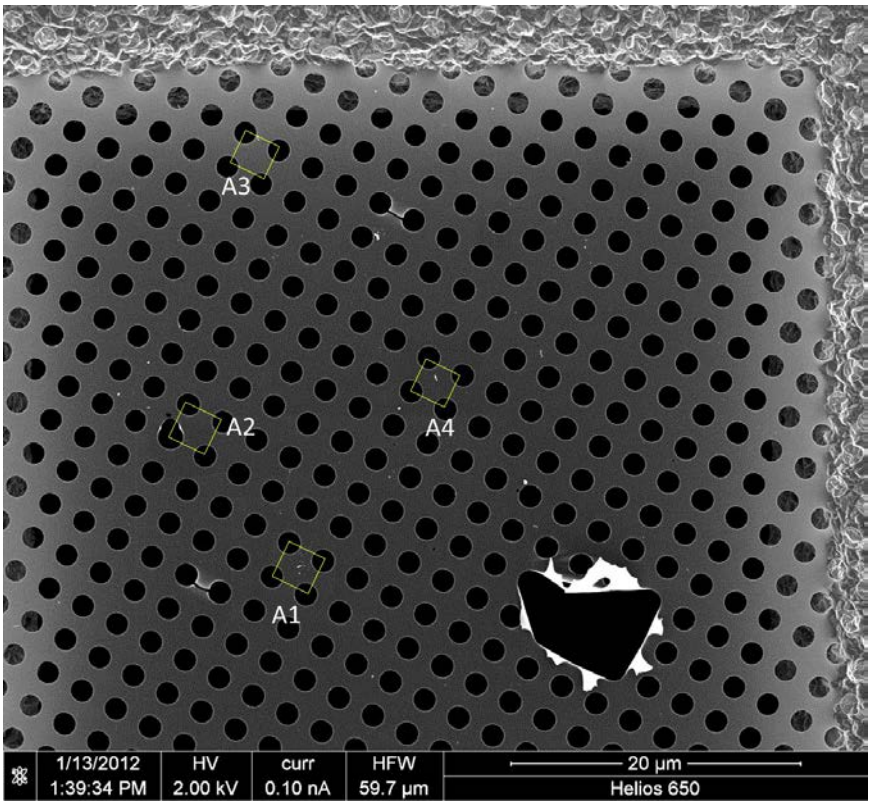

Figure 21: An overview image of one of the grid squares containing several nanoparticles. Small yellow squares mark locations of possible CNTs that should be analyzed further.

Figure 22 shows a set of high resolution images that correspond to the areas marked with yellow squares shown in Figure 21 and others like them. For example, Figure 22a corresponds to the area A1 in Figure 21. Most nano-rods were 10 nm to 20 nm in diameter and their lengths ranged from a few hundred nanometers to more than one micrometer. Nano-casings were more variable in their sizes. Some had similar sizes as nano-rods while others were several hundred nanometers in diameter.

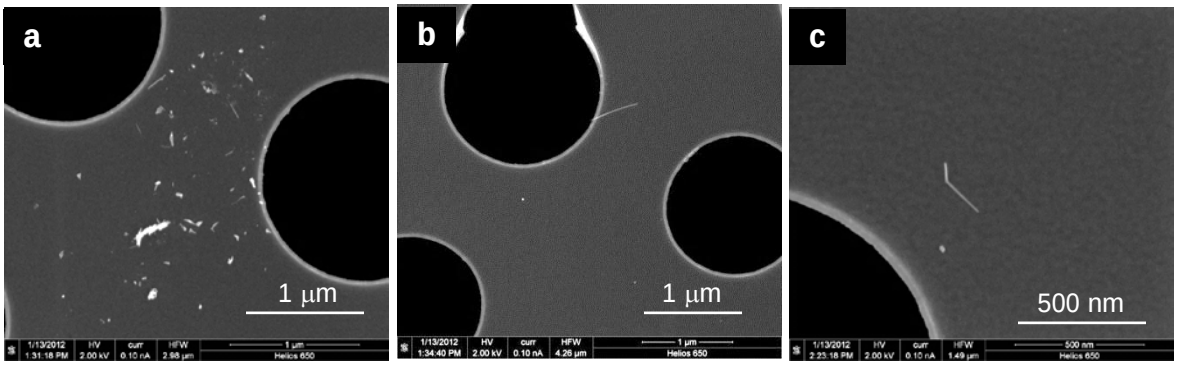

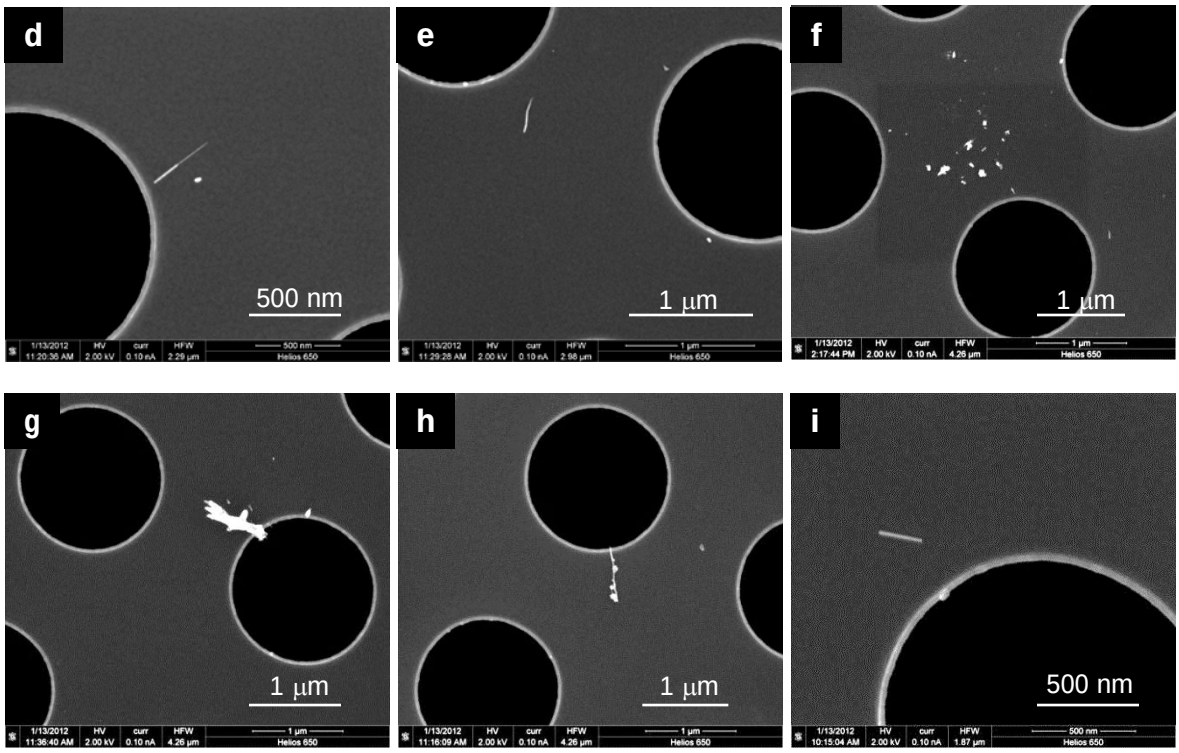

Figure 22: Nanoparticles from the cutting debris (Sample 1).

Comparing the number and the types of particles captured on the SEM stubs to those deposited on the TEM grids, it was clear that we were only collecting a fraction of the released particles using the dusting method. Several different types of functionalized and charged TEM grids were also tried to increase the collection efficiency without much success.

4.3.1.3. Sample 2

Sawdust

Figure 23 shows typical sawdust particles from Sample 2. As in Sample 1, most of the particles were hundreds of micrometers or greater in size and consisted of several different materials – resin, carbon fibers, fiberglass, paint chips, etc. The crisscross pattern of the resin on the carbon fibers indicated that the different layers of carbon fibers were oriented at an angle from each other (Figure 23a). This agrees with the braided or woven pattern seen in the low resolution images of the carbon fiber layers (Figure 6). While the carbon fibers in the Sample 1 had smooth surfaces, the carbon fibers in the Sample 2 were covered with longitudinal ridges (Figure 23b).

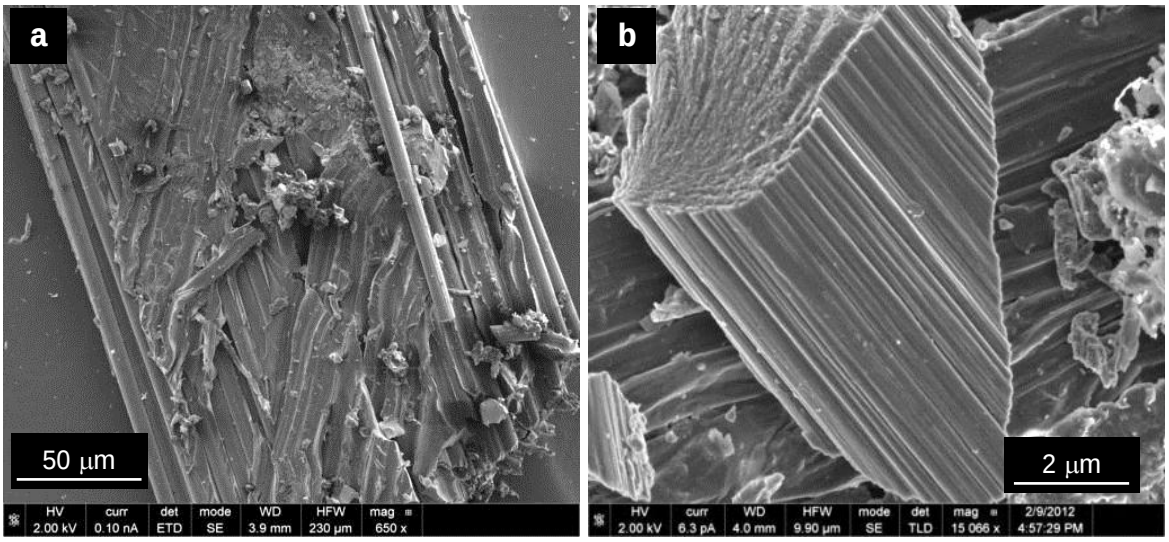

Figure 23: Typical saw dust particles from the Sample 2.

Cutting Debris

Several different types of particles and particle aggregates were found in the cutting debris from the Sample 2 (Figure 24). There were the expected carbon fiber-resin chunks (Figures 24a – 24c) and fiberglass-resin chunks (Figure 24d – note the differences in the fiber diameters and the smoothness of the fiberglass surface compared to the carbon fibers). Two other types of particle aggregates commonly seen were the aggregates of flake like particles (Figure 24e) and the dendritic aggregates with fine particles (Figure 24f). Figure 24g shows a thin layer of resin on a carbon fiber where some of the fibrous network in the resin (yellow oval) is visible. Also found in some of the carbon fibers are fibrous protrusions and loosely attached nano-sized fibers (Figures 24g – 24i). Both the fibrous network and the nano-sized fibers could be resin covered CNTs.

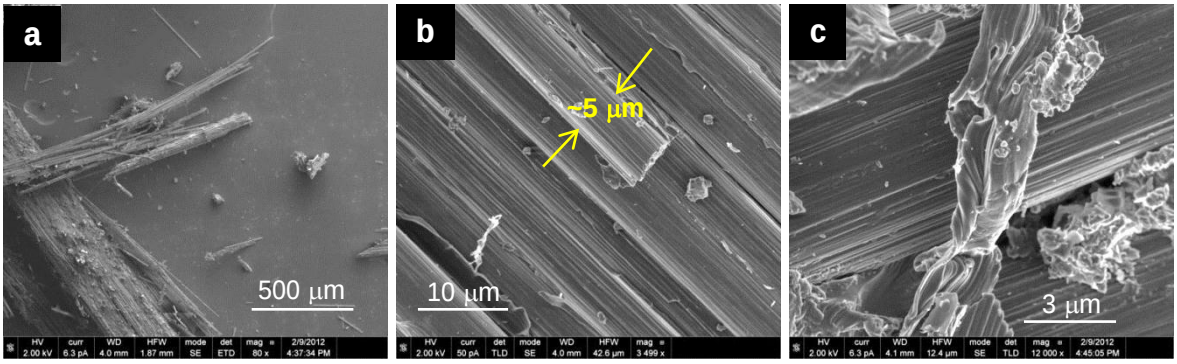

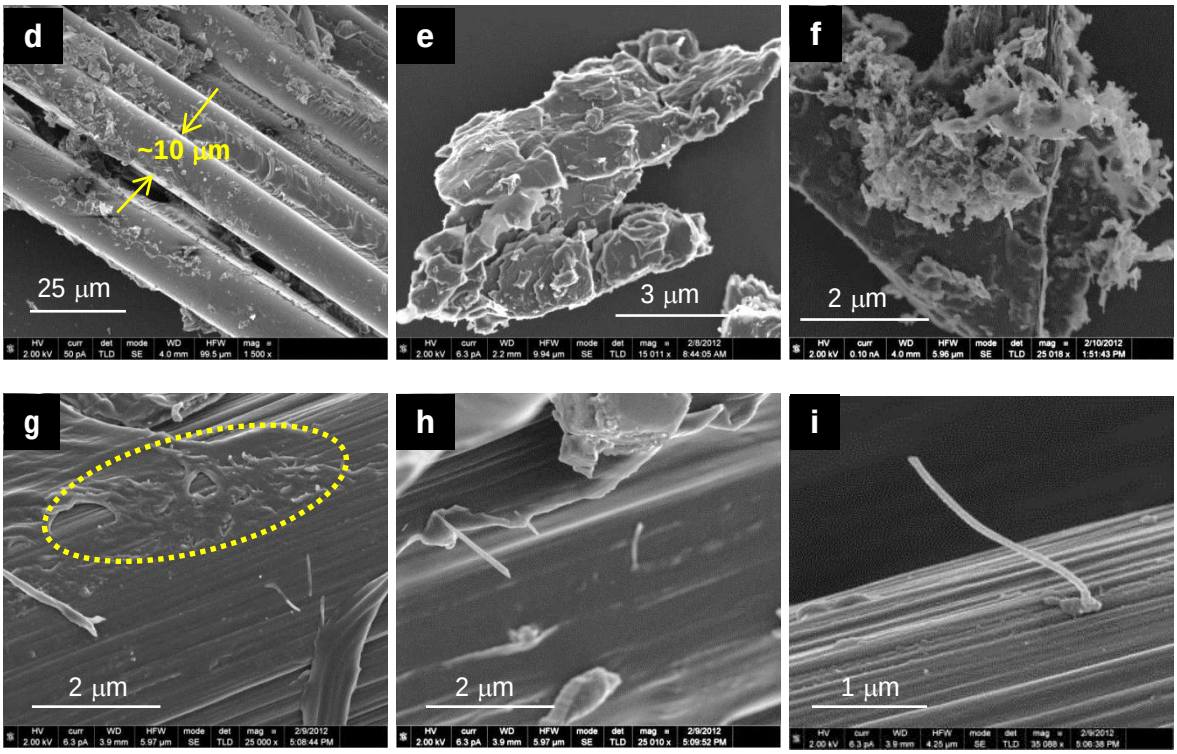

Figure 24: Particles from the cutting debris (Sample 2).

Fine Particles

Fine particles collected from the inside of the glove bag and from the cutting operation are shown in Figure 25. Several different types of nano-sized particles were found – dendritic aggregates of rounded particles and nano-rods (Figure 25a and 25c), aggregates of flake-like particles (Figure 25b and 25f), nano-casings (Figure 25d) and crumpled up graphene sheet-like particles (Figure 25e). In this sample, individual nano-rods were not found but nano-rods similar to those found in the Sample 1 were often seen complexed with other nano-sized particles (Figure 25a and 25c). Figure 26 is a higher resolution image of one of the dendritic aggregates clearly showing multiple nano-rods complexed with grain-like nanoparticles.

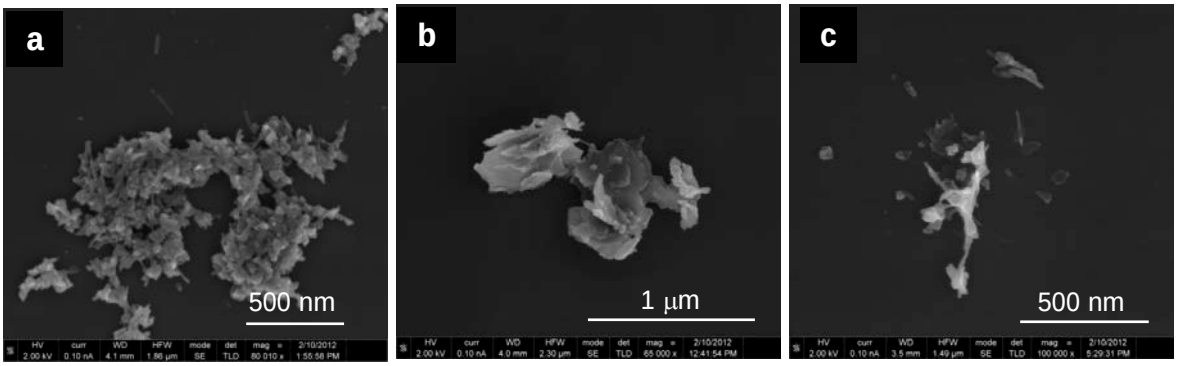

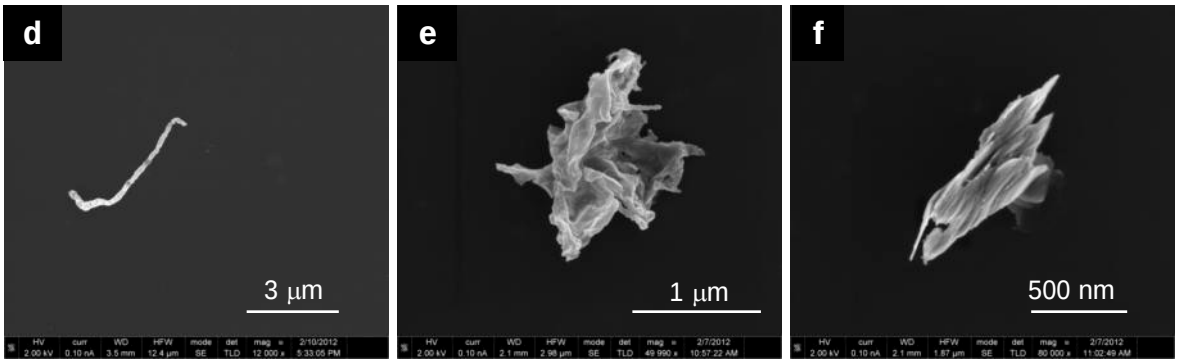

Figure 25: Fine particles collected from the Sample 2.

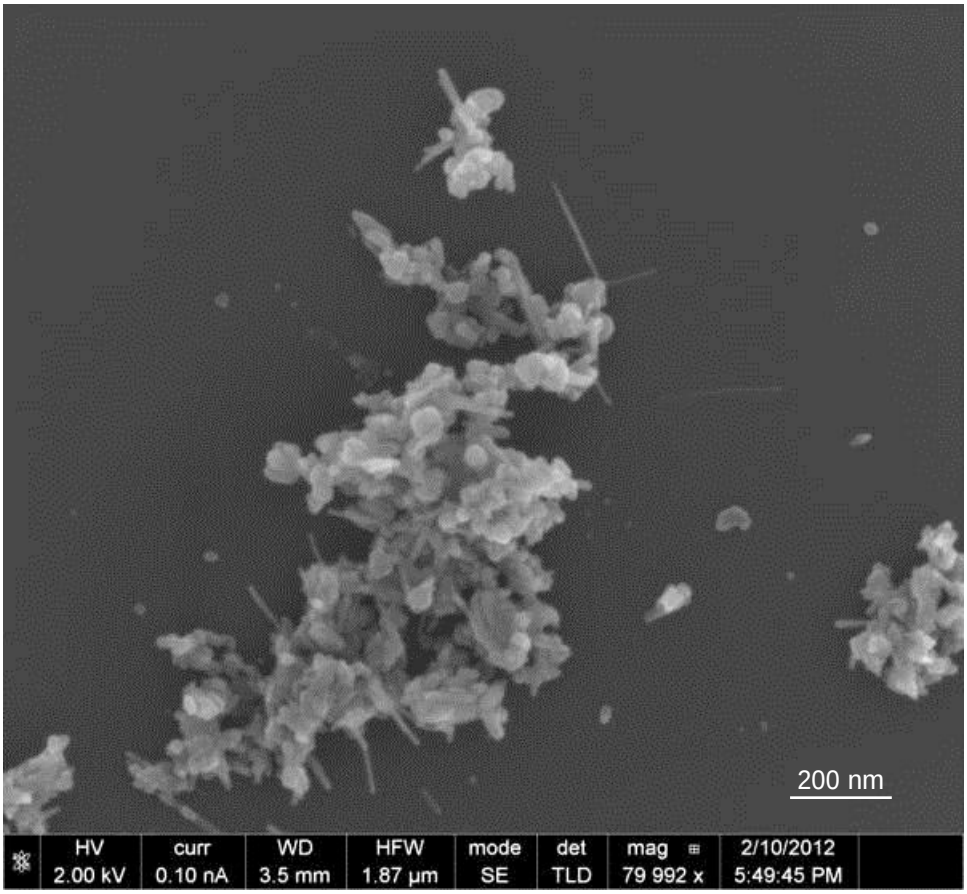

Figure 26: High resolution view of one of the dendritic aggregates clearly showing the rounded particles and the nano-rods.

Fine Particles on TEM Grids

Fine particles were deposited on TEM grids using the same dusting method used for the Sample 1. However, the collection efficiency was extremely low as before and we were unable to find any nano-rod like particles on these TEM grid samples. An active sampling approach may be needed to achieve the necessary collection efficiency for further analysis.

4.3.2 Transmission Electron Microscopy (TEM)

To confirm that the nano-rods and nano-casings found during the SEM analysis are CNTs, TEM analysis of the fine particles were performed. Only the particles from the Sample 1 were analyzed due to the problems in the sampling methods.

Figure 27 shows one of the nano-casings. The light gray background patterning in the TEM image (Figure 27b) is from the carbon film. Nominal thickness of the carbon film on the Cu TEM grid is 10 nm to 20 nm according to the product literature. This background noise from the film layer made clear imaging of the nanoparticles challenging. Ideally, the nanoparticle sample should be hanging over a hole in the carbon film so that there is no interfering substrate underneath the sample. But due to the low collection efficiency and the small size of the particles compared to the size of the holes (1.2 μm), most of the particles found on the TEM grids were on the carbon film rather than hanging over the edge of the holes. Although somewhat noisy, even in a low resolution bright field (BF) TEM image shown here, the tube like structure of the particle was apparent.

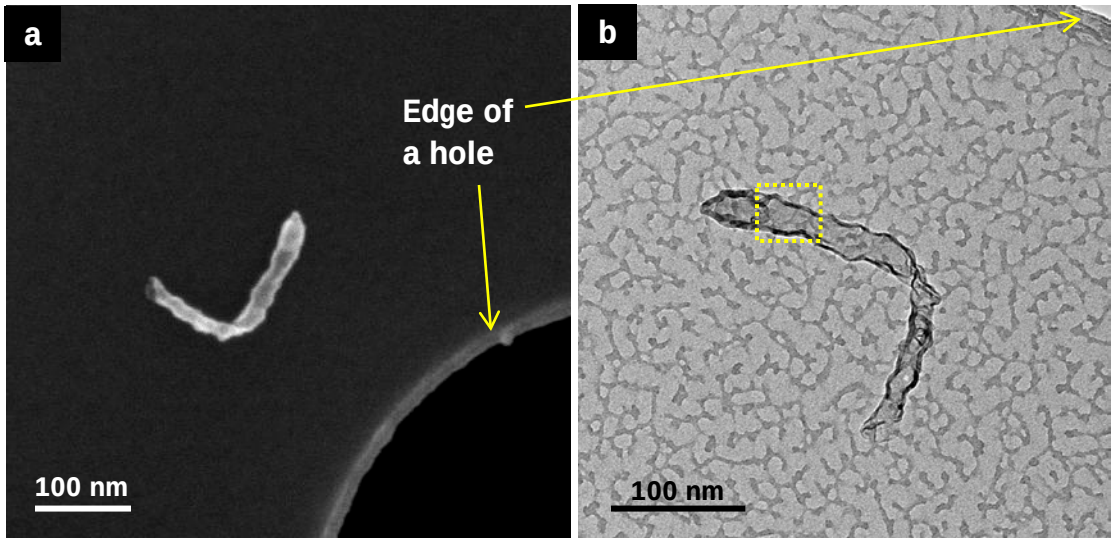

Figure 27: SEM (a) and BF TEM (b) images of a nano-casing. The yellow rectangular region in (b) denotes the region of the particle shown in Figure 28.

Figure 28 shows the high resolution (HR) TEM image of a section of the nano-casing shown in Figure 27. Again, the carbon film underneath the nano-casing makes it hard to see the multi-wall structure of the nano-casing. A close up image of the wall (Figure 28b) shows the multi-wall structure more clearly. Although the nano-casing exhibited the multi-walled structure of a carbon nanotube, it did not have the clean straight edge that classic MWCNTs exhibit. A closer examination of the wall structure showed that the nano-casing had many overlapping multi-layers.

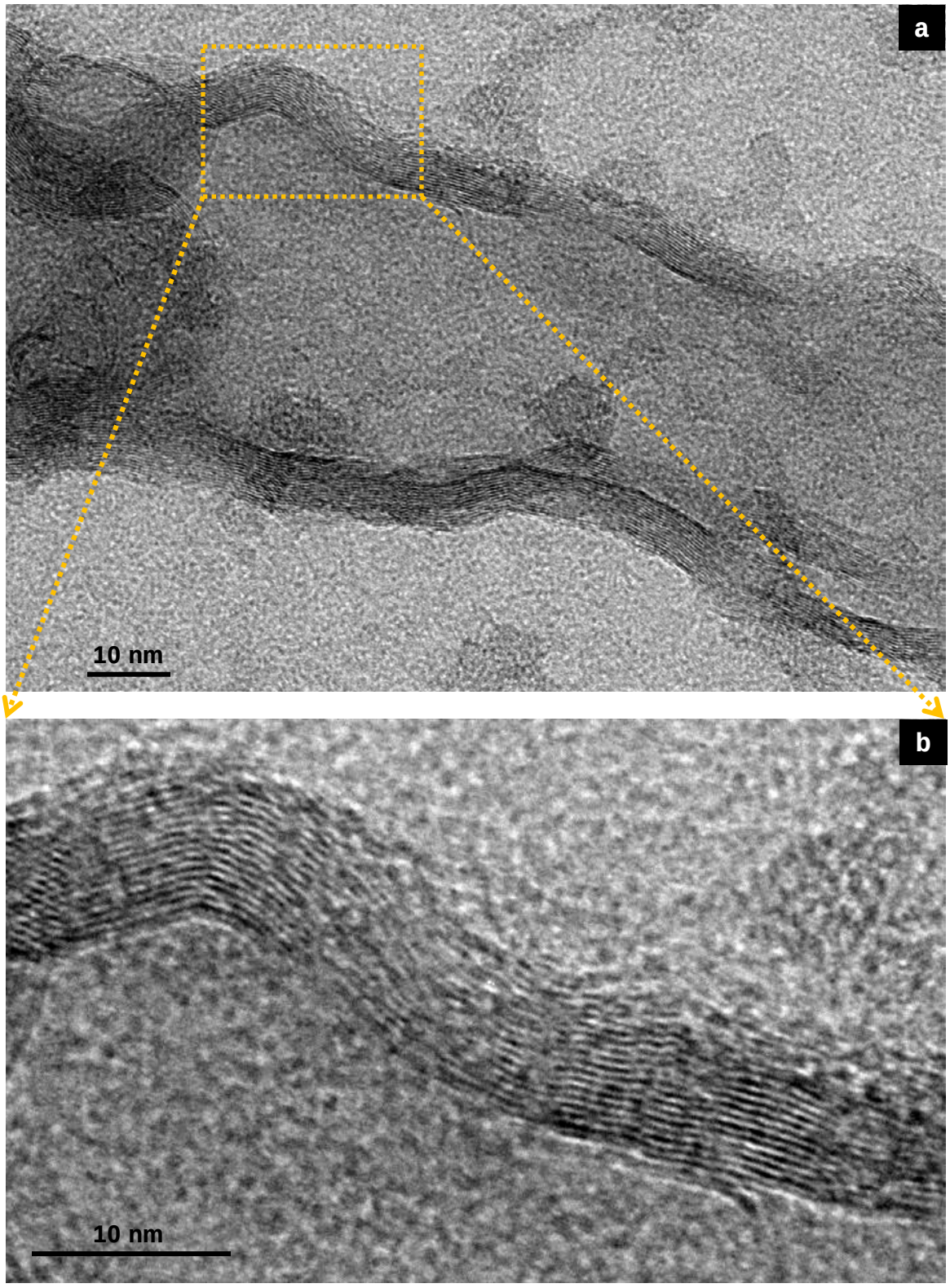

Figure 28: HR TEM images of a section of the nano-casing shown in Figure 27. (b) is a magnified view of the dashed rectangular region marked in (a).

Figure 29 shows an aggregate particle. In the SEM image (Figure 29a) the particle looks like an aggregate of short rod like particles. But the BF TEM image (Figure 29b) shows that the aggregate could be a single long tube that was folded up.

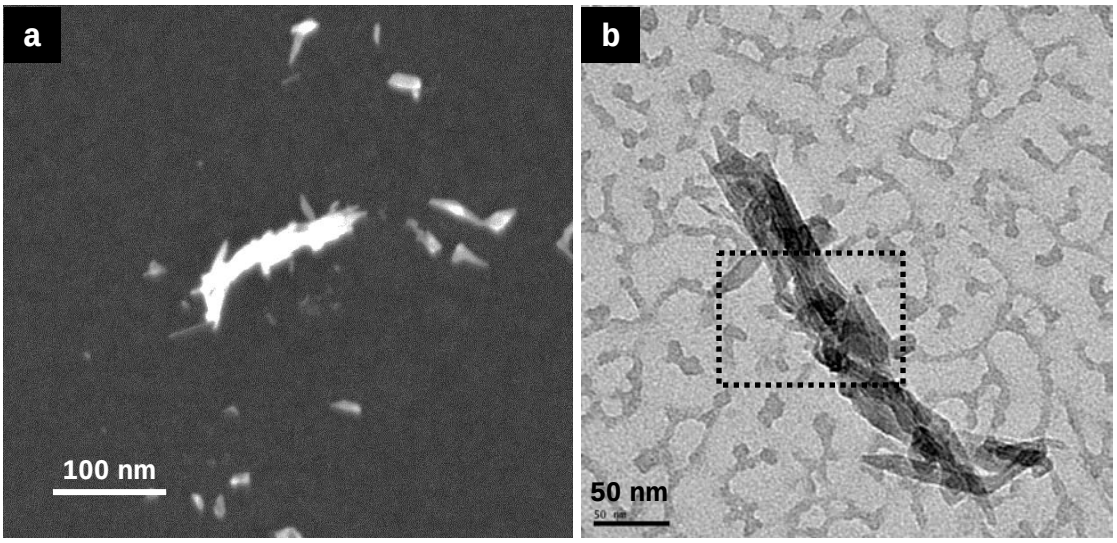

Figure 29: SEM (a) and BF TEM (b) images of an aggregate particle. Dashed rectangle in (b) marks the section of the particles shown in Figure 30.

Figure 30 is a HR TEM image of a section of the folded tube. Although the multiple layers forming the particle wall were easily discernible, the hollow center (tube structure) of the particle was difficult to see. Yellow rectangles in Figure 30a mark the locations of the close up views shown in Figures 30b and 30c. Figure 30b shows a hollow core surrounded by multiple walls. Overlapping structures resulting from the particle's complicated folds made it difficult to distinguish different sections of the nanotube structure and the hollow center/multi-wall structure shown the Figure 30b was not uniformly visible in this particle. Also, in some sections of the particle there was no discernible hollow core – probably due to a very small center opening. Folds in the tube are more apparent in another close up view of the particle (Figure 30c).

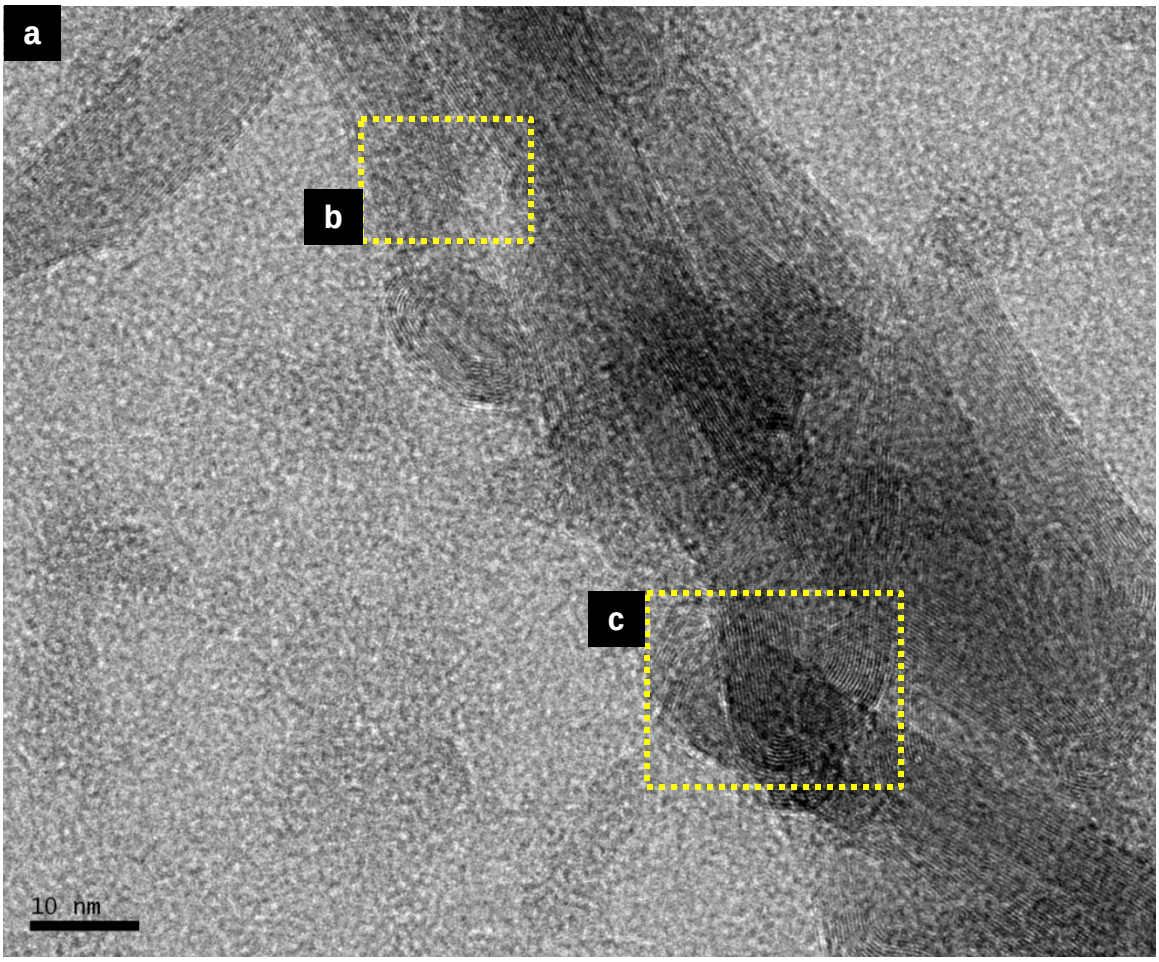
a
b
c
10 nm

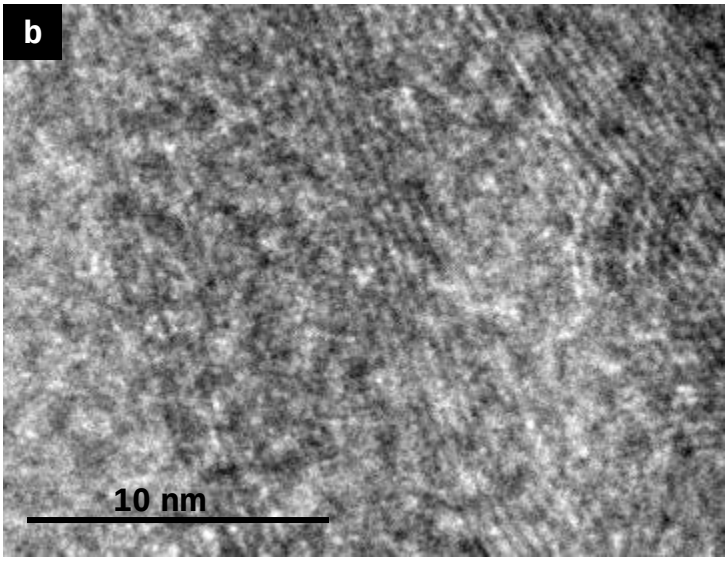
b
10 nm

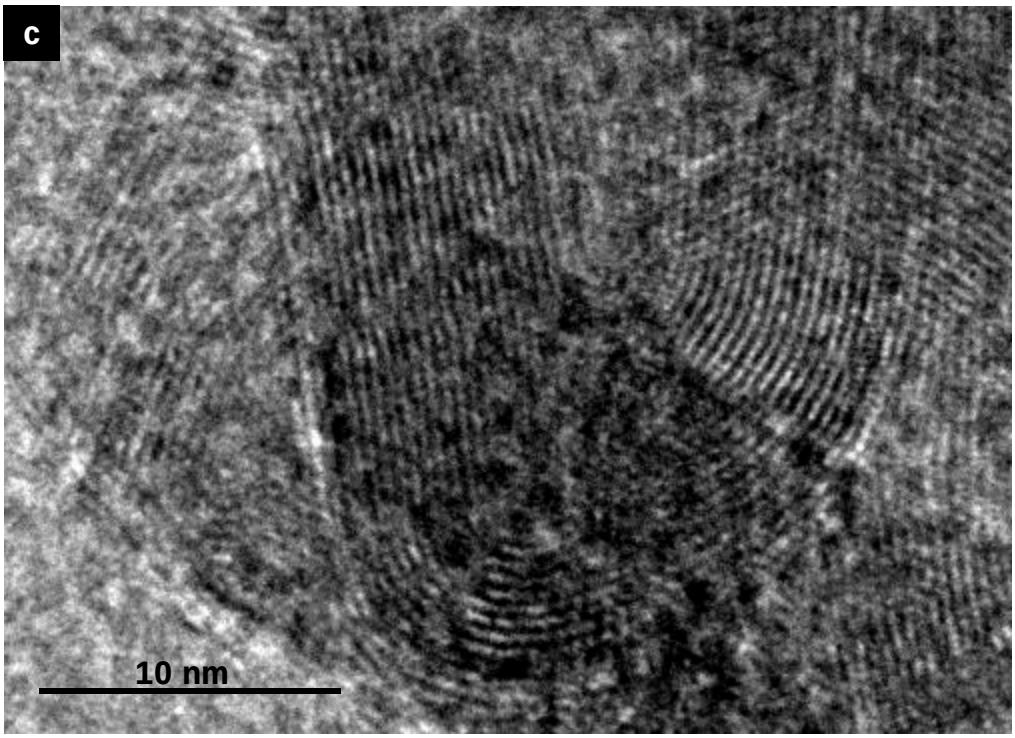

Figure 30: HR TEM image of a section of the folded up tube shown in Figure 29.

Figure 31 shows the SEM and BF TEM images of another commonly found particle – straight bare CNT like nanoparticle.

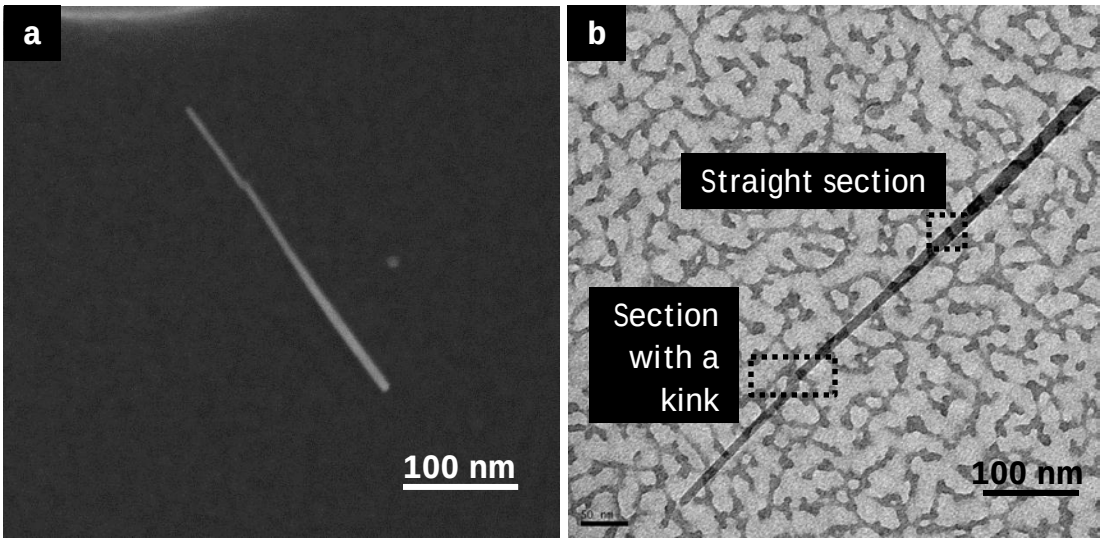

Figure 31: SEM (a) and BF TEM (b) images of a CNT-like particle. Two different areas of the particle were imaged – a straight section (Figure 33) and a section with a kink (Figure 32).

Figure 32 is a HR TEM image of the section with a small kink. The image is noisy but the multi-wall structure of the tube can be identified. Also the kink seen in the SEM image did

not look like a bend in a continuous tube. Rather it seemed to be two closed end tubes next to each other (see the dashed guidelines in Figure 32).

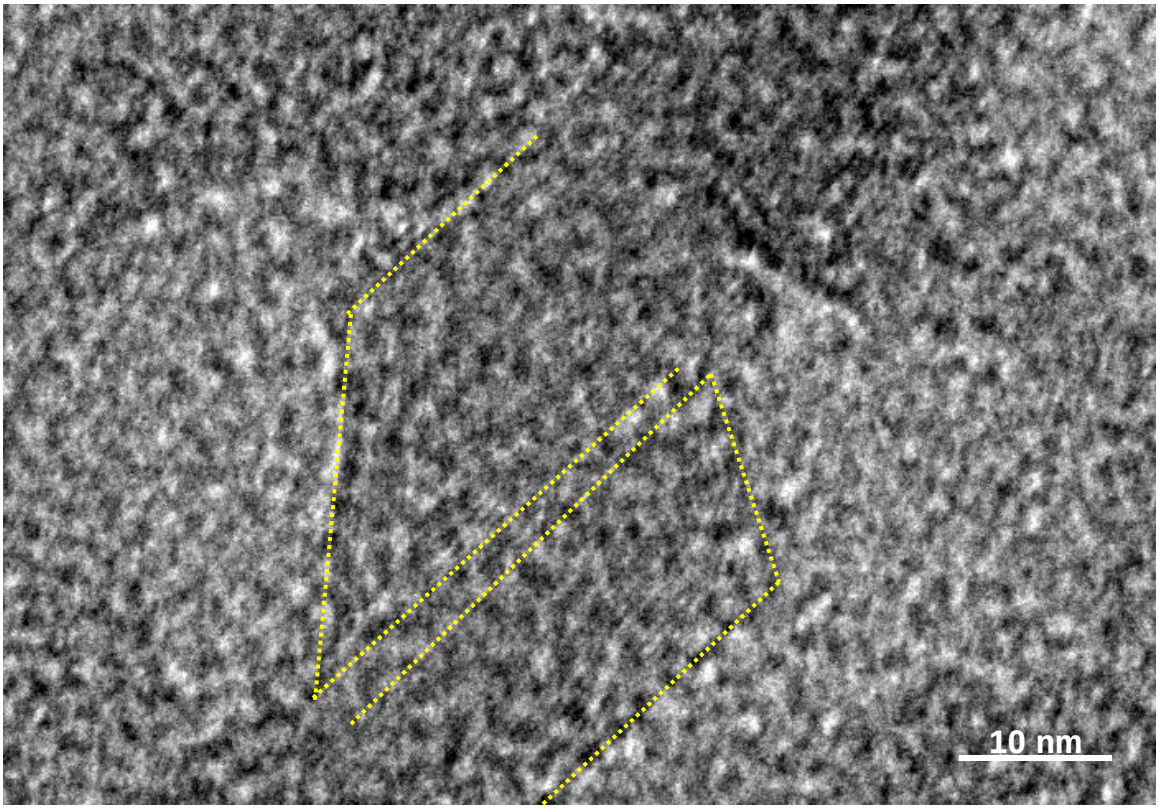

Figure 32: Close up view of the section with a kink. Yellow dashed lines are added as visual guides in identifying the locations of the multi-walls.

Figure 33 is the HR TEM image of the straight section of the particle shown in Figure 31. Hollow middle of the CNT is clearly visible in this case.

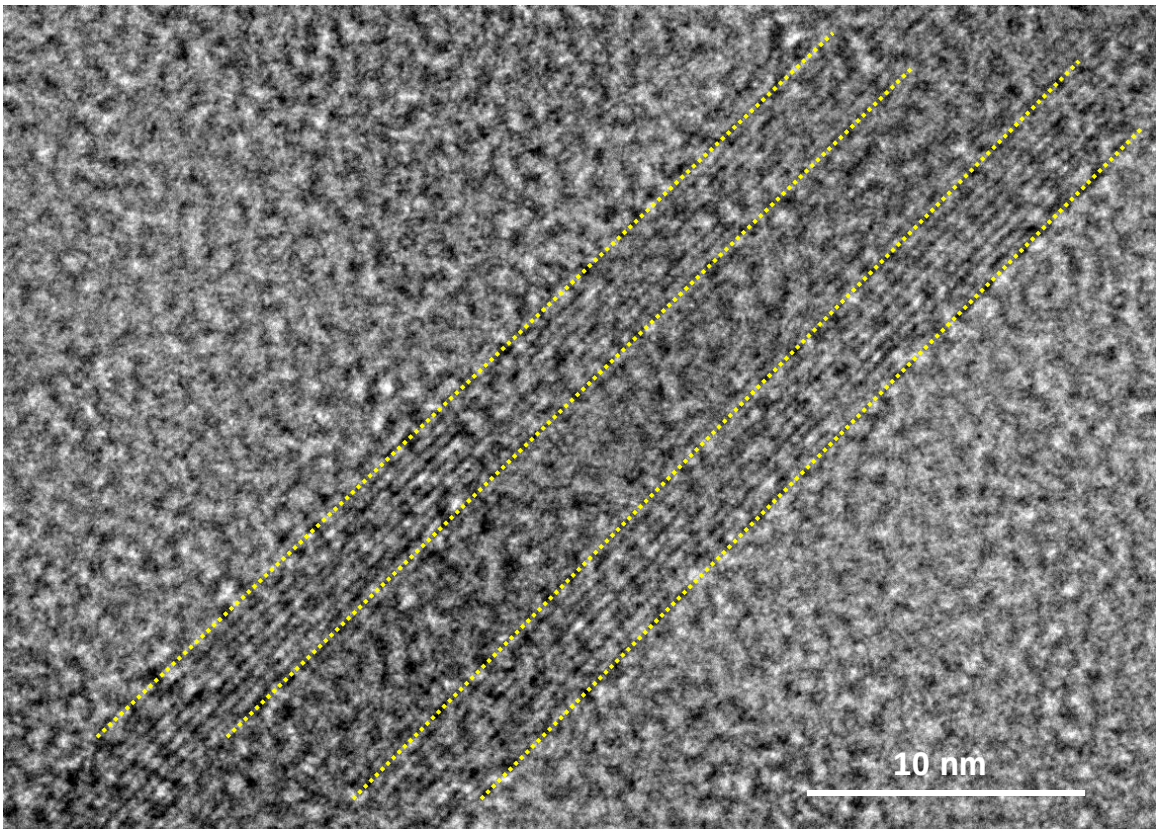

Figure 33: HR TEM image of a straight section of the CNT-like particle. Yellow dashed lines are added as visual guides marking the locations of the nanotube walls.

Figure 34a shows the SEM image of a particle that looks like a CNT with several grains of nanoparticles attached to it. When imaged in BF TEM mode, these granular nanoparticles turned out to be folded up nanotubes similar to the one shown in Figures 29 and 30.

Fortunately, the tip of this particle was hanging over the edge of a hole in the carbon film and we were able to obtain a clear TEM image of the CNT end cap (Figure 35) and the multi-layer structure of the tube wall.

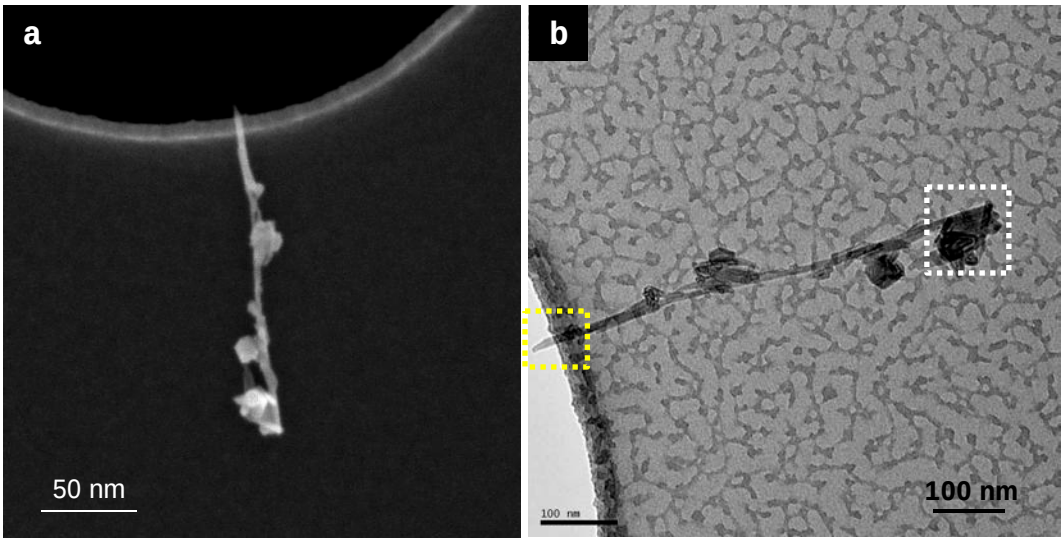

Figure 34: SEM (a) and BF TEM (b) image of a CNT-like particle with attached nanoparticles.

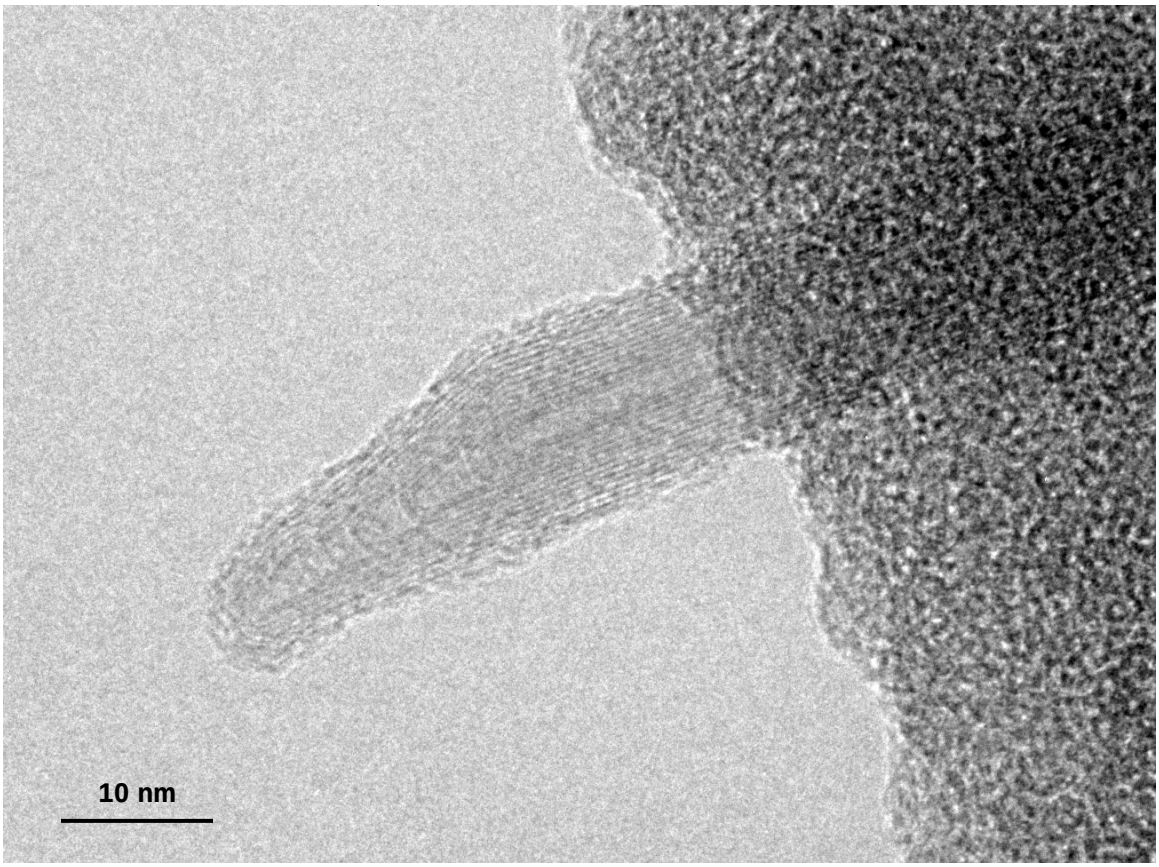

Figure 35: HR TEM image of the CNT end cap clearly showing multi-wall structure.

Figure 36 shows the bunched up section of the nanotube shown in Figure 34. As before, overlapping layers made it difficult to see the individual features of the nanotube, but the multiple walls of the particle were clearly visible in the rolled-up structure.

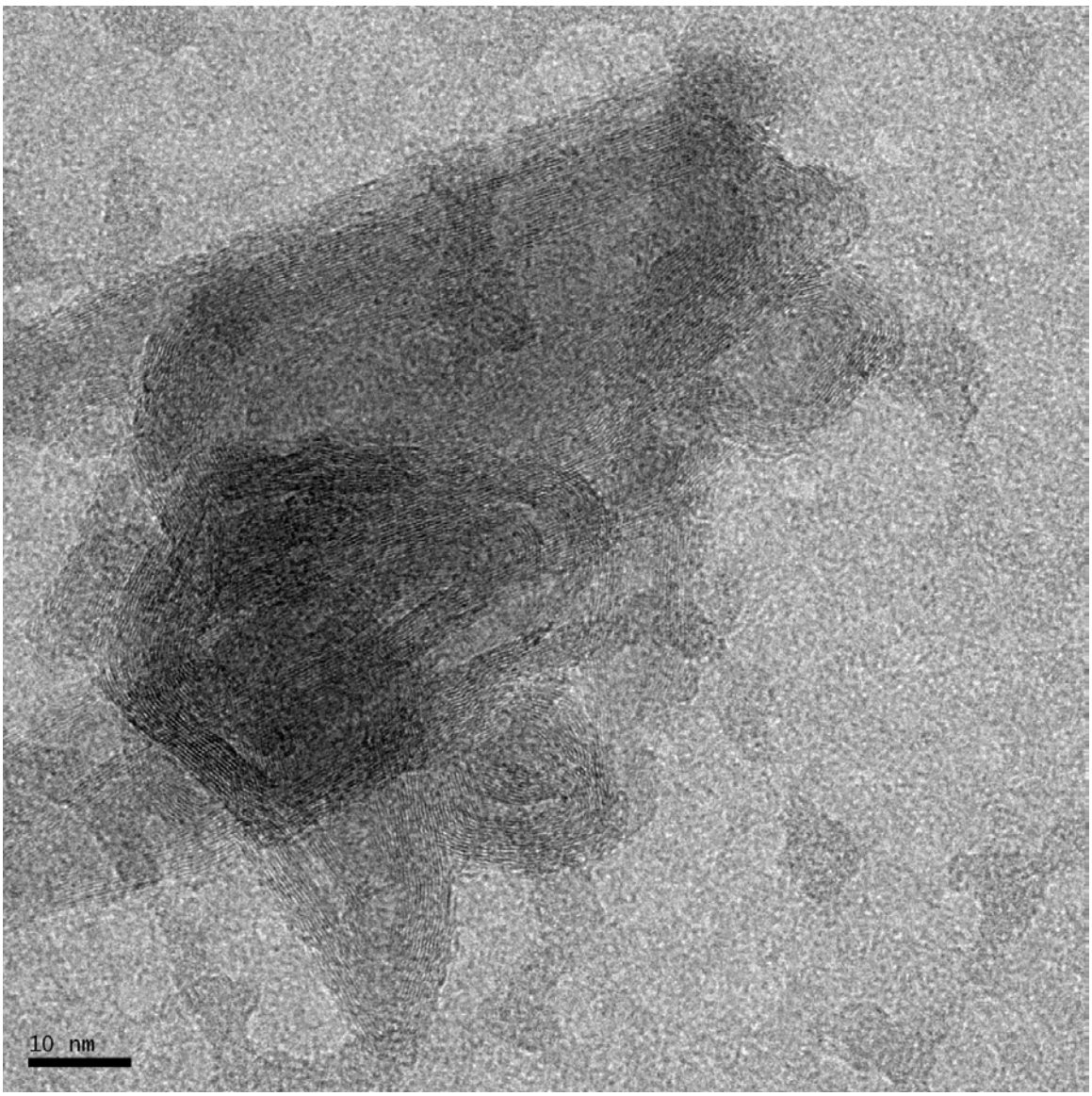

Figure 36: HR TEM image of the folded up section (marked in white rectangle) of the particle shown in Figure 34.

Figure 37 shows the SEM and BF TEM images of another bare CNT-like particle and Figure 38 shows the HR TEM image of the top end of the particle. In the HR TEM image, the classic hemispherical end caps and side walls of a MWCNT are clearly visible.

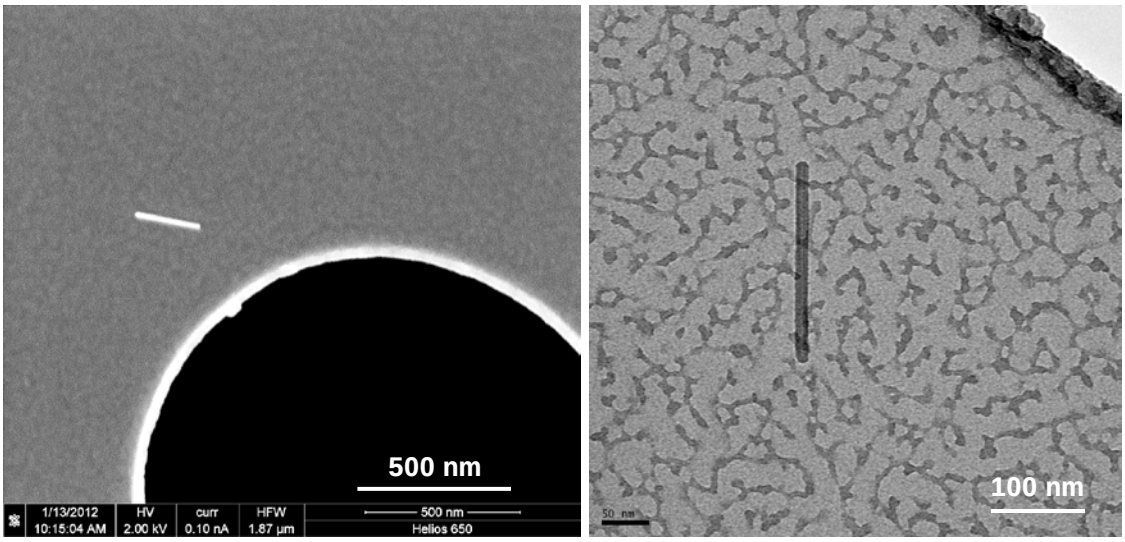

Figure 37: SEM (a) and BF TEM (b) images of a rod-like particle.

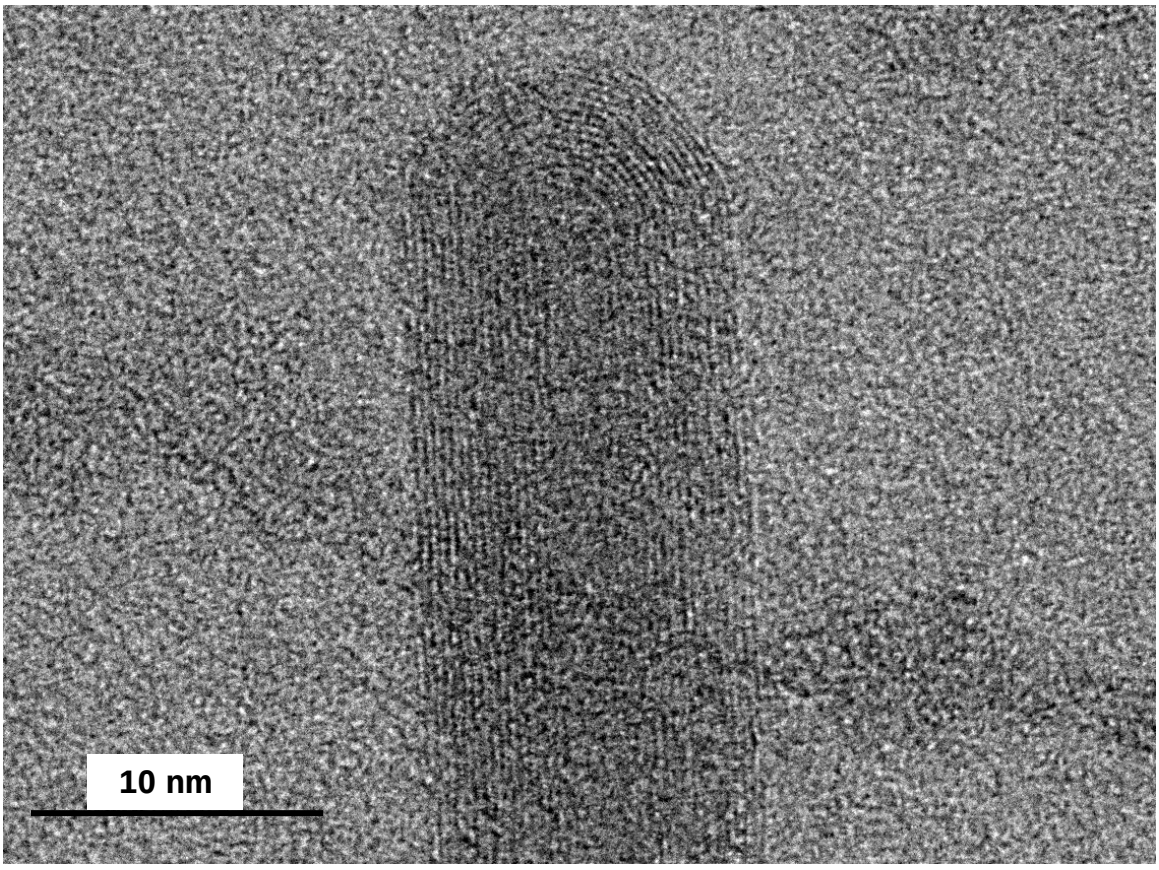

Figure 38: HR TEM of the rod-like particle shown in Figure 37. Hemispherical end caps and the side walls of the CNT are clearly visible.

5. Discussions and Conclusions

Product patents of baseball bats and other publically available literature on the use of CNTs in sports equipment clearly indicated that the CNTs in these bats are present as nanofillers in the carbon nanocomposite material. Initial LM and SEM analyses confirmed the laminate structure of the bat barrels and the presence of carbon fiber composite layers. Both bat barrels consisted of multiple layers of carbon fiber polymer composite and fiberglass polymer composite materials. High resolution SEM analysis of the flat polished cross-section samples of the bats did not show any CNTs in the carbon nanocomposite layers. However, Raman spectroscopy of the same layers did detect CNT signals. Subsequent SEM analysis of the carbon nanocomposite chunks from both bats did show surface protrusions and features in agreement with the reported images of resin-covered CNTs, indicating the presence of CNTs in the carbon nanocomposite layers.

Qualitative elemental analysis of the barrel cross-sections was performed to identify the locations of the carbon fiber and fiberglass composite layers. SEM-EDS showed that both bats had at least 1 mm thick layer of paint and fiberglass composite material on the surface. Carbon nanocomposite layers were located below the paint and the fiberglass layers. Since the CNT containing carbon nanocomposite layers are located relatively far below the surface, accidental release of CNTs due to minor abrasions and scratches on the bat surface was considered minimal.

Two additional CNT release scenarios were considered: 1) release from a broken bat and 2) release during bat disposal and recycle process. Bat breakage is relatively common in composite bats. Additionally, the conditioning process for these composite bats includes "rolling" where the barrel is repeatedly compressed to break the bond between different laminate layers, increasing the likelihood of CNT release from a broken bat. Many of the product disposal and recycle processes include cutting up or shredding of products into easily processable chunks. Both release scenarios involve exposed inner laminate layers and lead to possible release of CNTs during delamination and other destructive processes.

The release of CNTs from the exposed carbon nanocomposite layers was simulated through sawing and cutting. Sawdust, cutting debris and fine particles from these operations were collected and examined using SEM and TEM. Most of the particles released during the sawing and cutting operations were hundreds of micrometers or larger in size. However, high resolution analysis of some of the larger particles and fine particles did show that many CNT-like nanoparticles were present either attached to larger particles or singly. Some of these particles looked like resin covered nano-fibers/tubes (nano-casings) and others looked more like bare CNTs. TEM analysis of several CNT-like particles confirmed their multi-wall structures although some of them exhibited rather unusual, wrinkled side-wall shapes.

Based on the SEM and the TEM analyses of the release particles presented here, it was evident that the CNTs in the nanocomposite material can be released as bare CNTs and as aggregates of CNTs and other materials. However, to quantitatively assess the CNT release, more controlled and rigorous sampling procedures and faster detection methods are needed. The differences in the number of CNTs and other nano-sized particles deposited on the SEM stubs

(with sticky carbon tape) and the TEM grids indicated that many of the fine particles released during the simulated disposal process (cutting and sawing) were captured by the surrounding surfaces instead. Also, SEM and TEM, although effective, are very time consuming and laborious methods. TEM confirmation of each candidate CNT particle is not a viable approach for quantitative analysis of released CNTs.

For the next phase of the CNT release study, optimization of the current detection methods and sampling approaches are considered. The use of electrostatic precipitator or similar devices during the sawing and cutting operation may help to counteract the loss of fine particles during the sampling step. NIOSH Method 7400 for asbestos sampling will also be considered. A robust method to correlate SEM particle morphology to TEM confirmation of CNTs combined with an automated imaging routine can also be very helpful, especially when combined with a correlative SEM-Raman analysis approach.

Appendix I: Instruments and Experimental Settings

Light Microscopy

Macro scale imaging of the bat samples were collected using Nikon SZM stereo microscope.

Scanning Electron Microscopy

Low resolution imaging and x-ray analysis of the polished samples were performed using FEI Quanta 200F ESEM equipped with Bruker X-Flash 30 mm^2 SDD. Most of the images were collected at 15 keV or above beam energy.

Focused Ion Beam Scanning Electron Microscopy

Focused ion beam milling and TEM thin section preparation were performed using FEI Nova NanoLab 600 FIB SEM. Most of the SEM images were collected at 5 keV beam energy and ion beam milling was performed at 30 kV acceleration voltage. Milling currents varied depending on the specific operation – rough milling, fine milling and cleaning. Final cleaning of the TEM thin section was done at 5 kV.

Sawdust and fine particle imaging was performed using FEI Helios NanoLab 650 FIB SEM. Most of the high resolution SEM images were collected at 1 keV or 2 keV beam energy and 100 pA beam current. Survey images were collected at 4 mm working distance but individual nanoparticles were imaged at 2 mm or less working distance using the through the lens detector.

Transmission Electron Microscopy

TEM analysis was performed using FEI Titan 80-300 aberration-corrected AEM. All TEM images (BF and HR) were collected at 300 kV.

Appendix II: Supplementary Figures

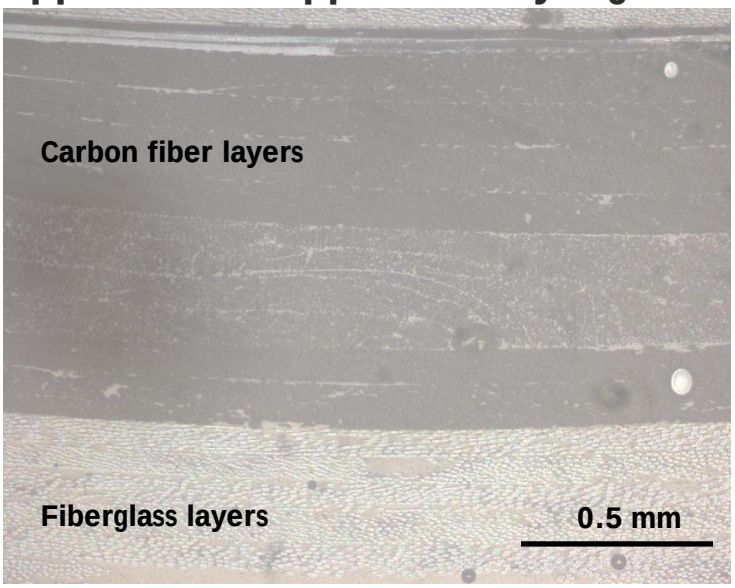

Figure A1: Bright field image of the Sample 1 thin section showing multi-layered structure of the carbon fiber layers and fiberglass layers.

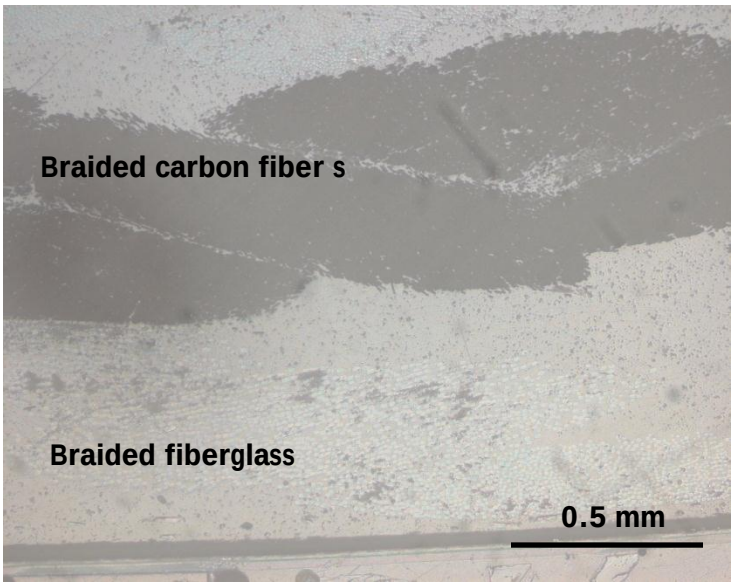

Figure A2: Bright field image of the Sample 2 thin section showing woven carbon fibers and fiberglass.

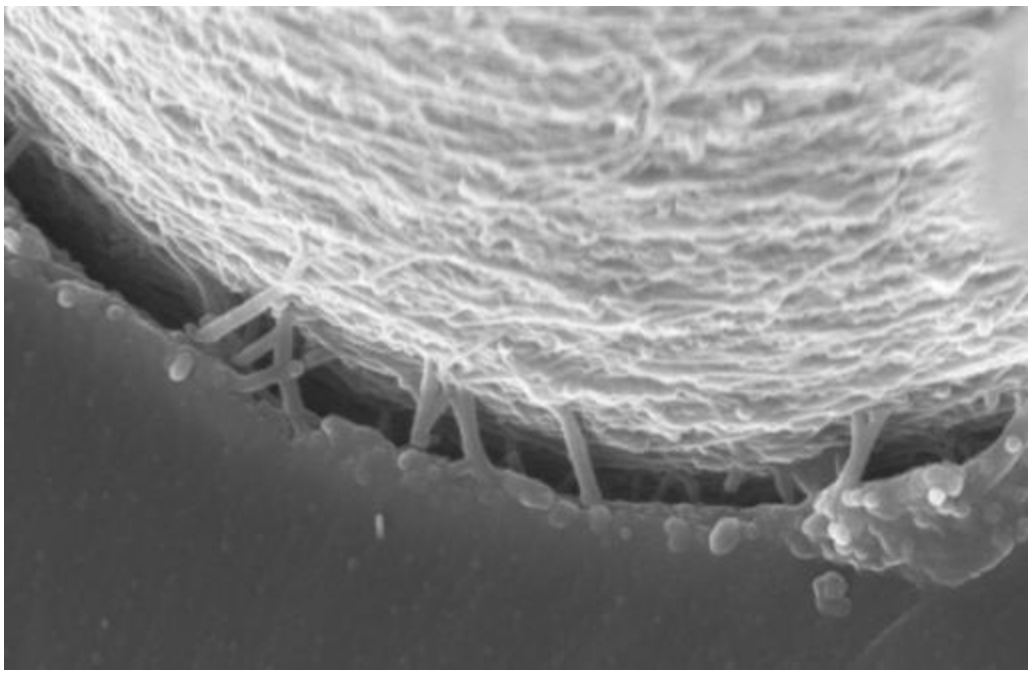

Figure A3: SEM image of Zyvex™ CNT composite material (http://www.zyvextech.com/media/)

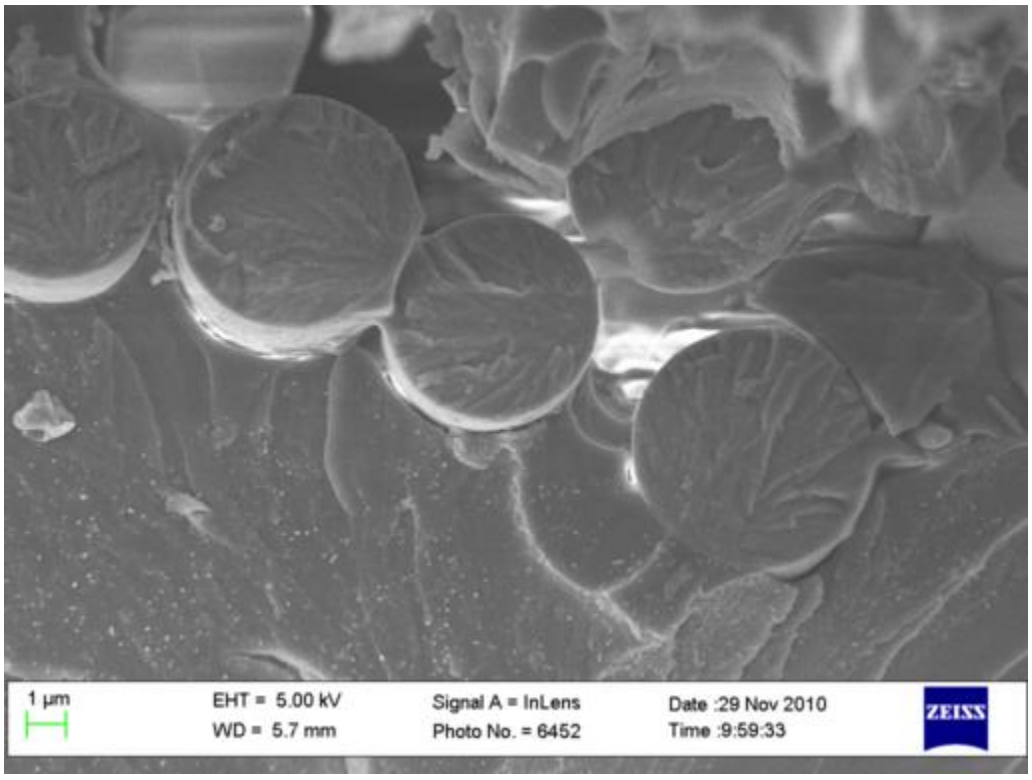

Figure A4: SEM image of Zyvex™ CNT composite material (http://www.zyvextech.com/media/)

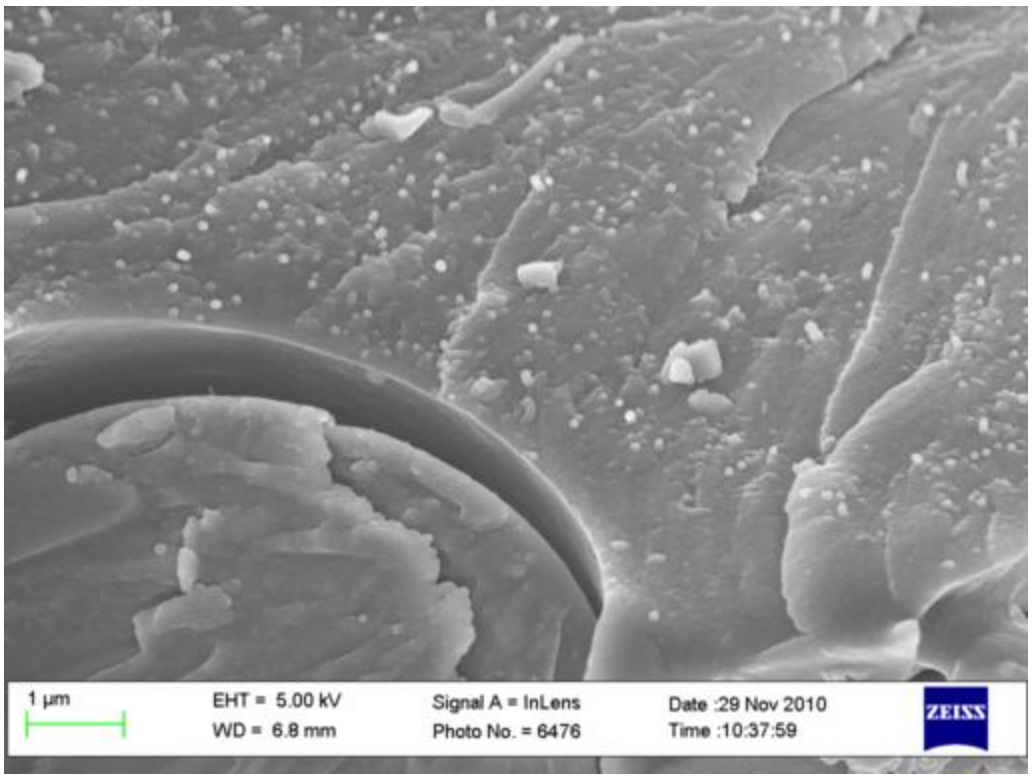

Figure A5: SEM image of Zyvex™ CNT composite material (http://www.zyvextech.com/media/)

Exposure Assessment of Carbon Nanotubes in Sports Equipment, Phase II

Final Report to the U.S. Consumer Product Safety Commission
Interagency Agreement # CPSC-I-12-0009

Report Date: January, 2015

Performed by:
Keana Scott
Grant Myers
Frederick Meisenkothen
Stephan Stranick
Andrew Herzing
John Henry Scott

Submitted by:
Keana Scott
Microanalysis Research Group
National Institute of Standards and Technology
100 Bureau Drive, MS-8372
Gaithersburg, MD 20877
(301) 975-4579
keana.scott@nist.gov

1 Table of Contents

2 EXECUTIVE SUMMARY

Two commercially available, multiwall carbon nanotube (MWCNT) containing composite bats were analyzed with microscopy-based techniques. The main objective of this study was to develop analytical methods for detecting, characterizing and quantifying MWCNTs in consumer products and any associated release fragments from wear and failure events such as accidental bat breakage as well as intentional wear through abrasive stressing. Both bats had hollow barrels made up of multiple layers of glass and carbon fiber reinforced composite material. Manufacturer's product information specified that the MWCNTs were added in the polymer resin that binded the carbon fiber layers.

Analysis of intact (unabraded) bat material showed no evidence of any MWCNTs and we suspect that this is due to the low MWCNT concentration level in the polymer resin. Raman imaging of control/model MWCNT epoxy nanocomposite samples indicated that the detectable MWCNT signals in these samples originated from MWCNT agglomerates and were not detectable at the low concentration levels found in the bat's epoxy matrix. To assess the release of MWCNTs during fracturing and abrasive stressing scenarios, an abrasion particle sampling system was implemented. Several different sampling configurations were evaluated and micro-orifice uniform deposit impactor based aerosol sampling of release particles was ultimately selected as the most effective approach. The detection of released MWCNTs required exhaustive surveying of large analysis area at very high imaging resolution. Automated hierarchical SEM imaging approach was implemented to accomplish this manually intensive task.

Using our released particle sampling and imaging methods, we found that polymer-free MWCNTs and polymer embedded MWCNT fragments were released during our simulated stressing process albeit in relatively low quantities. The low quantities of MWCNTs in the collected samples indicate that either the MWCNTs are not easily released from the polymer matrix or that the released MWCNTs are effectively sequestered through various loss mechanisms. Accurate assessment of MWCNT release rates from commercial nanocomposite products, however, is not feasible with our current suite of analytical and experimental techniques. To achieve the requisite accuracy will require a long term and sustained effort in the development of robust sampling systems coupled with novel real time visualization methods that probe MWCNT release mechanisms and dynamics.

3 INTRODUCTION

The National Institute of Standards and Technology (NIST) is tasked to refine and optimize microscopy-based analysis methods for detecting, characterizing and quantifying multiwall carbon nanotubes (MWCNT) in and release fragments from several commercially available CNT

containing consumer sporting and safety equipment under different use-case- scenarios for the Consumer Product Safety Commission (CPSC) in accordance with the Interagency Agreement # CPSC-I-12-0009.

Composite bats are popular because they can provide several performance advantages over aluminum or wooden bats. They are better control over swing weight, tunable trampoline effect (temporary deformation of the barrel during the collision with the ball) and bending stiffness, and highly damped bending vibrations which helps to lessen the "sting" effect [1,2]. However, one major disadvantage of the composite bats is their durability, especially in cold weather. Composite bats tend to break more easily than other types of bats because of the brittle nature of fiber reinforced polymer composites used in these products. In recent years, toughness of these composite materials are shown to improve with the addition of MWCNTs in the polymer resin [3].

In Phase I of the study (completed in June 2012), two types of CNT containing (based on the manufacturer's literature) baseball bats were identified by the CPSC and the NIST as the initial test products and purchased by the NIST. Analysis of these bat samples confirmed release of loose and partially embedded MWCNTs from both baseball bats in specific un-intended use scenarios such as cutting and shredding of bat pieces. Although a number of MWCNTs and MWCNTs embedded in resin fragments were found in the cutting and shredding debris in Phase I, there was no systematic effort to control the release rate or to effectively sample the released material.

Phase II effort focused on more systematic and controlled evaluation of release particles from these product. The three main topic areas research were 1) the development and optimization of Raman spectroscopy based MWCNT detection procedure where different sampling methods and experimental parameter space were explored, 2) SEM analysis of abrasion particles to determine MWCNT release in different use-case scenarios, and 3) feasibility testing of quantitative SEM analysis of MWCNTs in consumer products

4 APPROACH SUMMARY

Several CNT containing consumer products (based on the manufacturer's labeling) were considered and two types of baseball bats were identified by CPSC and NIST as the test sample products and purchased by NIST. Based on the manufacturer's product information and our earlier Phase I analysis of the bat components, we determined that the release of MWCNTs during normal use is not likely and the likelihood of MWCNT exposure through incidental contact with an intact bat is minimal. Our subsequent analyses were based on the release scenarios such as release during bat breakage, handling of broken bat fragments, and un-intended uses such as intentional damaging of the bat through cutting or sawing.

For detailed analysis of the bat's internal structure and nanomaterial release testing, the bats were cut into smaller pieces. Experimental protocols were reviewed and several exposure tests were performed by the NIST Office of Safety, Health and Environment (OSHE) during the sectioning of the bats to ensure safe handling of MWCNT containing products and materials.

Sectioned samples of the bats were analyzed for the presence of MWCNTs using various microscopy and spectroscopy techniques including focused ion beam (FIB) SEM, Raman spectroscopy, and transmission electron microscopy (TEM). MWCNT release scenarios (bat breakage and unintended use cases) were simulated using an abrasion particle sampling setup, designed for systematic and well controlled abrading of the bat samples and active aerosol sampling of the release particles. Custom fabricated epoxy nanocomposite samples with known MWCNT loadings were used to refine and optimize the abrasion particle sampling setup. Several iterations of sampling chamber design and sampling device configurations were tested during this process.

Debris from the simulated release scenarios were analyzed using SEM and Raman spectroscopy. SEM analysis of rerelease particles required systematic survey of a large area at high resolution and automatic image acquisition was used to accomplish this. For Raman analysis, custom prototype Raman microscope system was used for analyzing MWCNTs in nanocomposite material as well as MWCNTs in released particles.

5 METHODS AND RESULTS

5.1 Sample Preparation

5.1.1 Sample Description

Two CNT containing bats were analyzed. They were[1]:

Sample 1: Manufacturer 1 Youth Baseball Bat 32 inch/21 oz.
Sample 2: Manufacturer 2 Senior League, 30 inch/22 oz.

MWCNT enhanced composite bats have hollow barrels and filled or hollow handles. Barrels have layered structure of alternating fiber glass and carbon fiber (CF) layers as shown in the Figure 1. In a three phase (fiber/MWCNT/resin) composite system such as these, MWCNTs are used as nanofillers in the polymer resin to toughen the polymer and improve the

[1] Certain commercial equipment, instruments, or materials are identified in this talk to foster understanding. Such identification does not imply recommendation or endorsement by NIST, nor does it imply that the materials or equipment identified are necessarily the best available for the purpose.

polymer/carbon fiber adhesion. See Appendix 1 for a video explanation of nanocomposite technology.

The order of material layers and the orientation of fibers vary depending on the manufacturer. Figure 2 shows the cross-sectional images of two sample bats. Sample 1 consists of two bi-layer non-woven laminates of glass fibers and carbon fibers bonded together (Figures 2A and 3A). Sample 2 has alternating woven layers of glass fibers and carbon fibers (Figures 2B and 3B). Outermost layers of the bats are covered with a thick layer of paint that protects internal fiber layers from incidental scratches and gauges.

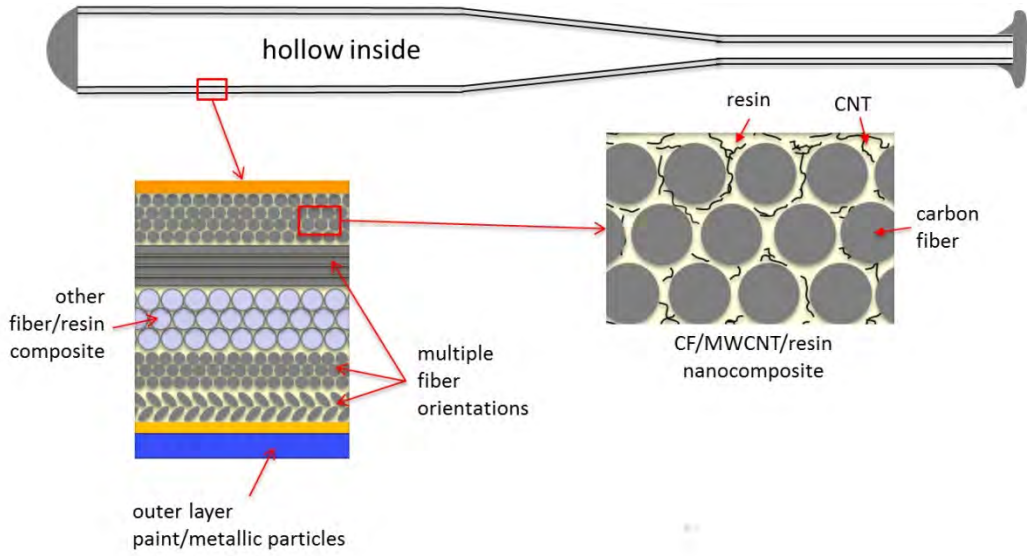

Figure 1: Schematic of MWCNT enhanced composite bat barrel structure.

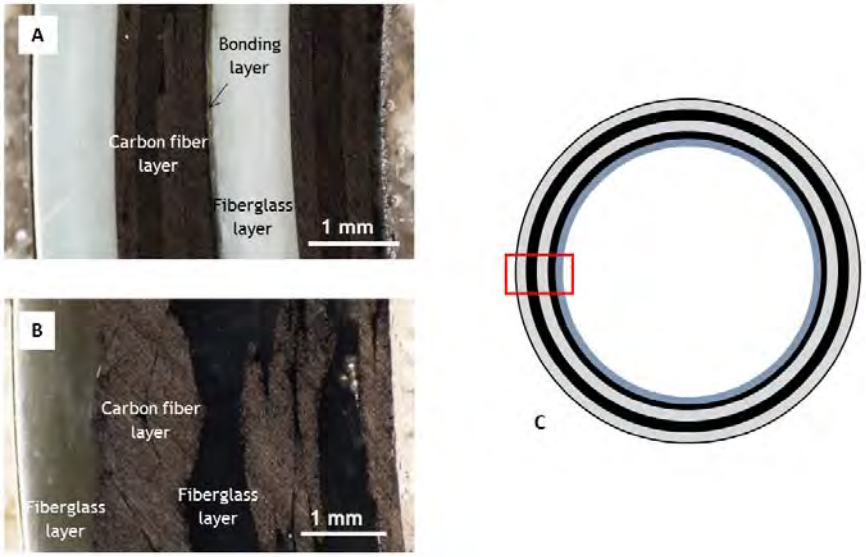

Figure 2: Cross-sectional view of A) Sample 1 and B) Sample 2. Red rectangular box in C) shows image orientation. For both samples, left edge is the outer surface of the bat and the right edge is the inner layer.

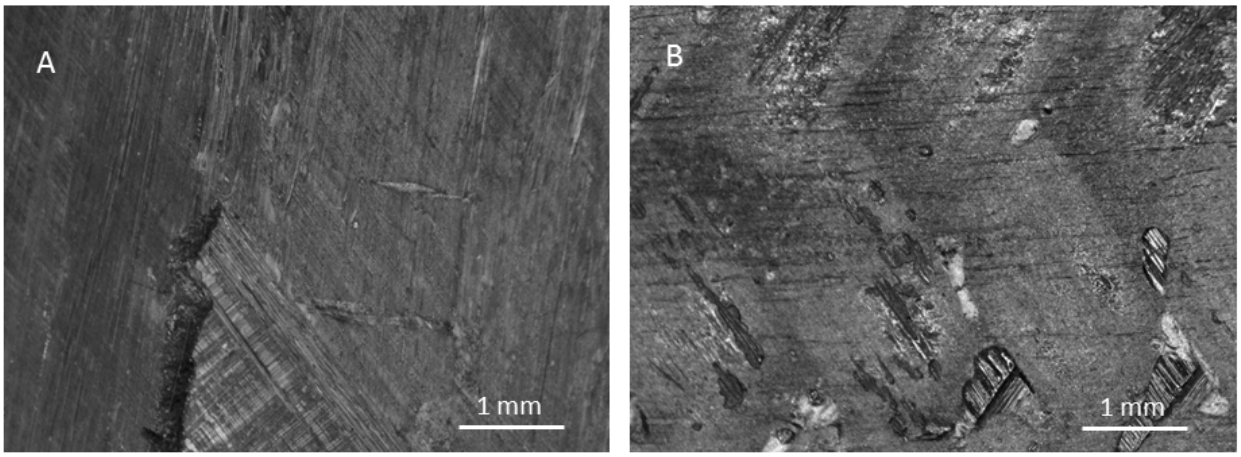

Figure 3: A) Stacked non-woven laminate structure from sample 1 and B) woven laminate structure from sample 2.

5.1.2 Bat Sectioning

For abrasion testing and microscopy analysis of the bat structures, bats had to be sectioned into small sample pieces. After an initial safety assessment where the sawing process was tested[2] and approved for nanoparticle safety by the OSHE, the bats were sectioned into roughly 2 cm by 5 cm pieces using a band saw equipped with a HEPA vacuum attachment. The sawing operation was performed while wearing a personal aerosol sampler and a HEPA filtered respirator. Surrounding room air was also monitored during the process. Breathing zone and work area air was found to be well within the regulatory limit for fine particle exposure.

Sectioned bat pieces were sonicated and rinsed in distilled water to remove any loosely attached particles and air dried in a HEPA filtered fume hood for several days before storing them in plastic containers. All subsequent testing and analyses were performed on these sectioned pieces.

5.1.3 Selective Matrix Dissolution

Polymer matrix binding both the glass fibers and the carbon fibers was selectively dissolved using n-methylpyrrolidone based solvents at 70 °C to facilitate detection of MWCNTs in the samples. After removing un-dissolved portion of the sample, the solution was vacuum filtered (0.1 μm pore size) to collect any free MWCNTs. The filters were rinsed with distilled water and dried overnight in a HEPA filtered fume hood. Dried filters were carbon coated for charge dissipation prior to SEM analysis.

[2] EC/OC analysis was performed on the filter samples and found acceptable.

5.2 Aerosol Sampling System

5.2.1 Nanocomposite Control Samples

Sampling of release particles from an abrasion experiment was more challenging than we anticipated. Initial aerosol sampling during abrasion of bat samples yielded very few particles at all and most were large (>100 μm in diameter) particles. There were no detectable free MWCNTs or MWCNT associated particles in the collected aerosol samples. Since the exact MWCNT loading levels of the composites used in the bats are not available, without a positive control, we could not confirm that the lack of MWCNTs in the collected aerosol samples was due to unaccounted losses or absence of release.

To ensure that the aerosol sampling method is valid, i.e., the method will collect MWCNTs if they are released during abrasion, we performed a systematic sampling study using a set of positive control samples. The control samples were three component MWCNT epoxy nanocomposites containing Bisphenol A diglycidyl ether (DGEBA, epoxy resin), Jeffamine (hardener) and Arkema MWCNTs with 9 different MWCNT loadings varying from 0.01 mass% to 1.0 mass%. SEM and TEM analysis of the control nanocomposite samples showed that the MWCNT dispersion was not very homogeneous. Instead of a uniform dispersion of individual MWCNTs throughout the epoxy matrix, we found that the control samples consisted of interspersed agglomerates of MWCNTs in epoxy matrix. These MWCNT agglomerates (or MWCNT rich domains) were up to several micrometers in diameter and their spacing decreased as the MWCNT loading increased. Figure 4 shows TEM images of the 0.01 mass%, 0.5 mass%, and 1.0 mass% nanocomposite samples. MWCNTs in these control samples were not homogeneously dispersed and, in all samples, we observed clumps (agglomerates) of MWCNTs and large regions of the samples that are relatively free of MWCNTs.

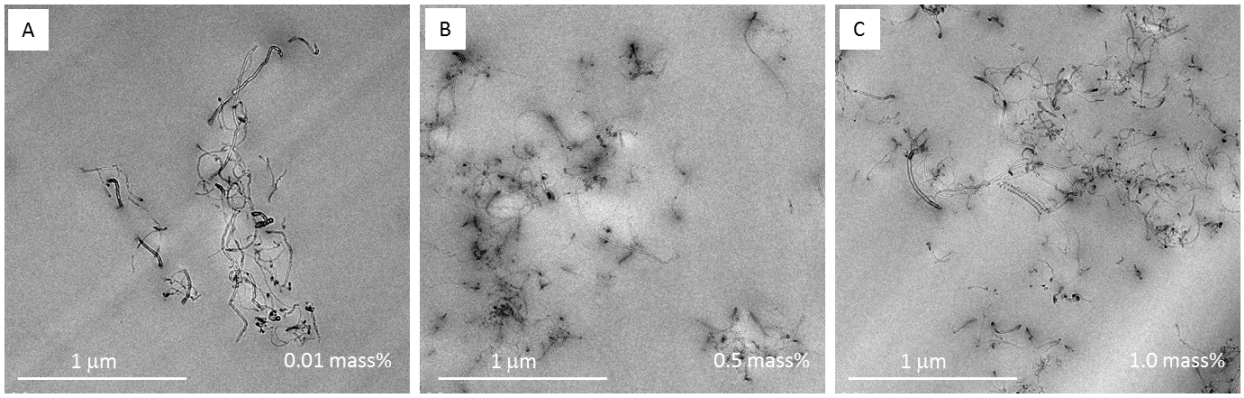

Figure 4: TEM images of the control nanocomposite samples showing MWCNT distributions in differently loaded samples.

5.2.2 Linear Abrader

Taber Linear Abraser Model 5750 abrader with T-slot universal table (Figure 5) is used for abrasion process. Abrasion stroke length, speed, applied force, and the number of cycles can be adjusted. Different abrading tip can be used to simulate a wide range of abrasive conditions. For MWCNT release testing, oval shaped double cut carbide burr was used as an abrading tip instead of commonly used abradant tip to minimize spurious particle generation.

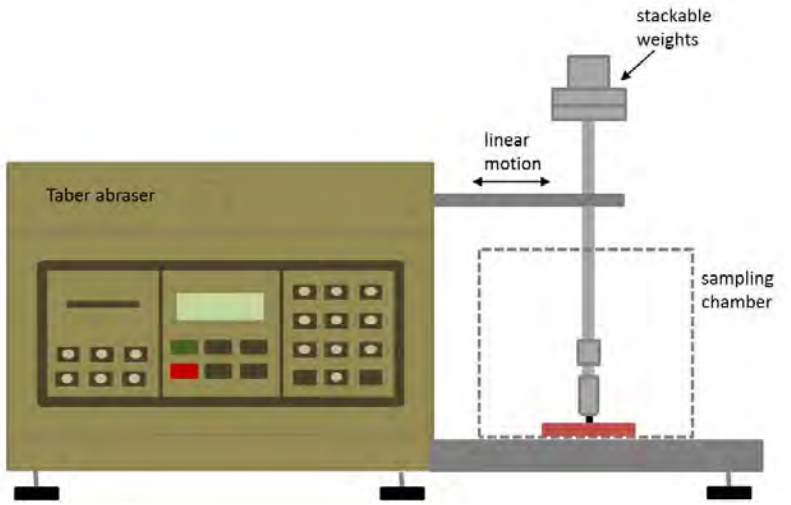

Figure 5: Schematic of Taber Abraser with universal stage and custom sampling chamber.

For aerosol sampling of abrasion particles, a fully enclosed sampling chamber was designed around the sample stage and the abrading (Figure 6). The sample chamber was designed to include as little portion of the abrader mechanism as possible 1) to minimize extraneous contributions such as particles from abrader motor and other friction induced particles and 2) to facilitate cleaning of the chambers and to prevent cross contamination between different sample runs.

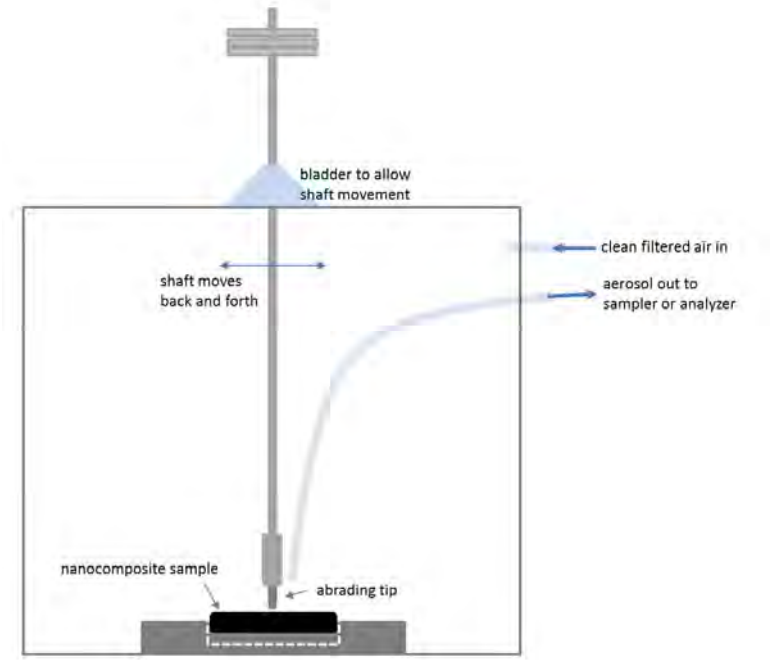

Figure 6: Schematic of the sampling chamber.

Several different intake port (aerosol inlet near the abrading tip) designs were tested. It was found that sampling very close to the abrading surface is necessary to collect sufficient particles, given the low speed and force used (60 cycles per min with 0.5 in stroke length under 1100 g of load). Small intake nozzle diameter (1/8 in) was also necessary to generate a sufficient pressure drop for effective sampling. To further minimize contamination, clean HEPA filtered air was fed into the chamber at flow rate near the sampling flow rate. Between each sampling run, inside of the chamber is vacuumed using a HEPA filtered vacuum and allowed to stabilize for at least 30 minutes.

5.2.3 Sampling System, SMPS Setup

The initial sampling setup consisted of a scanning mobility particle sizer (SMPS) for particle sizing and counting, an electrostatic precipitator (NAS) and a personal sampler for sample collection (Figure 7). Collection substrate types tested were Si wafers, nucleopore filters, and double-sided carbon tape.

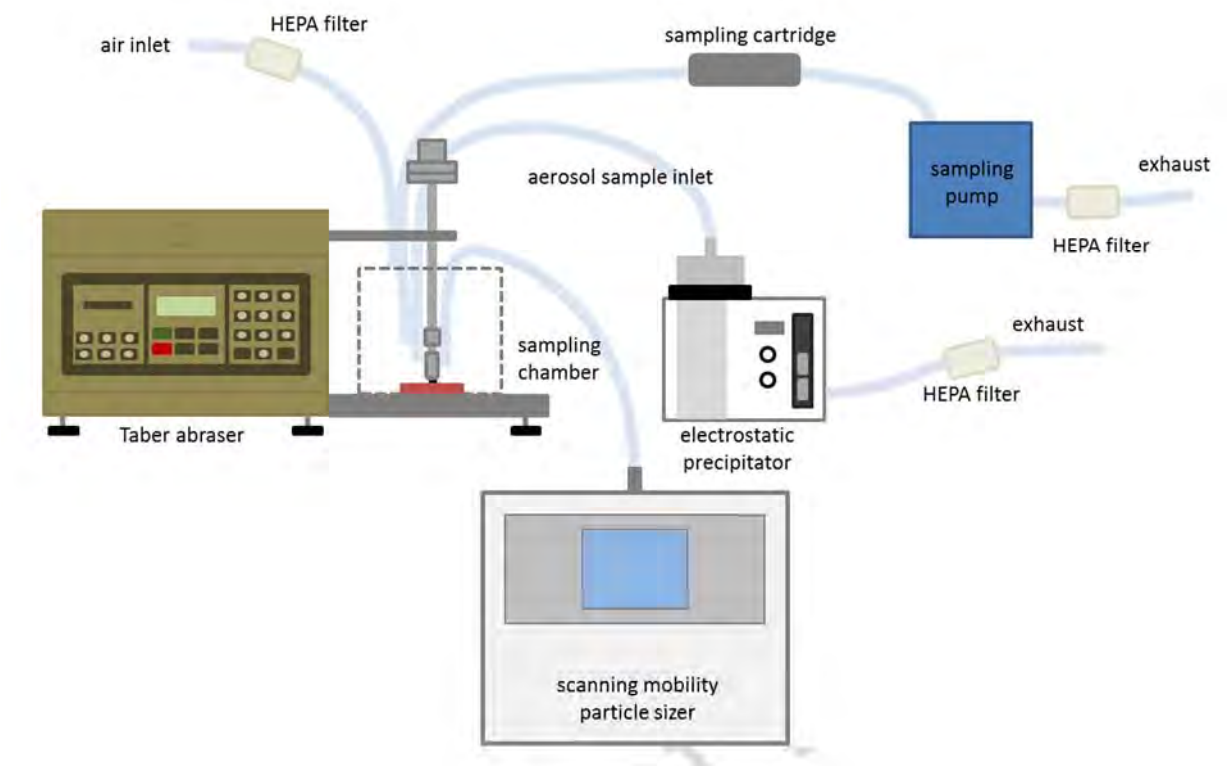

Figure 7: Schematic of the abrasion particle sampling station, SMPS-NAS setup.

5.2.3.1 SMPS Analysis

SMPS analysis was performed using MSP Model 1000XP scanning mobility particle sizer. 48 channel scan over 10 nm to 500 nm particle diameter was used. Average of 35 to 40 scans (about 2.5 hours) were used for the particle size distribution of each abrasion run. Figure 8 shows a typical particle distribution. For all nanocomposite sample, particles size distribution showed a peak around 100 nm while the abrader is running and this peak is missing when the abrader is not running. However, the particle number concentration was extremely low (few particles per cc) for all cases, making it difficult to draw any conclusions based on the SMPS results.

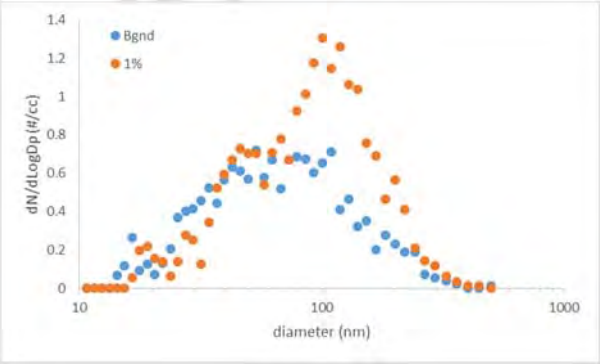

Figure 8: Average particle distribution from 1 % epoxy nanocomposite sample.

One possible explanation for this low number concentration is the slow speed of the abrader (maximum of 60 cycles per min) and the low flow rate of the SMPS (0.3 LPM). To compensate for the low particle generation rate and low flow rate, we experimented with the placement of intake port for the sampling tube with limited improvement in particle detection when the intake port is at or very near the abrading surface.

5.2.3.2 Electrostatic Precipitator Sampling

TSI Nanometer Aerosol Sampler (NAS) electrostatic precipitator was used to collect fine aerosolized particles generated during abrasion process. Three different bias voltages (0 kV, 5 kV, and 10 kV) and two different flow rates (1 LPM and 2 LPM) were tested. There were significant variations in the sampling efficiency. Figure 9 shows optical images of abrasion particles collected using different sampling conditions. For 1 mass% nanocomposite samples, many more particles were collected at 0 kV and 10 kV bias voltages compared to 5 kV bias voltage. High flow rate (2 LPM) sampling exhibited more evenly distributed particles over a larger area compared to a low flow rate (1 LPM) sampling.

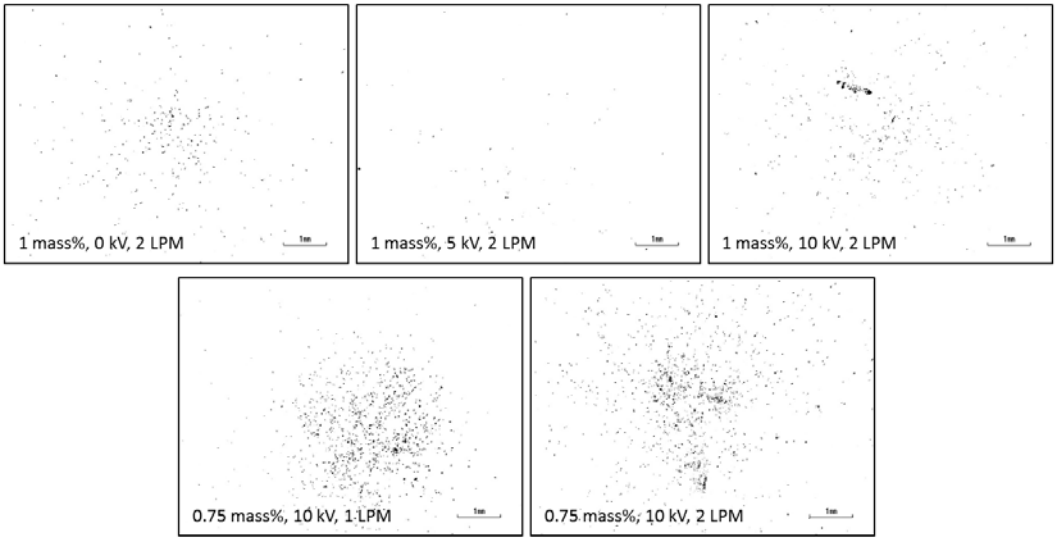

Figure 9: Effects of bias voltage and flow rate on electrostatic precipitator sample collection.

Figure 10 shows SEM images of typical abrasion particles collected on Si substrate and double sided carbon tape using an electrostatic precipitator. Most of the particles were several micrometers or larger and highly charging, necessitating the use of additional conductive coating for charge dissipation. Even with a thin layer of conductive coating, these samples tended to charge because abrasion particles had very rough surfaces that made it difficult to evenly coat the particles.

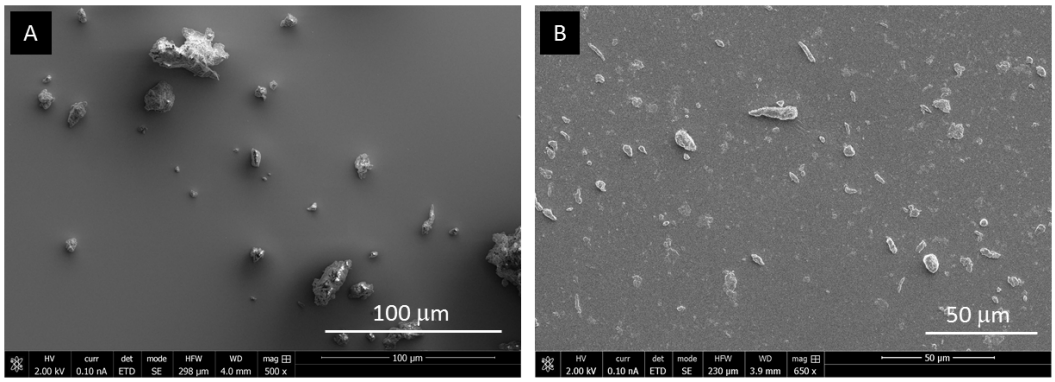

Figure 10: Typical aerosol particles using electrostatic precipitator. A) 1 mass% MWCNT epoxy composite sample collected on Si wafer, B) 0.5 mass% MWCNT epoxy composite sample collected on double sided carbon tape.

Although there were a number of particles collected, most of the particles were very large (several tens of micrometers in size). Careful analysis of the collection substrate showed presence of very few sub-micrometer sized particles. In general, detecting a singly appearing nanoparticle among larger, poorly conducting particles are extremely challenging. Figure 11 illustrates some of these difficulties. Some form of conductive coating is needed to dissipate charging but it is difficult to achieve very thin (5 nm to 10 nm) and uniform coating on uneven surfaces. The abrasion sample shown in Figure 11 was coated with 5 nm of Os but this was insufficient to fully dissipate charging in the larger particles. Nanoparticles adjacent to larger particles can easily be shadowed and undetectable unless the samples are imaged in several different rotational and tilt positions. Additionally, limited depth of focus at high resolution imaging conditions prevent effective detection of individual nanoparticles when present alongside larger particles.

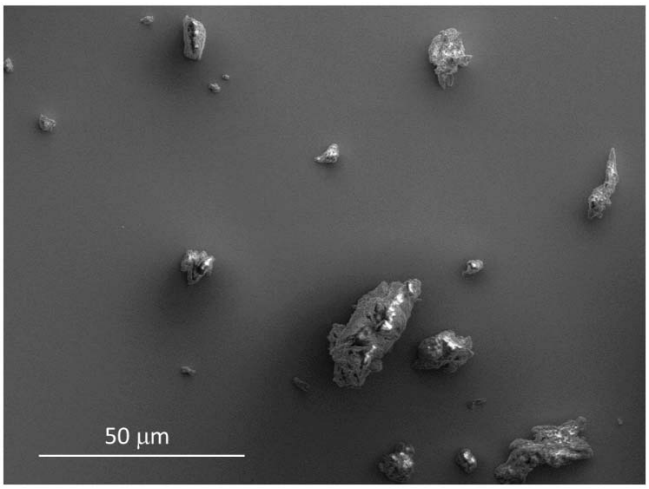

Figure 11: Close-up image of 1 mass% MWCNT sample. This sample was coated with 5 nm of Os for charge dissipation but there is still significant amount of charging, obscuring fine features on the larger particles.

Electrostatic precipitator based sampling was found impractical because of the difficulties associated with imaging and detecting individual MWCNTs in the polydisperse particle samples. Size selective precipitation method is needed for effective analysis of collected particles.

5.2.3.3 Filter Sampling

Several different types of filter sampling methods were tested for collecting aerosol samples during abrasion runs. Asbestos style filter cartridges and impactor based personal samplers were used but both methods had similar issues as the electrostatic precipitator – polydispersity of collected particles and found unsuitable for effective detection of released MWNCTs without the addition of a size selection step prior to filter sampling.

5.2.4 Sampling System, MOUDI setup

Preliminary test results from the positive control samples indicated that the abrasion experiments are either not generating aerosols that can be collected using the current set up or generated aerosols are getting lost through various mechanisms, electrostatic loss being one. Loss by unintentional deposition such as diffusion, inertial impact, electrostatic deposition, etc. at the sampling inlet and during transport is an important factor in determining the overall sampling efficiency [4].

One way to mitigate the low sampling efficiency problem due to transport loss is to use sufficiently high flow rate to collect as many particle as possible. We used micro-orifice uniform deposit impactor (MOUDI) to collect size selected sample collection at high flow rate. While the flow rates used for the earlier electrostatic precipitator and filter sampling devices ranged from 1.5 LPM to 3 LPM, flow rate required for MOUDI sampling is 30 LPM, much higher than those used for other sampling devices. Additionally, MOUDI produces size selected particle samples, eliminating some of the charging issues in highly polydisperse samples. For example, higher stage samples (small particle diameter samples) on Si wafers can be imaged without additional charge mitigation measures such as conductive coating, thus preventing additional loss of imaging resolution through coating artifacts. Figure 12 shows the schematic of the MOUDI based abrasion particle sampling setup.

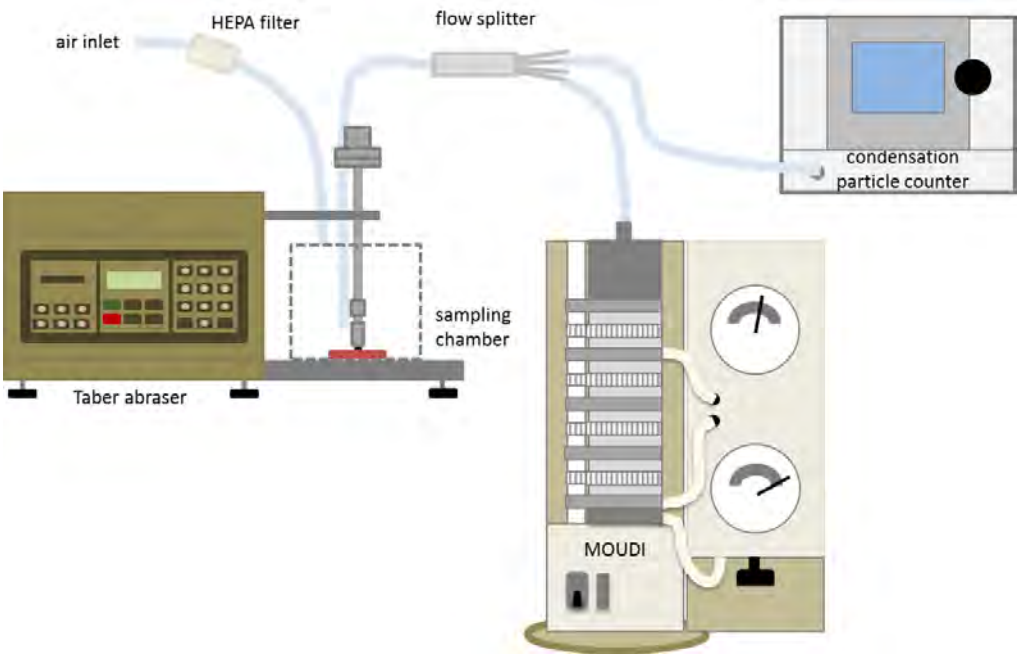

Figure 12: Schematic of the abrasion particle sampling station, MOUDI-CPC setup.

5.2.4.1 MOUDI (micro-orifice uniform deposit impactor)

MSP model 100 MOUDI, an inertial cascade impactor with multiple nozzles, was used. Detailed discussions of the aerosol sampling using cascade impactor can be found elsewhere [5,6]. MOUDI consists of a series of impaction plates where particles of specific size ranges can be collected based on the nozzle sizes. See Appendix 2 for the list of different impaction stages and corresponding nozzle sizes. MOUDI can be used in a rotating or non-rotating mode. If used in a rotating mode, collected particles are distributed more evenly on the sampling substrate.

The initial testing of MOUDI sampling using traditional Al foil substrates showed very poor collection efficiency. Track-etched polycarbonate membrane filters, although more effective in collecting particles than Al foils, were difficult to handle without disturbing the collection surface and required conductive coating to mitigate charging. To avoid these problems, MOUDI impaction plates were customized as shown in Figure 13 to accommodate 1 inch Si wafers as sample substrate instead of the traditional Al foils or membrane filters.

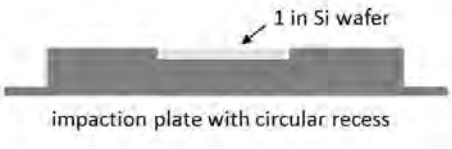

Figure 13: Custom modified impaction plate with 1 inch circular recess to accommodate a Si wafer.

For the abrasion particle sampling, a subset of impaction plates, namely stages 6 through 9, were used in a non-rotating mode. In a non-rotating sampling configuration, each stage

produces differently sized honeycomb-like particle distribution pattern where the size of the cells depend on the number of nozzles on the stage. See Appendix 2 for the table of nominal particle size and number of nozzles for each stage. Figure 14 shows optical images of samples from different stages. Inlet stage sample does not show any pattern because there is only one nozzle at this stage.

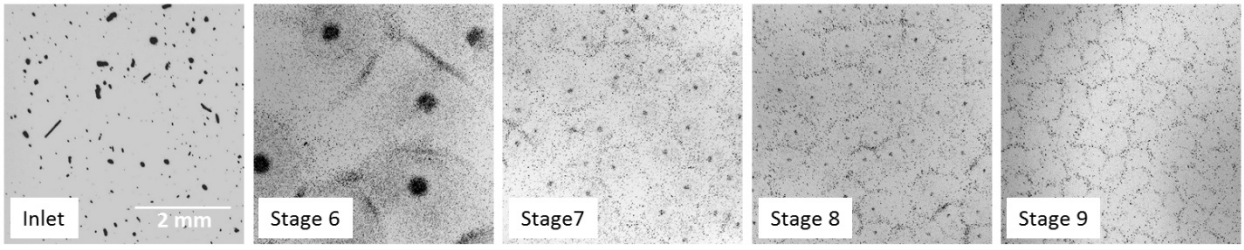

Figure 14: Particle distribution patterns from different MOUDI stages. Particles are collected on 1 in Si wafers. All images show 5 mm x 5 mm field of view.

5.3 Raman Spectroscopy

5.3.1 Raman Microscope

The scanning Raman microscope was constructed in-house based on an upright microscope with a fiber-coupled HeNe (632.8 nm) laser source. The collimated laser is filtered and reflected via an inject-reject scheme into the rear of the microscope and through either an IC50x air objective or a UIS2 UPlanSApo 100x oil-immersion objective. The scattered light was collected with the same objective and passed through the inject-reject filter and focused into a multimode fiber connected to either a holographic spectrograph with thermoelectrically cooled, charge-coupled device camera for spectral analysis or a single photon counting module for discrete Raman mode analysis (single channel detector with spectrally narrow bandpass filtering judiciously selected for individual Raman modes of MWCNTs). The sample was mounted on a closed-loop piezoelectric stage for sample scanning, where 10-nm stage resolution allowed for diffraction limited (~200 nm) spatial resolution with oversampling. Individual spectra were measured with ~1mW laser power and 1s integration time for a signal-to-noise ratio > 500:1 and then fit to a Pearson-VII function to assess the MWCNT Raman spectral peak positions. The resulting peak position maps were taken over micro-scale regions with (128×128) pixels.

5.3.2 Raman Analysis of Bat Samples

MWCNT containing (3.5 mass% MWCNT loading) epoxy nanocomposite samples were made and used as control samples. Figure 15 shows a Raman spectrum collected from a 3.5 mass% samples. MWCNT peaks (at wavenumbers 1330 cm^{-1}(D), 1600 cm^{-1}(G) and 2660 cm^{-1}(G')) are clearly visible in these samples. Raman analysis of loose carbon fiber also displayed broad

peaks around 1330 cm^{-1} and 1600 cm^{-1} but none around ~2650 cm^{-1}. Based on these initial test data, the G' peak around 2650 cm^{-1} is used as the indicator of MWCNTs in the bat samples.

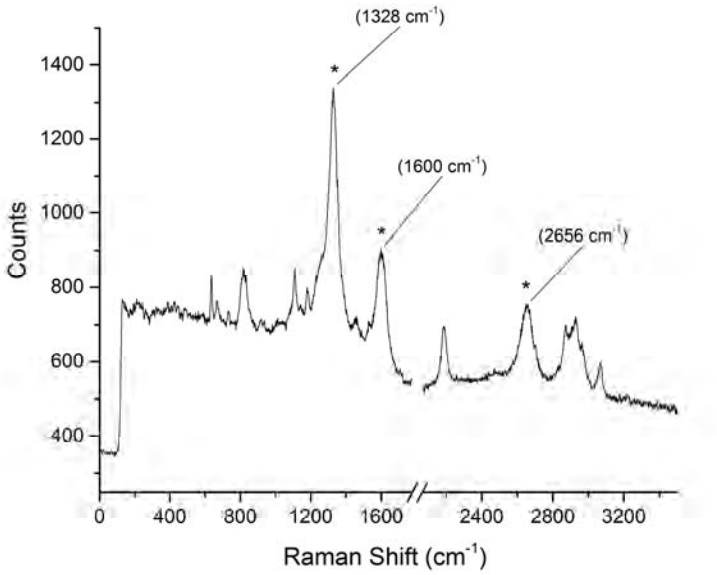

Figure 15: Raman spectrum of MWCNT epoxy nanocomposite sample.

Raman analysis of bat fragments were difficult because of uneven sample surface and high background signal. Figures 16A and 17A show typical bat carbon fiber layer fragments from bat 1 and bat 2. To minimize spurious contributions from surrounding material and provide smooth analysis surfaces, several thick coupons of bat resin material and carbon fibers were made for Raman analysis. Figures 16B and 17B show coupons fabricated from bat 1 and bat 2, respectively.

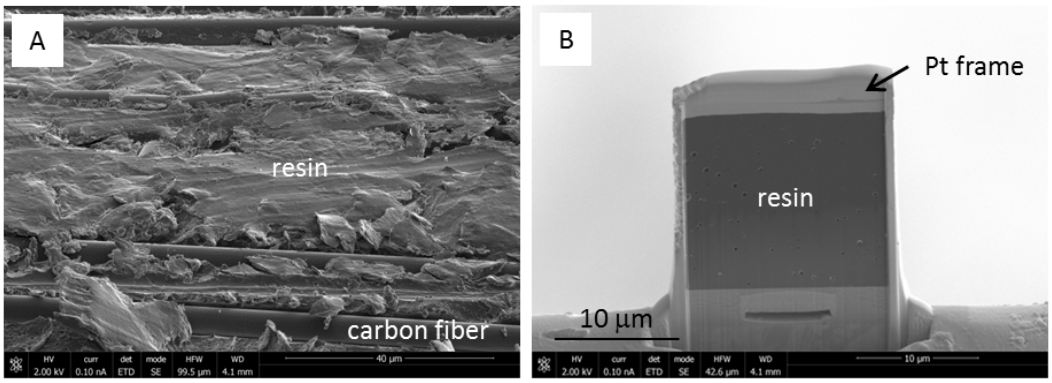

Figure 16: Fragment of bat sample 1 showing carbon fibers cover with resin (left) and a thick coupon made from the resin (right). The dark square area is the resin and surrounding light material is Pt frame used to stiffen the polymer coupon.

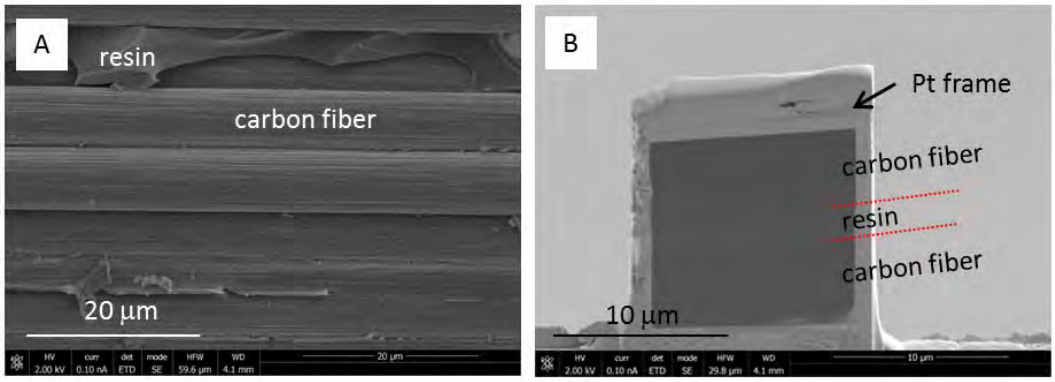

Figure 17: Fragment of bat sample 2 showing carbon fibers and resin filling in area between the carbon fibers (left) and a coupon made from the resin (right). The dark square area is separated into three sections - top and bottom dark gray sections sandwiching a slightly lighter gray section. The top and bottom sections are the carbon fibers and middle section is the resin. Light material surrounding the carbon fiber and resin is frame formed with Pt to stiffen the polymer coupon.

According to the manufacturer's claim, MWCNTs are mixed in the resin but Raman analysis of the resin sections from bat 1 and bat 2 did not show detectable MWCNT signature (G' peak). Fluorescence background from polymer resin was generally very strong and even the D and G band peaks from the residual carbon fiber were barely identifiable (Figure 18A). Raman spectrum from a loose carbon fiber is shown in Figure 19B as a comparison. Broad D and G band peaks are visible in the carbon fiber spectra, but there is no discernable G' peak at 2560 cm^{-1}, characteristic of MWCNT. Raman analysis of resin sections were problematic because resin sections were readily damaged under the incident laser beam and probe laser power had to be reduced significantly to collect usable spectra from resin sections. Raman spectra of resin sections did not show any discernable MWCNT peaks.

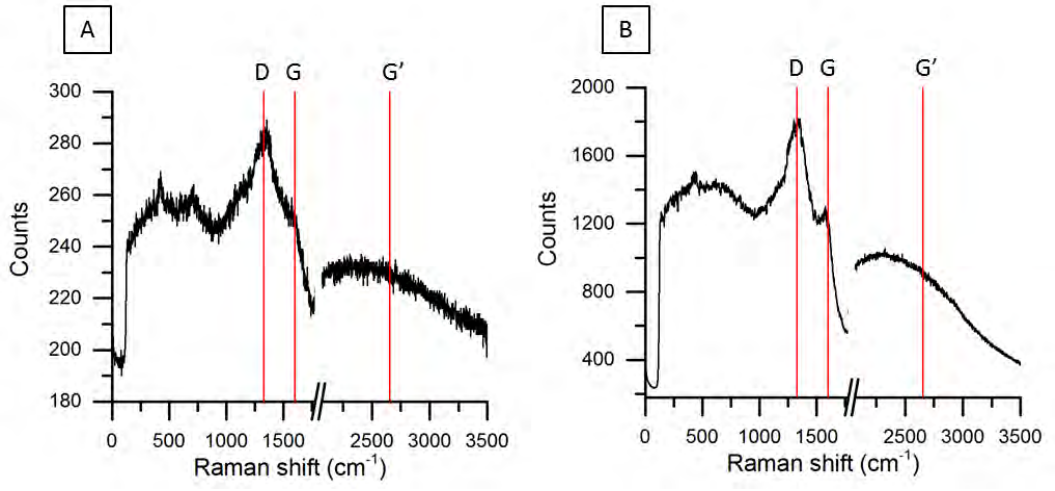

Figure 18: Raman spectrum from bat 1 carbon fiber coupon prepared using FIB SEM (left) and from a bat 1 loose carbon fiber (right).

5.3.3 Raman Analysis of MWCNTs in Control Samples

The positive control nanocomposite samples described in Section 5.2.1 were used to evaluate the Raman microscope's detection limit for MWCNTs dispersed in epoxy matrix. Figure 19 shows Raman images of MWCNTs in three different control samples (0.01 mass%, 0.5 mass%, and 1.0 mass%).

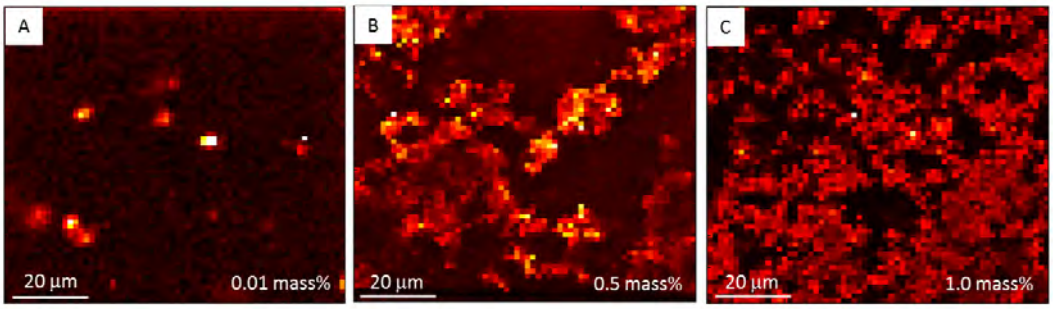

Figure 19: Raman images of MWCNT nanocomposite control samples showing differences in MWCNT (based on D peak) distribution in differently loaded samples. 90 µm x 90 µm field of view. Lighter color represents stronger MWCNT D peak signal.

Localized hot spots of MWCNTs were detected in all control samples including the lowest concentration 0.01 mass% sample. The distributions of the MWCNTs in the control samples were very inhomogeneous. This agreed well with previous TEM analysis of these samples (see Figure 4) and we suspect that the detected MWCNT Raman signals were originating from MWCNT agglomerates. In Figure 19A, we can see that the localized MWCNT signals are unevenly distributed and the MWCNT agglomerates were several micrometers or larger in size. Spacing between the MWCNT agglomerates ranged from a few micrometers to several tens of micrometers. As the MWCNT loading increased, the MWCNT agglomerate sizes increased and also started to form a connected network of MWCNTs. In the 1 mass% sample, several large regions of connected network of MWCNTs were seen although there were occasional, isolated small clusters of MWCNTs as well.

5.4 SEM & TEM imaging

All SEM analysis was performed using FEI Helios NanoLab 650 focused ion beam scanning electron microscope. TEM analysis was performed using FEI Titan 80-300 transmission electron microscope.

5.4.1 SEM Imaging of Bare MWCNTs

Aerosolized bare MWCNTs were collected on a Si wafer and used as a test sample for evaluating and optimizing SEM imaging conditions. Various imaging parameters such as beam voltages, beam currents, detection modes, bias voltages, and charge mitigation methods were evaluated using these samples. MWCNTs used for commercial nanocomposite products are

relatively heterogeneous in size and shape and often contain many residual catalyst particles. Figure 20 shows these variations in MWCNT size and shape clearly. Figure 20A shows MWCNTs coated with Os and Figure 20B shows MWCNTs coated with Au/Pd coating. MWCNT lengths varied from few tens of nanometers to multiple micrometers. In the Os coated sample, MWCNT diameter varies from ~10 nm to 20 nm and some of the smaller diameter MWCNTs are difficult to see while in the Au/Pd coated sample, MWCNTs are much more clearly defined and the diameter ranges from 20 nm to > 30 nm.

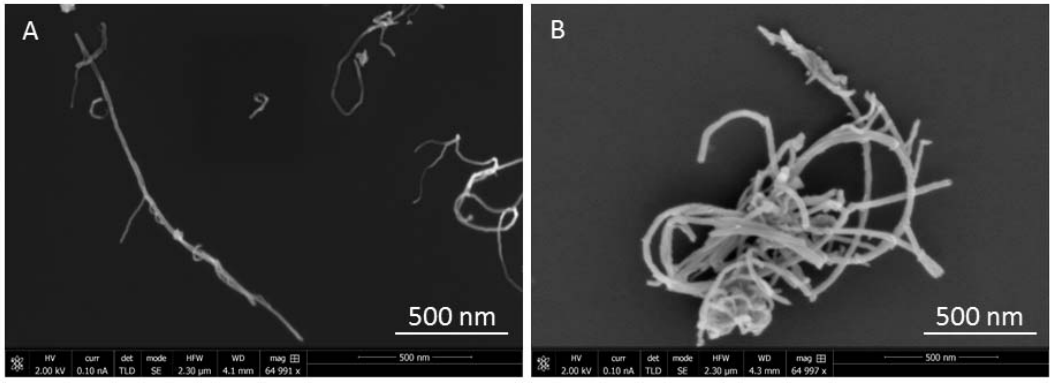

Figure 20: Bare MWCNTs on Si wafers A) with Os coating and B) Au/Pd coating.

Conductive carbon coating using a carbon evaporator was also tested. Carbon coating is often desirable because it provides a very thin conductive layer without introducing artifacts such as altered material contrast or added surface texture. However, one main concern is the possibility of MWCNT like contaminants from the evaporation process itself. Several blank Si wafers were carbon coated using a carbon evaporator and analyzed for contaminant particles. No MWCNTs or particles with similar morphology were found on these coated blank samples.

In general, Imaging with low electron beam acceleration voltages (1 kV to 2 kV) and low beam currents (50 pA to 200 pA) using the through lens detector at shorter working distance of 4 mm or less were desirable for bare MWCNT imaging. Uncoated samples are preferable but some amount of conductive coating may be necessary.

5.4.2 Bat Samples

Several TEM thin sections were made from the bat 1 and bat 2 fragments. All samples were made from the carbon fiber/resin regions of the bats. Figure 21 shows an image of a typical TEM thin section made from a carbon fiber/resin area of the bat. The dark, roughly circular regions are the carbon fiber cross sections and the light gray area is the polymer resin that bind the fibers together. Dark rectangular region around the thin section is the Pt support frame used to stabilize the <100 nm thick TEM section.

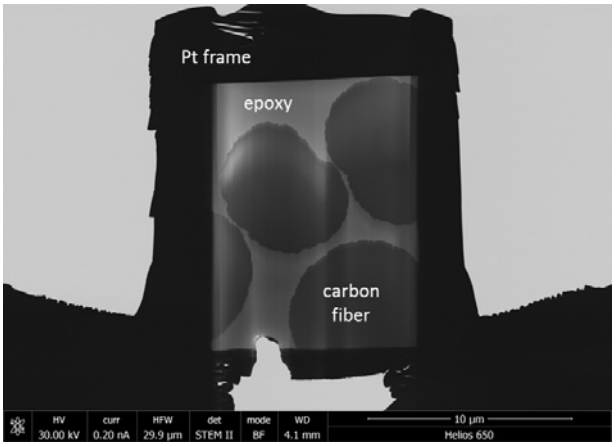

Figure 21: TEM thin section of bat 2 carbon fibers and surrounding polymer resin. Differences in material hardness between the carbon fiber and resin caused uneven film thickness.

MWCNTs but were not seen in any of the TEM thin sections (Figure 22). One possible cause for this lack of MWCNTs is poor sampling statistics. Overall volume sampled by one TEM thin section is roughly 10 μm^3 (10 μm x 10 μm x 100 nm). Although not likely, for nanocomposites with less than 1 mass% MWCNT loading, it is possible to not detect MWCNTs in any given 10 μm^3 volume.

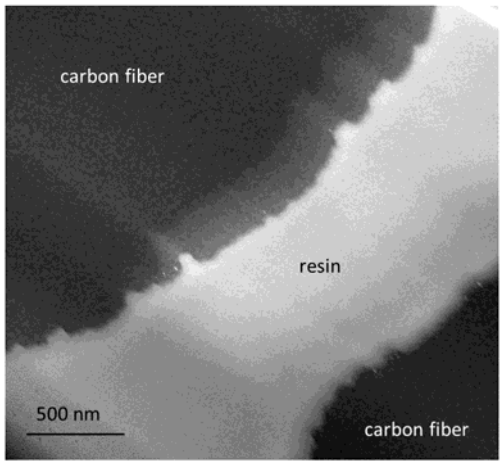

Figure 22: TEM image of the bat 2 thin section. No MWCNTs were detected in the resin between the carbon fibers.

5.4.3 MWCNTs on Bat Fragments

Fragments of bat 1 and bat 2 were dusted onto Si wafers and carefully examined for the presence of any exposed or free MWCNTs. SEM examination of the bat fragments did show few MWCNTs embedded in the resin, loosely attached on the particle surface, and on the Si surface as free MWCNTs. Figures 23 and 24 show several examples of these MWCNTs from bat 1 and bat 2 respectively.

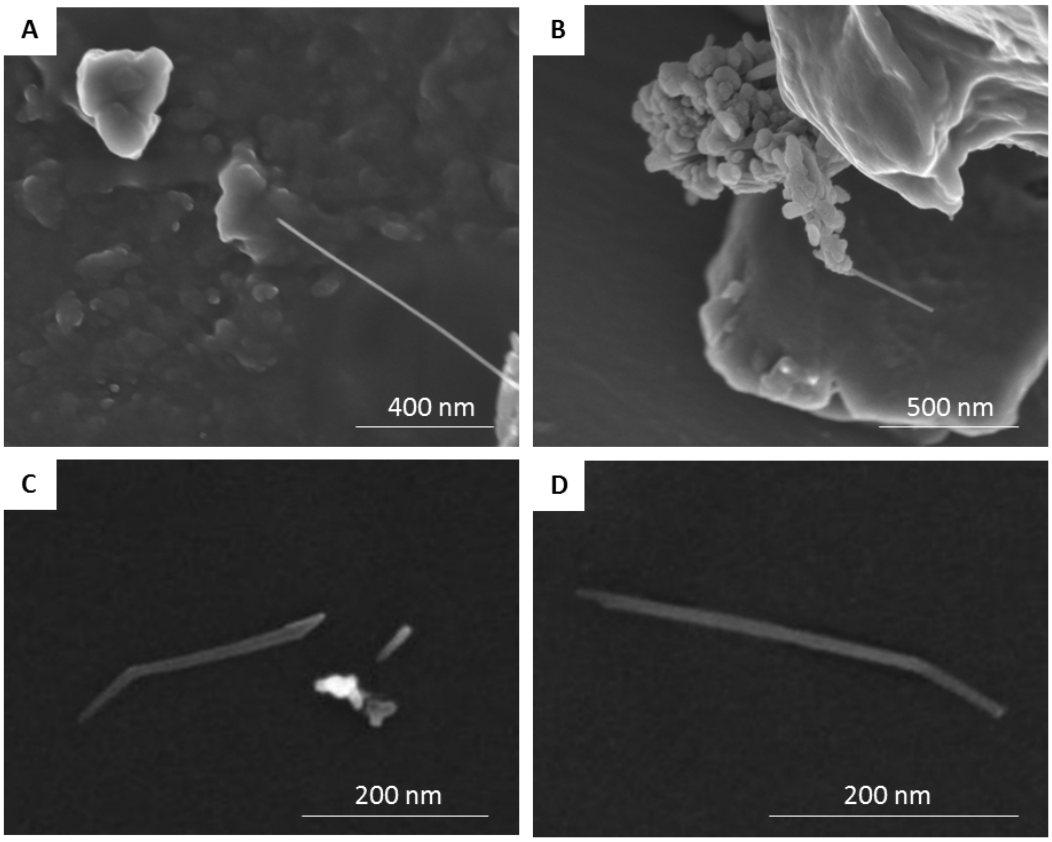

Figure 23: Bat 1 fragment sample collected onto a Si wafer showing A) exposed, B) loosely attached, and C & D) free MWCNTs.

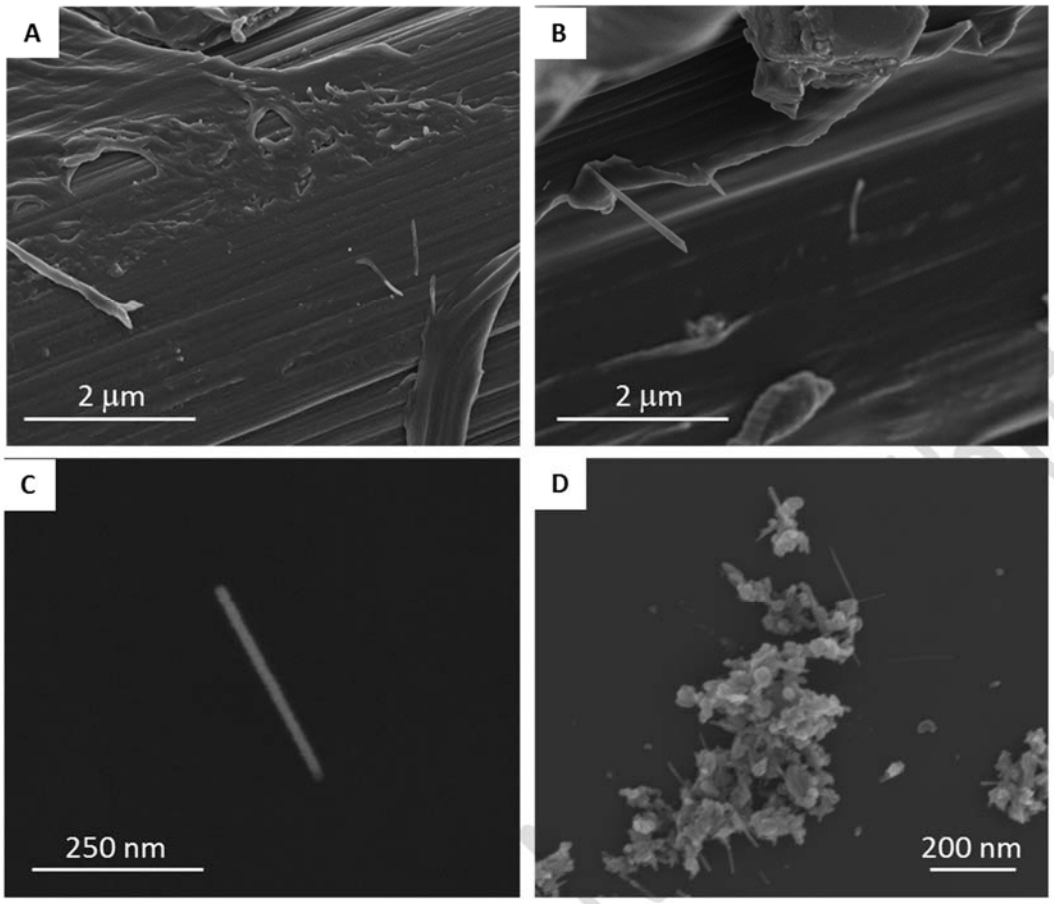

Figure 24: Bat 2 fragments collected on a Si wafer showing A & B) exposed, C) free, and D) in loose agglomerate with other MWCNTs and polymer fragments.

These images of MWCNTs confirm the presence of MWCNTs in the bats and the release of MWCNTs during some fracture or breakage events. However, detecting these free or exposed MWCNTs took many hours of manually intensive high resolution imaging of Si wafer samples and each one of the Si wafers represent only a few mg of bat material. For more comprehensive analysis of bat fragments, automated imaging approach is required.

5.4.4 Automatic Imaging of MOUDI Samples

As discussed in Section 5.2.4, MOUDI can generate relatively monodisperse particle samples. Although there are unavoidable size variations and few particles outside of the expected cut size ranges, higher stage (small particle size) samples can usually be imaged without any additional coating.

One main challenge of SEM imaging of abrasion particle samples is the need to cover a large sampling area at extremely high resolution. Cursory scan of the sample substrate at low resolution can easily overlook nanoparticles and manual survey of large sample area at very high resolution is not practical. Ideally, we would want to use an automated imaging routine

where the entire sample substrate is analyzed at various resolutions and likely nanoparticles are imaged at requisite resolution but this is beyond our current capability. However, we were able to implement automated imaging of large sample areas to handle the bulk of the imaging needs. Manual evaluation of automatically collected images was still required to identify regions of interest for subsequent imaging session and to confirm the presence of nanoparticles and MWCNTs.

Automatic large area imaging (mapping) routine was used to search for exposed and free MWCNTs in the MOUDI samples. We found that the pixel resolution of 50 nm or less and 1 μs or greater pixel dwell time are needed to detect individually occurring bare or a small cluster of MWCNTs on an uncoated Si substrate. This is what we termed "survey" resolution. However, at this survey resolution, we cannot usually resolve the shape and size of MWCNTs clearly. For example, a 200 nm MWCNT would appear as a barely visible spot that is roughly 4 pixels long. These survey scan can pin point areas of sample substrate that contain higher number of nanosized particles. Another set of images at higher resolution is acquired and reviewed for MWCNTs.

Figure 25 shows an example of this process in terms of image arrays and their relative positions and resolution. In this example, about 10 mm x 10 mm area of the 1 in Si wafer was surveyed at a low resolution imaging condition. Depending on the imaging parameters used, this could take a couple of hours to several hours. Collected low resolution images are reviewed using a web based multi-resolution visualization tool to identify areas for subsequent high resolution analysis. Images collected from the high resolution imaging sessions were manually reviewed to identify features that may be individual MWCNTs or clusters of MWCNTs. Likely candidates were reimaged at much higher resolution (2 nm pixel resolution, for example).

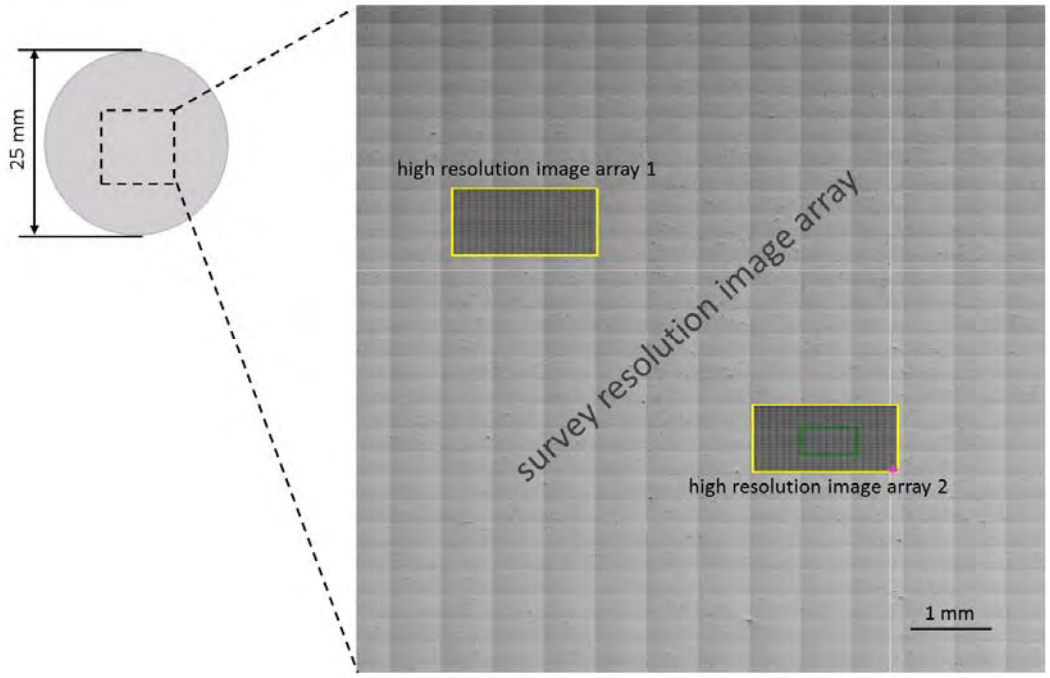

Figure 25: Diagram showing relative scales and locations of automated array imaging data set. Automated array imaging was combined with a hierarchical imaging strategy to perform intelligent surveying of a large sample area at multiple imaging resolutions.

As mentioned before, non-rotating MOUDI samples have distinctive honeycomb-like particle distribution patterns. Figure 26 shows an optical image of a stage 6 MOUDI sample showing many "cells". The size of the cells varied depending on the nozzle spacing (higher stage cells were smaller in overall size than lower stage cells). In the example shown in Figure 26, each cell is about 2 mm in diameter.

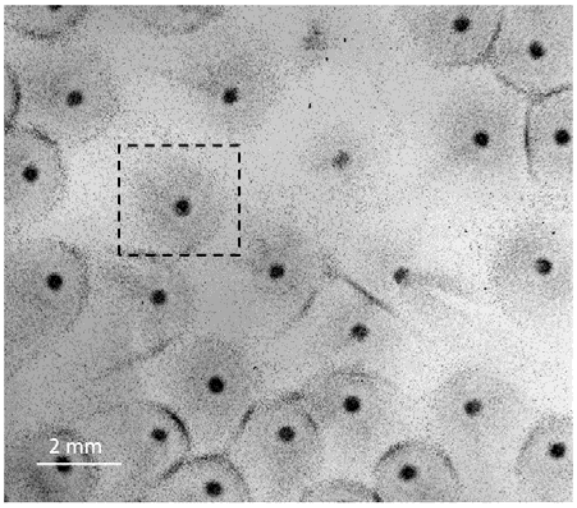

Figure 26: Particle distribution pattern from a stage 6 MOUDI sample.

Each cell consisted of a central bull's eye with a relatively high particle concentration, cell boundary that is formed when particles entering through adjacent MOUDI nozzles collide with each other and form a high particle concentration edge, and a lower particle concentration mid-region. Figure 27 shows close-up views of one of the cells from a stage 9 sample. To ensure that a representative particle population on each MOUDI stage sample was analyzed, high resolution SEM mapping was performed on areas large enough to cover at least one complete cell. For higher stage samples where cell sizes are relatively small, multiple cells were analyzed.

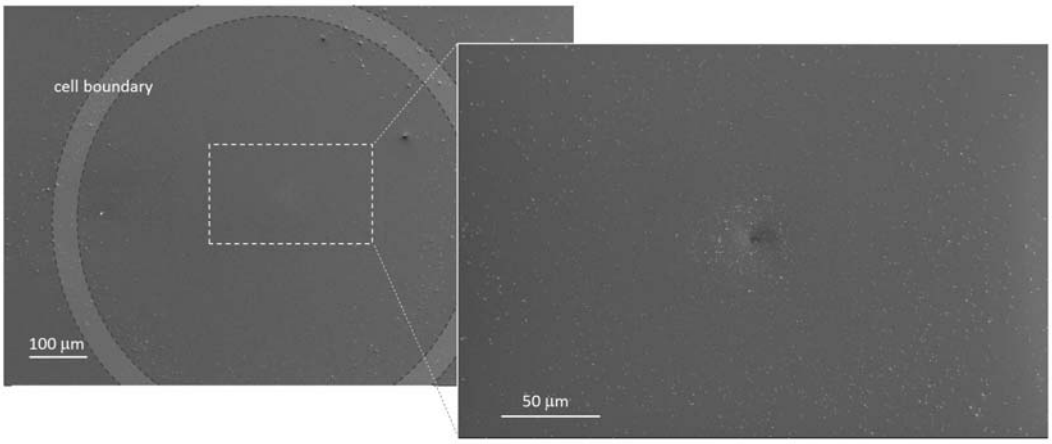

Figure 27: Overview images of a "cell" from a stage 9 MOUDI sample showing larger particles along the cell boundary (marked with gray ring) and very fine particles within the barely visible bull's eye region (rectangular inset).

5.4.5 Release Particles from the Bats

5.4.5.1 Abrasion Particles for the Bats

Abrasion particles collected using MOUDI were analyzed using the hierarchical automated imaging strategy described in the previous section. Average particle size varied depending on the MOUDI stage that sample was collected on but the shape of the particles, in general, were relatively uniform. Many of the larger particles (particle diameter > 1 µm) have a rounded or rolled shape. Figure 28 shows a typical particle morphology for samples from MOUDI stages 6, 8, and 9. Also, as the particle size increased (with the decreasing stage number), charging artifacts became more pronounced as can be seen in Figure 28A.

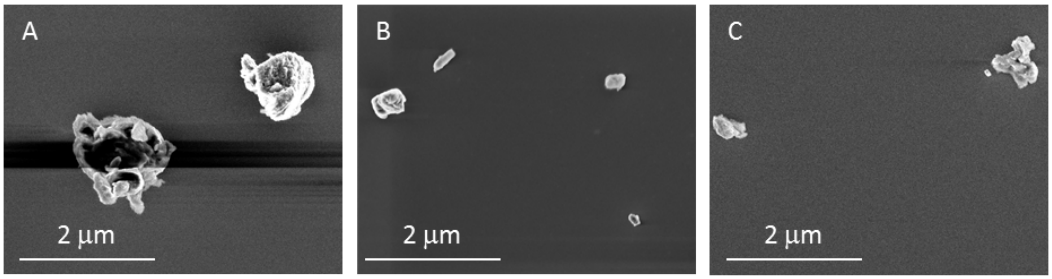

Figure 28: Typical abrasion particles from different MOUDI stages: A) stage 6, B) stage 8, C) stage 9.

Particles in the nanometer size range did not have the rounded morphology that the larger particles exhibited. Figures 29 shows several classes of nanoparticles sampled during the bat 1 abrasion process. The most abundant were small, irregular shaped particles with varying surface textures, as shown in panels J-M. There were also many fractal-like aggregates of very small spherical particles reminiscent of combustion particles (panels H & I). Less abundant were rod-like particles that are either polymer coated MWCNTs (panels B-G) or, in some cases, bare MWCNTs (panel A).

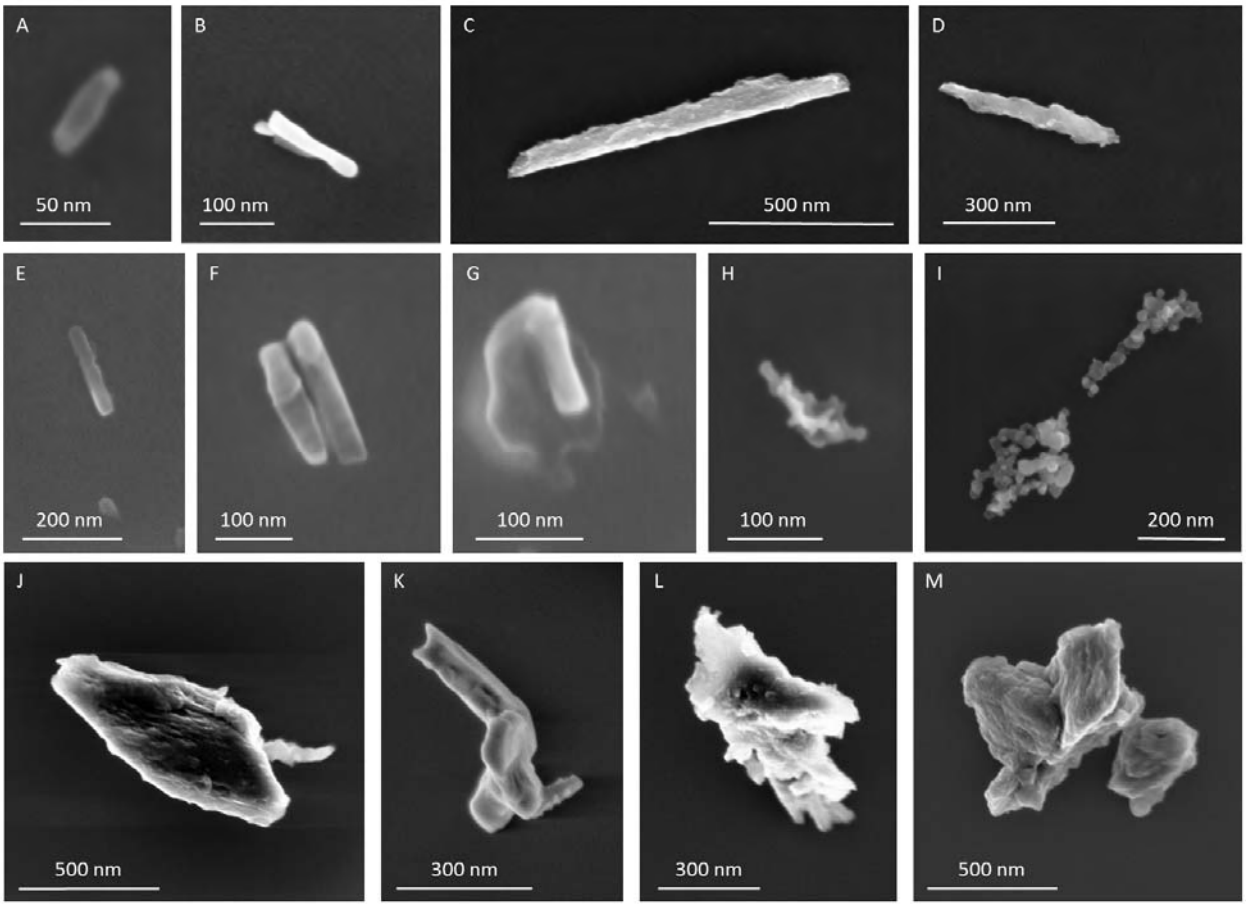

Figure 29: Released abrasion nanoparticles from bat 1 collected using MOUDI. These and similarly shaped and sized particles were present in all the MOUDI stage samples.

Figure 30 shows the types of nanoparticles sampled during the bat 2 abrasion process. Particle shapes and sizes were similar to those found in the bat 1 samples. There were many irregular shaped particles, individually occurring nanometer range spherical particles, fractal aggregates, and agglomerates of different particles. Rod-like particles were usually partially embedded in some other material or loosely attached to another particle and were relatively short in length, most of them in 100 nm to 500 nm range. Based on earlier analysis of similar rod-like particles, we suspect that all the particles except for Figure 30B are either bare MWCNTs or MWCNTs embedded in resin.

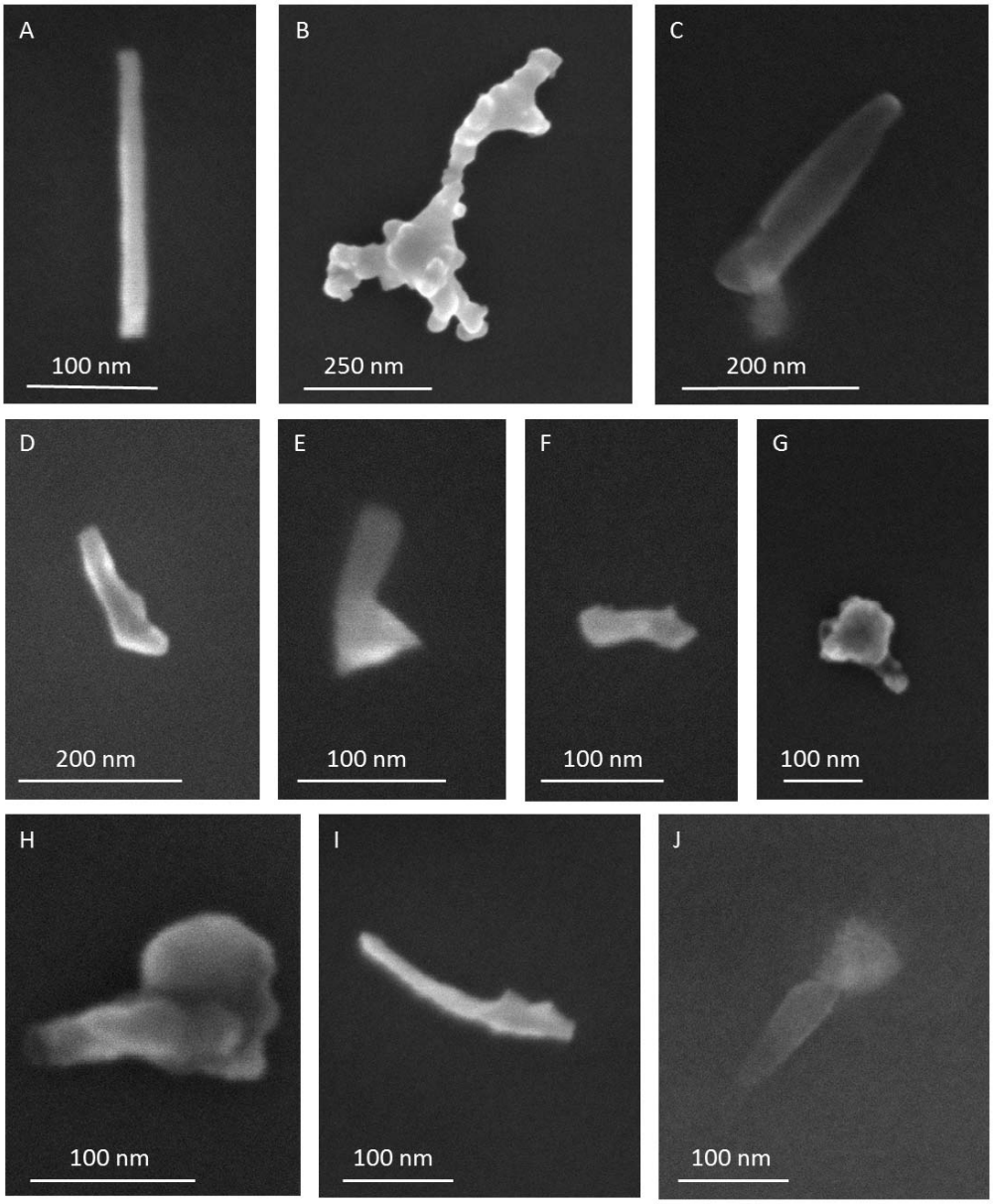

Figure 30: Released abrasion nanoparticles from bat 2 collected using MOUDI. These and similarly shaped and sized particles were present in all the MOUDI stage samples.

5.4.5.2 Fracture Particles from the Bats

Release particles were also collected using MOUDI while manually fracturing the bat carbon fiber layers. These operations were relatively short in duration (2 min to 3 min) and consumed one or two small, sectioned pieces of the bat. Release particle morphology was similar to that of abrasion release particles. However, in the fracture sample, larger particles were more angular and jagged and lacked the rounded morphology we saw earlier. Figure 31 shows some of the nano-sized particles from the bat 1 fracture sampling. As before, many of the rod-like particles are relatively short and usually attached or embedded in another material. However, there were occasional longer (1 μm or longer) particles. Fractal aggregates were usually larger and more complex in structure than those we saw in the abrasion release particles.

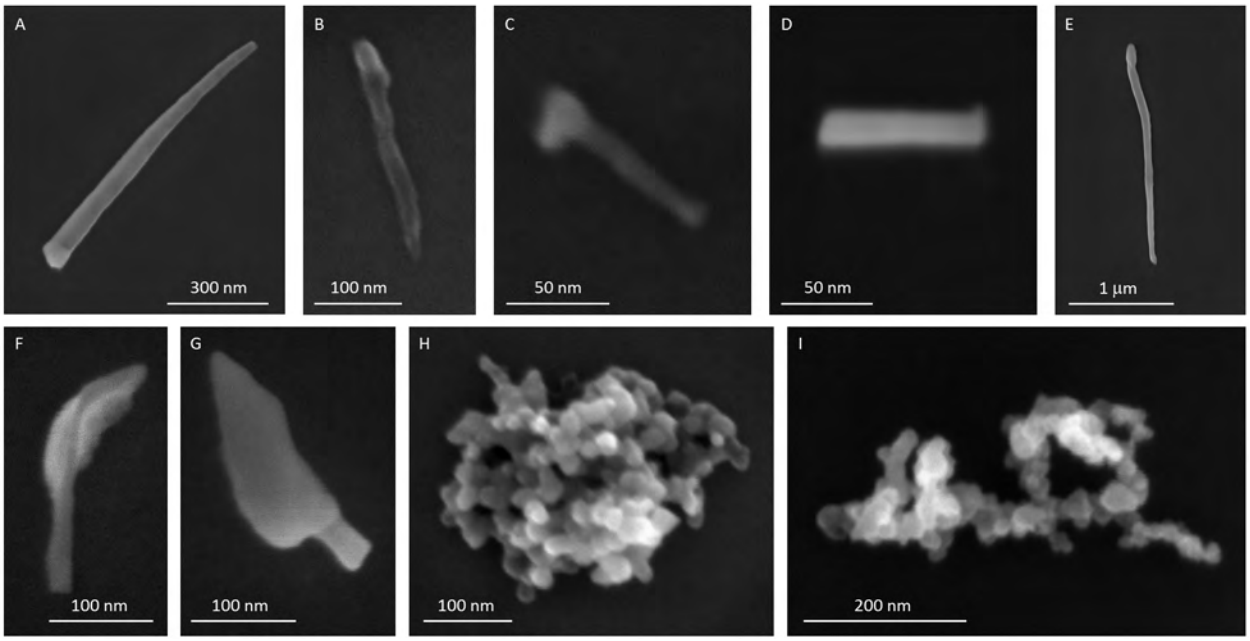

Figure 31: Release particles from bat 1 fracture sampling. Particles were collected with MOUDI using the same stage configurations as in the abrasion sampling.

Figure 32 shows the nanoparticles from the bat 2 fracture sampling. Again, the most abundant particles were the irregular shaped singly occurring particle or particle agglomerates. Rod-like particles were present but not common. In general, we were able to find about a dozen or more rod-like particles in each cell.

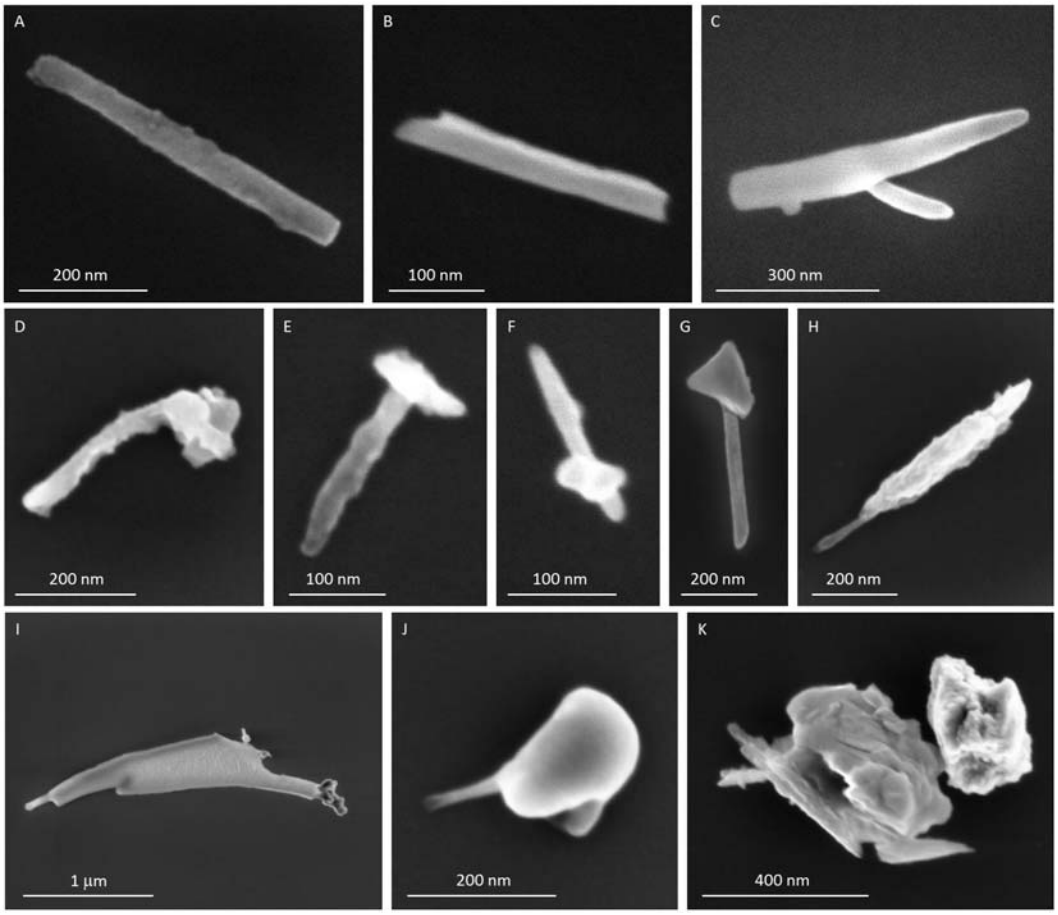

Figure 32: Release particles from bat 1 fracture sampling. Particles were collected with MOUDI using the same stage configurations as in the abrasion sampling.

Some of the MWCNTs were also found in the fracture samples collected at the MOUDI inlet stage. There is no size selection mechanism at the inlet of MOUDI and the size of the particles collected at this stage ranged widely (from few tens of nanometers to several hundred micrometers). Many of the particles are hundred micrometers or larger and a conductive coating was needed for effective imaging. Even with a thin layer of carbon coating, larger particles caused significant charging artifacts as shown in Figure 33. In the fracture samples, many of the larger particles are broken pieces of carbon fibers or large chunks of resin that were peeled off from the fibers. In contrast, inlet stage of the abrasion sampling showed very few particles larger than 50 μm and particle morphology was, again, relatively rounded.

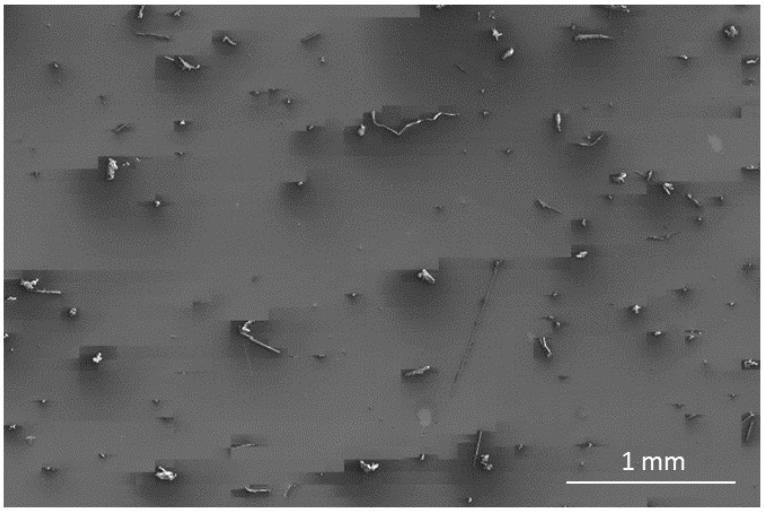

Figure 33: Montage of survey images of MOUDI inlet sample from bat 1 fracture sampling process.

In between the larger particles, there were a number of smaller particles and some areas where initial impact had broken larger particles into smaller pieces. These were where many of the MWCNTs and MWCNT associated fragments were found in the inlet sample. Figure 34 shows some of these particles and Figure 35 shows SEM and the corresponding TEM images of several commonly occurring release particle types.

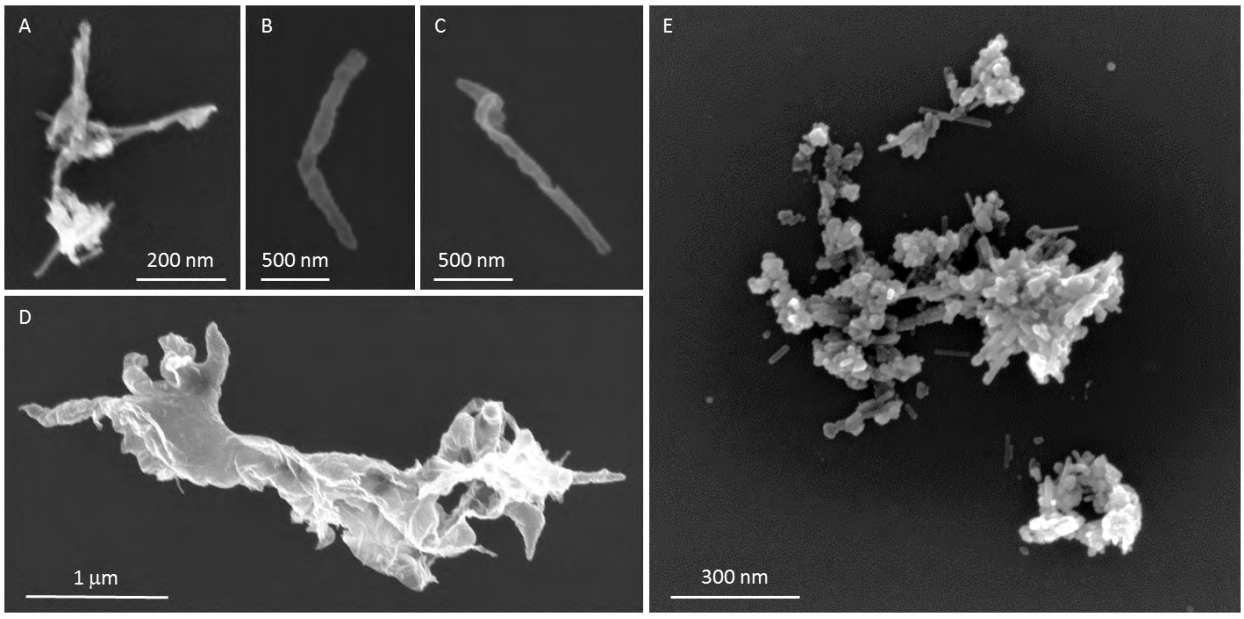

Figure 34: Released particles from the bat 1 fracture sampling collected at the MOUDI inlet stage.

Figure 34A shows a clump of coated and bare MWCNTs. Similar release particles were collected in our preliminary release study and confirmed to be MWCNTs (See Figures 35E & F). Figures 34B and C show individual, uneven diameter tubes. TEM analysis of similar particles

showed that these have clear multiwall structure as shown in Figures 35C and D. Figure 34D shows a thin membrane like particle with several tubular projections. Similar membranous material analyzed in TEM showed no multiwall structure. Figure 34E shows a couple of agglomerates of several short MWCNTs with polymeric nanospheres frequently seen in fractal aggregate morphology. Figure 35 A and B are the SEM and TEM images of similar rod-like MWCNTs.

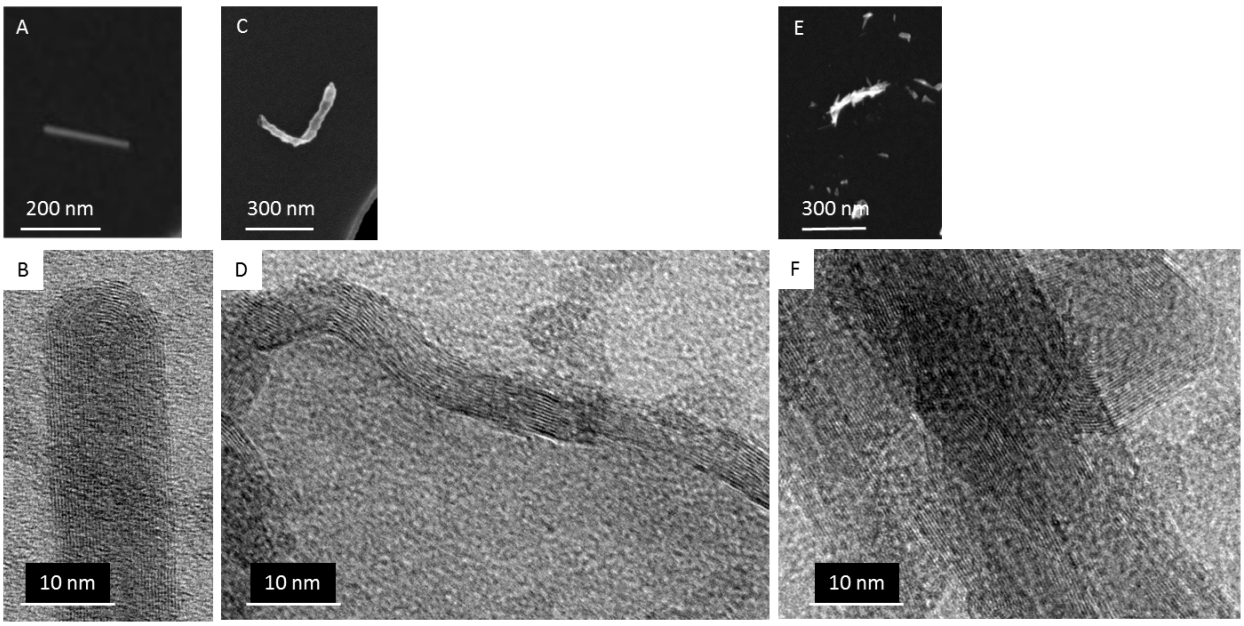

Figure 35: SEM images of three commonly occurring MWCNT particle types and corresponding TEM images showing the multiwalled structure of the particles.

6 DISCUSSIONS AND CONCLUSIONS

In our preliminary analysis of the MWCNT nanocomposite bats, we found that free MWCNTs and clusters of MWCNTS with and without polymer fragments were released during rigorous abrasion and rubbing of the bat composite layers. However, effective sampling (collection) of release particles, especially very fine particles, were difficult and free MWCNTs were detected only by sampling the enclosed chamber walls or by dusting TEM grids with a large quantity of abrasion debris. In the current phase of the release study, we used a more systematic approach for collecting release particles by incorporating several well established aerosol sampling techniques. Our aerosol sampling system consisted of a Taber linear abrader, a custom sampling chamber, real time particle analyzers (SMPS and CPC), and several impactor based sampling devices (MOUDI, electrostatic precipitator, and personal samplers). However, we quickly found that the collection efficiency problem we experienced during our preliminary analysis phase was not limited to passive air sampling.

Previously reported results from several groups confirmed the release of free standing MWCNTs and polymer fragments that clearly contain protruding MWCNTs from sanding (fast abrasion) or sawing operations [7-9]. In these studies, MWCNTs were detected on filter samples but none of the aerosol measurements showed corresponding particle size distribution. Several factors could account for the discrepancy. Low total number of MWCNTs released, low sampling flow rate, diffusion loss during transport, etc. can result in particle population that is too small for detection by real time particle analyzers. Similar factors can probably be attributed to our system's poor collection efficiency.

A set of custom fabricated control epoxy nanocomposite samples with known MWCNT loadings was used to evaluate and optimize the performance of our aerosol sampling process. We found that nanocomposite abrasion particles were not effectively aerosolized and we were also incurring a significant transport loss through various mechanisms (gravitational settling, diffusion loss, inertial impact, electrostatic deposition, etc.) at the sampling inlet and along the transport path. We were able to address some of these problems through careful configuration of sampling parameters and proper positioning of sampling ports and were successful in generating sufficient number of size selected release particles from commercial bats using the new abrasion sampling system.

A custom Raman microscope system was used for the analysis of MWCNTs in the nanocomposite samples. Although we were able to detect MWCNTs in nanocomposite control samples with MWCNT loading as low as 0.01 mass%, we were not successful in detecting MWCNTs in the bat samples. The most likely explanation for this lack of MWCNT signals in the bat samples is that the MWCNT loading in the commercial bats is lower than the Raman system's detection limit. Based on the visual inspection of the resin fragments from the bats, we suspect that the MWCNT concentration in the resin must be fairly low because the resin fragments appeared translucent rather than black. MWCNT nanocomposites with MWCNT loading higher than 0.1 mass% should appear black. Raman analysis of the control samples showed that we were able to detect MWCNT agglomerates regardless of the average MWCNT concentration in the sample, but because the MWCNT dispersion was not homogeneous, this finding did not necessarily indicate that the detection limit of Raman imaging is as low as 0.01 mass% MWCNTs in epoxy matrix. In fact, the detection limit could be much higher in nanocomposites where MWCNTs are fully dispersed. Figure 36 is a schematic representation explaining this situation. Figures 36A and B show the schematic representations of a well dispersed and a poorly dispersed MWCNT composite sample, respectively. The red dashed circle represents the Raman probe diameter showing where the detected MWCNT Raman signal is coming from. Both samples contain the same number of MWCNTs but the poorly dispersed sample will generate a much higher intensity MWCNT Raman signal when the probe is on a MWCNT agglomerate while the MWCNT Raman signal from the well dispersed sample

may be too weak for detection. In commercial nanocomposite materials, proprietary polymer formulation or functionalized MWCNTs are used for much improved dispersion characteristics and this could be the reason why we were unable to detect any MWCNTs in the bat samples [10].

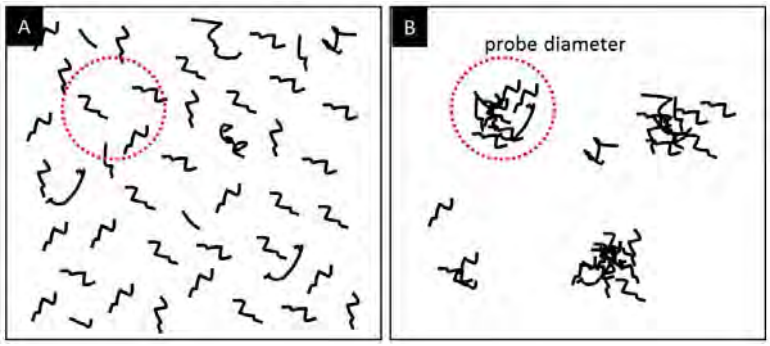

Figure 36: Effect of MWCNT dispersion on MWCNT detection capability in Raman imaging.

Currently there is no established data on the lower limits of detection for MWCNTs in polymer nanocomposites using Raman imaging. Current literature on Raman spectroscopy of MWCNT or MWCNT nanocomposites mostly focuses on the spectral details of detected MWCNTs and the samples used in these studies have relatively high MWCNT loadings (3 mass% or higher). Although there are several significant advances in Raman imaging methods, for example, tip-enhanced Raman imaging has shown promising results in nanoscale Raman imaging [11], detection of MWCNTs in polymer matrices is still very challenging. Better characterization of MWCNT detection sensitivity with and without surrounding polymer matrix and also a better understanding of MWCNT dispersion in polymer matrices are still needed to determine whether Raman imaging can be used as a routine detection method for MWCNTs in consumer nanocomposites and their release products.

Due to their extreme small size and the lack of unique elemental and chemical signature that can be easily detected using traditional microscopy techniques, direct imaging by SEM and TEM are still the most reliable and effective methods to detect and identify MWCNTs. However, to effectively search large samples such as the 1-in wafers used for our MOUDI sampling for nanometer size particles with low inherent contrast, painstaking surveys of the sample at a very high resolution are required. Although TEM imaging is necessary and critical in confirming the structural details of individual MWCNTs, high throughput TEM analysis of large population particle samples is not a practical option. We addressed this requirement for exhaustive searching by automating our SEM imaging process and also by instituting a hierarchical search strategy. Although it takes several days to fully examine one sample wafer, most of this time is spent in automated imaging of the sample and the actual 'eyes-on' time by a person is relatively short since manual scan of acquired image stack for MWCNTs or likely features can be

performed relatively quickly. Using the automated imaging approach, we were able to detect and confirm a number of released MWCNTs in the abrasion and fracture aerosols from the bat samples.

Our results showed that free MWCNTs and MWCNTs embedded in polymer fragments are released from commercial nanocomposites bats during slow abrasion and also during fracturing operations. However, the number of particles identified as MWCNTs was small compared to the total number of particles collected. The size and surface texture of the detected MWCNTs indicated that most of them were MWCNTs encased in polymer matrix similar to those described in Ding, et al. (Appendix 4) [12]. A number of free MWCNTs were also detected. On average, we found several free MWCNTs or MWCNT clusters in a 300 μm x 200 μm area of the sample wafer. This roughly translates into 7000 to 10000 MWCNTs per sample wafer. Although this number sounds large, since most of the free MWCNTs we found were relatively short (several hundred nanometers in length), these MWCNTs collectively could easily have been broken fragments from several long MWCNT fibers.

Our analysis of MOUDI samples helped us better understand the types of particles that were released during abrasion and the relative abundance of free and encased MWCNTs versus non-MWCNT particles. We did notice that some of the release particles on the MOUDI samples looked as though they were broken apart upon impact. We often detected multiple free MWCNTs in these locations. We also noted that the MWCNTs detected at the inlet stage were in general longer than those detected on the subsequent MOUDI stages. This seems to imply that sampling with MOUDI was influencing the released particle morphology and may not be representative of actual released particles and care should be taken in translating our MOUDI sample results to real world release scenario.

We were not able to assess the MWCNT release rate from our findings because we do not know how many particles were generated during the abrasion process and how many of released particles were lost during sampling through various loss mechanisms such as gravitational settling, electrostatic deposition, inertial impact, etc. For a quantitative assessment of MWCNT release rate, we need much more robust characterization of the particle abrasion system with real time analysis and visualization of release particles as well as realistic estimates of particle losses along the entire sampling path.

In summary, our results show that free MWCNTs are released from commercially available nanocomposites bats. However, the number of detected MWCNTs is very small compared to the number of total release particles. Although we cannot quantify the release rate of MWCNTs from the bats using our current analytical capability, the fact that we are detecting relatively few MWCNTs, whether that is due to the lack of MWCNT release or due to the loss of

particles through unintentional deposition along the particle sampling path, indicate that the environmental availability of MWCNTs from these products is limited.

ACKNOWLEDGEMENT

We would like to acknowledge Robert Fletcher, Julie Bitter and Matthew Staymates for their help with MOUDI stage modification and aerosol sampling setup; Jeremiah Woodcock, Chelsea Davis and Jeffrey Gilman for providing the MWCNT nanocomposite control samples; and Alline Myers and Joshua Schumacher for TEM sample preparation and imaging of the MWCNT nanocomposite control samples.

ABBREVIATIONS & TERMINOLOGY

FIB: focused ion beam

MOUDI: micro-orifice uniform deposit impactor

MWCNT: multiwall carbon nanotube

NAS: nanometer aerosol sampler

SEM: scanning electron microscope

TEM: transmission electron microscope

mass%: percent mass fraction

REFERENCES

1. Nathan, A.M. (2004) “Characterizing the performance of baseball bats” Am. J. Phys. 71, 134-143.
2. Russell, D.A. “Are Composite Bats better than Aluminum Bats?” http://www.acs.psu.edu/drussell/bats/compalum.html (last accessed 1/15/2015).
3. Mirjalili, V., Ramachandramoorthy, R. & Hubert, P. (2014) “Enhancement of fracture toughness of carbon fiber laminated composites using multi wasll carbon nanotubes” *Carbon* **79**, 413-423.
4. Brockmann, J.E. (2001) “Sampling and Transport of Aerosols”, in Baron, P.A. & Willeke, K. (Eds.), Aerosol Measurement: Principles, Techniques, and Applications (2nd Ed.) (143-195). Toronto, Wiley and Sons.
5. Kuhlmey, G.A., Liu, B.Y.H., Marple, V.A. (1981) “A Micro-Orifice Impactor for Submicron Aerosol Size Classification”, *Am. Ind. Hyg. Assoc. J.* **42**, 790-795.
6. Marple, V.A., Rubow, K.L., Ananth, G.P. & Fissan, H.J. (1986) “Micro-orifice Uniform Deposit Impactor” *J. Aerosol Sci.* **17**, 489-494.
7. Huang, G., Park, J.H., Cena, L.G., Shelton, B.L. & Peters, T.M. (2012) “Evaluation of airborne particle emissions from commercial products containing carbon nanotubes” *J. Nanopart. Res.* **14**, 1231-1244.
8. Schlagenhauf, L. Chu, B., Buha, J., Nuesch, F.A. & Wang, J. (2012) “Release of carbon nanotubes from an epoxy based nanocomposite during an abrasion process” *Env. Sci. Tech.* DOI: 10.1021/es300320y.
9. Schlagenhauf, L., Nuesch, F. & Wang, J. (2014) “Release of Carbon Nanotubes from Polymer Nanocomposites” *Fibers* **2**, 108-127.
10. Chen, J., Lie, H., Weimer, W.A., Halls, M.D., Waldeck, D.H., Walker, G.C. (2002) “Noncovalent Engineering of Carbon Nanotube Surfaces by Rigid, Functional Conjugated Polymers”, *J. Am. Chem. Soc.* 124, 9034-9035.
11. Yano, T., Ichimura, T., Kuwahara, S., H’Dhili, F., Uetsuki, K., Okuno, Y., Verma, P. & Kawata, S. (2013) “Tip-enhanced nano-Raman analytical imaging of locally induced strain distribution in carbon nanotubes” *Nat. Comm.* **4**, 2592 | DOI: 10.1038/ncomms3592.
12. Ding, W., Eitan, A., Fisher,F.T., Chen, X., Dikin, D.A., Andrews, R., Brinson, L.C., Schadler, L.S. & Ruoff, R.S. (2003) “Direct Observation of Polymer Sheathing in Carbon Nanotube−Polycarbonate Composites”, *Nano Lett.* **3** 1593-1597.

APPENDIX 1:

Video frame showing the structure of a baseball bat. Inset states that the resin matrix is reinforced with CNTs.
http://www.youtube.com/watch?feature=player_embedded&v=ORWyDSluw8g

APPENDIX 2: CONDUCTIVE COATING FOR CHARGE MITIGATION

Typical Au or Au/Pd coatings are 10 or more nanometers thick and form nanoscale islands, potentially obscuring very fine structures in the sample. Figure 11 illustrates how different charge mitigation methods can affect the resulting images. Figure 11A shows MWCNTs on Si coated with Au/Pd. MWCNTs are very well defined but also present are nanoscale islands on Si substrates, artifacts from Au/Pd coating. Figure 11B shows MWCNTs on Si coated with Os. Here, there are no discernable artifacts on Si substrate but the MWCNTs are less well defined.

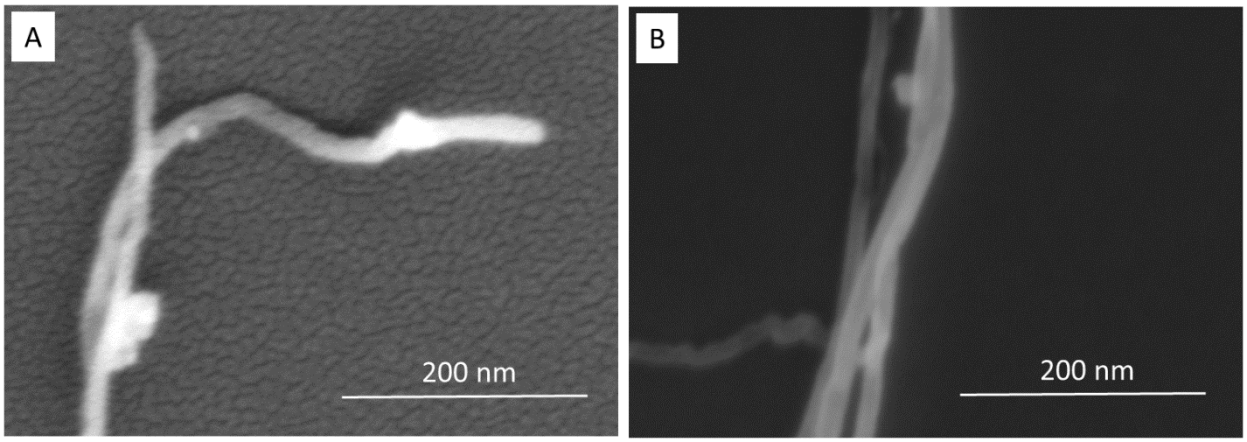

Figure A2: Close-up image of A) Au/Pd coated MWCNT on Si and B) Os coated MWCNT on Si.

APPENDIX 3: IMPACTION STAGE PARAMETER

Nominal cut size and number of nozzles of MOUDI stage is given below.

Stage Number	Nominal Cut size, μm	Number of Nozzles
inlet	15	1
1	10	3
2	5.6	10
3	3.2	10
4	1.8	20
5	1.0	40
6	0.56	80
7	0.32	900
8	0.18	900
9	0.10	2000
10	0.05	2000

APPENDIX 4: FIGURE 5 FROM DING ET AL. SHOWING POLYMER SHEATHED MWCNTS

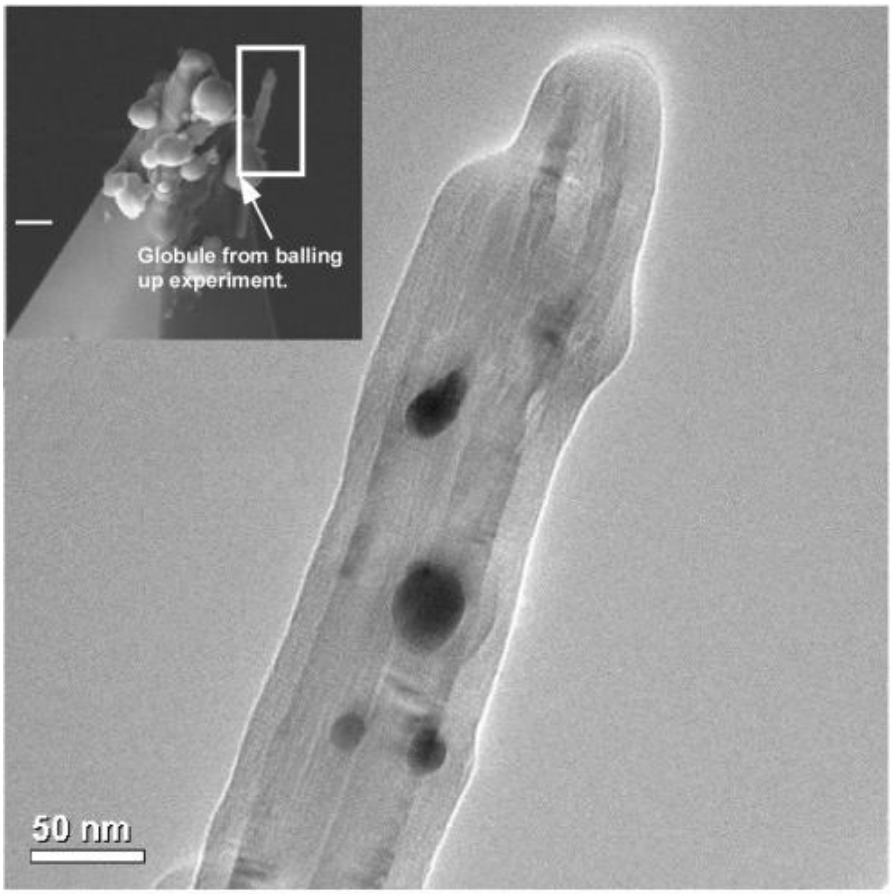

Figure 5: TEM image of a sheathed MWCNT after the outer layer of polymer has been removed during a "balling up" experiment. Even after the balling up experiment a thin layer of polymer remains adhered to the nanotube. (Inset) SEM image of the sheathed MWCNT still attached to the AFM tip after the balling up experiment, highlighting the location of the TEM image. Scale bar in the inset) 300 nm

Ding, W., Eitan, A., Fisher,F.T., Chen, X., Dikin, D.A., Andrews, R., Brinson, L.C., Schadler, L.S. & Ruoff, R.S. (2003) "Direct Observation of Polymer Sheathing in Carbon Nanotube−Polycarbonate Composites", *Nano Lett.* **3** 1593-1597.